UNIVERSITY OF CALIFORNIA,
IRVINE

# Characterization of the Iron/Heme Acquisition Pathways in *Mycobacterium tuberuclosis*

DISSERTATION

submitted in partial satisfaction of the requirements
for the degree of

DOCTOR OF PHILOSOPHY

in Biological Sciences

by

Rodger de Miranda

Dissertation Committee:
Professor Celia W. Goulding, Chair
Professor Thomas L. Poulos
Professor Michael Green

2023

# DEDICATION

To Alex, you have been the most amazing and supportive partner anyone could ever wish for. I would never have been able to succeed without you by my side.

To Jujubee and Katya, your fuzzy comfort has been instrumental in helping me persevere through COVID and get to the finish line.

To my friends and family (especially Elle and Jashana) who were always ready to listen to my rants, you are amazing.

To my mentors along the way who pushed me to continue, and even consider taking this path, I am committed to paying it forward to the next generation of scientists.

# TABLE OF CONTENTS

# LIST OF FIGURES

# LIST OF TABLES

# ACKNOWLEDGEMENTS

My journey to becoming a scientist has been far from linear, and I have been fortunate to have an outstanding group of mentors along the way who pushed me and guided me. Thank you Dr. Elizabeth Migicovsky for being that initial voice to ask "Have you ever considered doing a PhD?" Thank you Dr. Alberto Rascon and Dr. Laura Miller Conrad for teaching me how to be a researcher. And of course, thank you to Dr. Celia Goulding for being my PhD research advisor. Your guidance and enthusiasm for science have been instrumental in shaping me as a scientist. Finally, a special thank you to my husband Alex, without whom I would never have made it to the end. Your unfailing optimism, love, and support are truly what keep me going.

Chapter 1 all figures except for Figure 1.1 (which is from the 2022 World Health Organization World Tuberculosis Report), were made using Biorender.com.

Chapter 2 figure 2.8 was made using Biorender.com.

Chapter 3 I would like to acknowledge and thank Jessica Mendoza for her hard work assisting me in generating the FGD *M. smeg* expression construct, and for her friendship, support, unfailing optimism, and dedication for being the best scientist she can be. You are truly an inspiration. I would also like to thank my undergraduate researcher, Vanessa Saldivar, for her work on helping express and purify the putative *M. tuberculosis* biliverdin reductases, as well as for choosing me to be her mentor. I have learned a lot working with you theses past two years.

Chapters 4 and 5 are part of a manuscript in preparation. I would like to acknowledge Alex Chao and Bonnie Cuthbert for solving and refining the crystal structure of FecB, as well as the Esienberg lab at UCLA for solving and revining the crystal structure of FecB2, and Thaís Klevorn from the Ehrt lab at Cornell for performing the co-immunoprecipitation assays in *Mycobacterium tuberculosis*. And finally, Figure 5.1b was made using Biorender.com.

I also appreciate financial support from the National Institutes of Health (NIH) (P01-AI095208, T32AI141346).

# VITA

**Rodger de Miranda**

## EDUCATION

**Ph.D.—Biological Sciences** June 2023
University of California—Irvine, Irvine, CA

**Master of Science—Biological Sciences** June 2022
University of California—Irvine, Irvine, CA

**Bachelor of Science with Honors—Chemistry** December 2017
San José State University, San Jose, CA

**Associate of Science—Chemistry** May 2012
Cabrillo College, Aptos, CA

## RESEARCH AND TEACHING EXPERIENCE

**Graduate Student Researcher** Fall 2018-Summer 2023
Goulding Lab, Department of Molecular Biology and Biochemistry

**Graduate Student Teaching Assistant** Winter 2020 and 2022
University of California—Irvine, Department of Molecular Biology and Biochemistry

**Undergraduate Research Assistant** Fall 2016-Spring 2018
Miller-Conrad Lab, Department of Chemistry, San Jose State University

**Lecturer** Spring 2018
San José State University, Department of Chemistry

**Lead Biochemistry Tutor** Spring 2017-Spring 2018
San José State University, College of Science Advising Center

## PUBLICATIONS

**de Miranda, R.**, Cuthbert B.J., Klevorn, K., Chao, A., Arbing, M., Sieminski, P.J., Papavinasasundaram, K., Abdul-Hafiz, S., Chan, S., Sassetti, C.M., Eisenberg, D., Ehrt, S., and Goulding, C.W. Differentiating the roles of *Mycobacterium tuberculosis* periplasmic binding proteins, FecB and FecB2, in iron uptake. (*Manuscript in review at PLOS Pathogens*)

Chao, A., Burley, K.H., Sieminski, P.J., **de Miranda, R.**, Chen, X., Mobley, D.L., and Goulding, C.W. Structure of a *Mycobacterium tuberculosis* heme-degrading protein, MhuD, variant in complex with its product. *Biochemistry*. 2019; 58(46): 4610-20.

## PRESENTATIONS

"Elucidating iron transport in the periplasm of *Mycobacterim tuberculosis*." March 2023
Oral Presentation at the Annual American Society for Biochemistry and Molecular Biology Meeting, Seattle, WA.

"Characterization of periplasmic iron transport in *Mycobacterium tuberculosis*." April 2022
Poster presentation at the Annual American Society for Biochemistry and Molecular Biology Meeting, Philadelphia, PA.

"*In vitro* biochemical studies of ArnA from *Pseudomonas aeruginosa*." April 2018
Poster presentation at the Annual American Society for Biochemistry and Molecular Biology Meeting, San Diego, CA.

"Recombinant experission and purification of ArnA from *Pseudomonas aeruginosa*." Nov. 2017
Oral presentation at the Annual Biomedical Research Conference for Minority Students, Phoenix, AZ.

## AWARDS AND HONORS

| | |
|---|---|
| Robert Warner Award for Excellence in Research | Spring 2022 |
| ASBMB Travel Award | Spring 2022 |
| T32 in Microbiology and Infectious Disease | Fall 2020-Spring 2021 |
| College of Science Research and Teaching Scholar Award | 2016-2017 |
| Student Affiliates of the American Chemical Society Scholarship | Fall 2017 |
| San José State University Dean's Scholar | Spring and Fall 2017 |

## OTHER ACTIVITIES AND PROFESSIONAL MEMBERSHIPS

| | |
|---|---|
| MBB Rep. for Diverse Educational Community and Doctoral Experience | 2020-2023 |
| California Unified Taekwondo Association SoCal Referee Vice Chair | 2021-2023 |
| American Society for Biochemistry and Molecular Biology | 2018-Present |
| USA Taekwondo Level B-1 National Referee | August 2017 |
| Kukkiwon 2nd Degree Taekwondo Black Belt | May 2017 |

# ABSTRACT OF THE DISSERTATION

Characterization of the Iron/Heme Acquisition Pathways in *Mycobacterium tuberculosis*

by

Rodger de Miranda

Doctor of Philosophy in Biological Sciences

University of California, Irvine, 2023

Professor Celia W. Goulding, Chair

*Mycobacterium tuberculosis* (Mtb), the causative agent of tuberculosis, poses a great threat to human health. With the emergence of drug resistant Mtb strains, new therapeutics are desperately needed. As iron is critical to the growth and survival of Mtb, the mechanisms through which Mtb acquires host iron pose attractive therapeutic targets. Mtb scavenges iron from the host via Mtb siderophores, carboxymycobactin and mycobactin, and heme uptake. Heme uptake culminates in degradation by the cytosolic protein MhuD, a noncanonical heme degrading enzyme in the IsdG family, in Mtb. In a recent study, a product-bound structure of the MhuD-R26S mutant with α-biliverdin was determined and revealed the formation of a novel secondary structural element, α3, stabilized by the $^{75}$HisXXXR$^{79}$ motif. In Chapter 2 I investigate the biological relevance of this motif by examining the heme binding and degradation of a MhuD R79S variant. I also determined that IsdI, another IsdG-family protein, binds with high affinity to the β- and δ-biliverdin isomers which will enable structural studies of product-bound IsdI. The fate of the heme breakdown product generated by MhuD, mycobilin, remained unknown. In Chapter 3, I demonstrate that Rv2074 is a novel mycobilin reductase and determined the chemical structure of the novel reduced mycobilin product, coined "mycorubin," utilizing tandem mass spectrometry. Little is known regarding the transport of siderophores across the periplasm and cell-wall environment, but the Mtb periplasmic binding proteins FecB and FecB2 have been implicated

in host iron acquisition. In Chapter 4 *in vitro* ligand binding experiments and structural comparisons for FecB and FecB2 were performed, revealing that both FecB and FecB2 bind heme, while only FecB binds Fe-cMB. Subsequent structure-guided mutagenesis of the FecB ligand binding site identified a single glutamate residue—Glu339—that significantly contributes to Fe-cMB binding. In Chapter 5, a role for FecB in the Mtb siderophore-mediated iron acquisition pathway was corroborated by *Mycobacterium smegmatis* pull-down experiments, which revealed interactions between FecB and known members of the mycobacterial siderophore export and import machinery, like MmpS5, a protein involved in apo-siderophore efflux. Finally, the FecB interacting partner MmpS5 was confirmed in Mtb by co-immunoprecipitation.

# CHAPTER 1

## Iron Acquisition in *Mycobacterium tuberculosis*


### Abstract

The disease tuberculosis is caused by the bacterium *Mycobacterium tuberculosis* (Mtb), which initially infects the lungs as the primary site of infection. One of the immune responses to bacterial infection is sequestration of iron by macrophages, which puts stress on intracellular pathogens such as Mtb, and has led to the evolution of a sophisticated array of iron acquisition mechanisms in pathogenic bacteria. These mechanisms include secretion of siderophores and uptake of heme to scavenge host iron, and are discssued in more detail in this manuscript.


### The Current State of Tuberculosis

*Mycobacterium tuberculosis* (Mtb) is the causative agent of tuberculosis (TB), and responsible for approximately 1.6 million deaths per year, and has infected about one third of the world's population with latent TB.[1] Sine 2019, the number of deaths has increased by 14%, and the number of new infections has increased by 6% after almost two decades of steady decline, particularly in every region except for the African region (Figure 1.1).[1] These increases have been linked largely to COVID-19, which shifted resources away from TB testing, treatment, and isolation programs, and also hindered access to preventative medical care.[1–3] Furthermore, there has been a rise in multi-drug resistant strains from 2020 to 2021, after years of relative stability (2015-2020), also thought to be largely caused by COVID-19 impacts. Finally, TB remains one of the leading causes of death in patients with HIV.[1] The treatment for TB is long and harsh; The Centers for Disease Control recommends a nine month treatment of a cocktail of antibiotics including isoniazid, ethambutol, rifampin, and pyrazinamide, which can have severe side effects contributing to patient noncompliance and a rise in multi-drug resistant strains.[1,4]

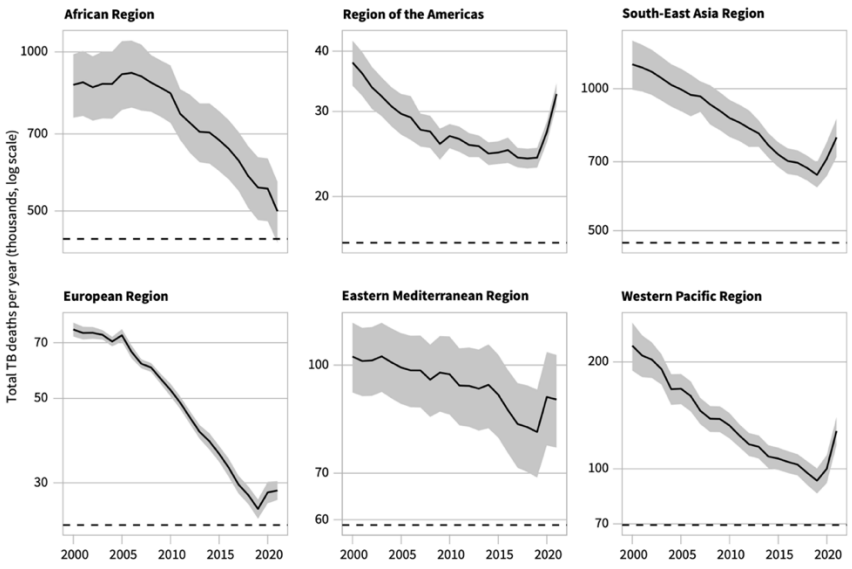


**Figure 1.1.** [1] Trends in the total number of TB deaths from the WHO 2022 Global Tuberculosis Report. The shaded regions indicate the 95% confidence interval. The dashed lines indicate the goals from the WHO End TB Strategy (which was aiming for a 35% reduction in deaths).

Mtb infection occurs when infected droplets are inhaled and settle in the lungs and begin to proliferate.[4] Mtb can then extravasate from the alveoli of the lungs into the lung parenchyma via an unknown mechanism (Figure 1.2). It has been proposed that Mtb may disseminate by four mechanisms: 1) Mtb has been shown to directly infect and kill lung epithelial cells[5], 2) a model has been proposed in which Mtb infects alveolar macrophages and then is transported across the lung epithelium intracellularly based on zebra fish models[6,7], 3) dendritic cells are known to sample antigens within the alveoli, and may become infected and traffic Mtb to nearby lymph nodes[8], 4) Mtb may be transported by specialized M cells which transport antigens to the parenchyma for display to antigen-presenting cells[9], or 5) dissemination may be achieved by some combination of all of these pathways. Once in the lung parenchyma the innate and adaptive immune responses work together to sequester the bacteria into granulomas, which drives Mtb into a latent stage but does not eradicate the infection (Figure 1.2).[10] This latent stage is characterized by dormant Mtb with low metabolic activity, and sequestration of the bacteria intracellularly in macrophages or

extracellularly in granulomas, preventing further spread and tissue damage.[11–13] In a patient with a healthy immune system the bacteria may be maintained in this latent stage for decades, resulting in an asymptomatic infection that can persist and become reactivated if the immune system becomes weakened or compromised later in life.[4,10] If the bacteria remains actively replicating and left untreated, the granuloma can rupture leading to dissemination of Mtb infection and death (Figure 1.2).[4]

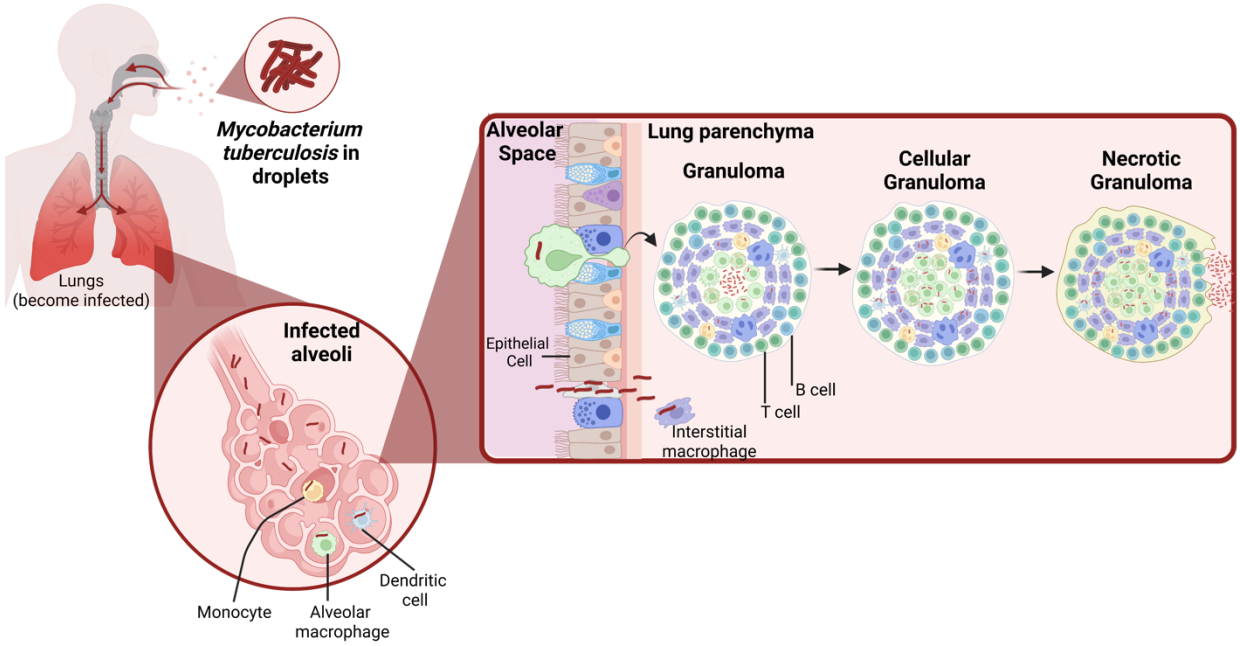


**Figure 1.2.** Stages of TB infection in the lung.

The latent stage of Mtb infection presents a large hurdle to developing treatments for TB, and necessitates the long treatment strategies currently prescribed as they help treat metabolically dormant Mtb which can persist intracellularly in various cell types, including macrophages, to reactivate later in life.[14,15] The challenges in treating TB are compounded by the cell wall architecture as they have a thick, waxy cell wall made up of complex lipids that causes low permeability, hindering the diffusion of hydrophilic drugs across the mycobacterial membrane and contributing to intrinsic antibiotic resistance.[16]

## The Importance of Iron

Iron is an essential micronutrient for almost all cell types as it is a vital component crucial for many cellular functions including the electron transport chain, drug detoxification, and oxygen transport.[17–19] Iron catalyzes these redox reactions by transitioning between its ferrous ($Fe^{2+}$) and ferric ($Fe^{3+}$) oxidation states.[20] While iron is highly abundant in the environment, host iron is tightly regulated and typically sequestered in proteins including transferrin or lactoferrin as free iron is toxic in its oxidized form.[17,21] The majority of the labile iron pool in humans is incorporated into heme and hemoglobin, or iron sulfur clusters, further limiting the availability of free iron.[21] Free iron is also largely insoluble in aqueous environments at a neutral pH as iron becomes oxidized to $Fe^{3+}$ in the presence of oxygen, which then forms insoluble ferric hydroxide.[18] This iron limited environment is exacerbated by the fact that macrophages utilize a multitude of mechanisms to further sequester iron as an antimicrobial defense mechanism, further limiting pools of iron available for Mtb.[17,18,22] Due to this lack of iron availability, Mtb has evolved multiple mechanisms to scavenge host iron.

**Siderophore-mediated Iron Uptake Pathways in Bacteria**

Many pathogenic bacteria have siderophore-mediated iron and heme uptake pathways. Both Gram-negative and Gram-positive bacteria have been shown to produce siderophores to scavenge and transport iron.[23–25] Bacterial siderophores are classified by their ferric iron-binding moieties including catecholates, carboxylates, hydroxamates, and phenolates which tend to form hexadentate, octahedral complexes with iron (Figure 1.3a).[23,26] Siderophores can be composed of a single type of iron-binding moiety such as enterobactin from *Escherichia coli* that contains catecholate moieties (Figure 1.3b), or can be of a mixed-type iron-binding moieties such as mycobactin from Mtb which has both hydroxamate and phenolate iron binding moieities (Figure 1.3b). Mtb actually synthesizes and secretes two siderophores: mycobactin and

carboxymycobactin that have different lengths and functional groups associated with their tail regions that lead to different localizations (Figure 1.3b).[26]

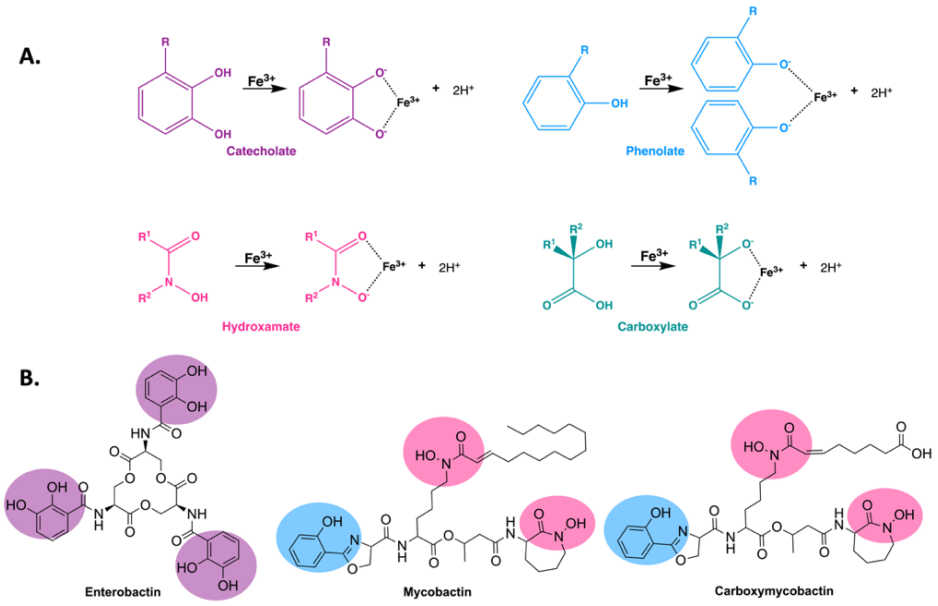


**Figure 1.3.** Overview of the diversity in siderophore structures. (A). There are four main moieties which confer siderophore iron-binding capacity: catecholate (purple), hydroxamate (pink), phenoloate (blue), and carboxylate (green). (B) *E. coli* and Mtb siderophores, enterobactin and mycobactin/carboxymycobactin, respectively, with the iron-binding moieties highlighted.

Other species of mycobacteria produce various mycobactins which share a similar iron-binding core, but have different derivatizations. *Mycobacterium smegmatis* and *Mycobacterium paratuberculosis* produce distinct siderophores mycobactin S and J, which are also coordinate iron via hydroxamate and phenolate moieties, but have slightly different R-groups incorporated.[18] *M. smegmatis*, and other nonpathogenic saprophytic mycobacteria, have also been shown to produce a third type of siderophore known as exochelin, which is formed by a formylated pentapeptide containing two hydroxamate groups key for iron binding.[27]

The most well-characterized siderophore-mediated iron uptake system in Gram-negative bacteria to date is that of *E. coli*. The siderophore, exochelin (Figure 1.3b), is synthesized in the

cytoplasm before being transported across the inner membrane and to the periplasmic space by an ATPase of the major facilitator superfamily (MFS, Figure 1.4).[28] The apo-siderophore is then exported to the extracellular space via TolC, a multifunctional efflux channel, with the aid of a periplasmic membrane fusion protein and resistance nodulation cell division (RND) transporter (Figure 1.4), where it can scavenge iron from host transferrin.[28,29] The ferric siderophore is then imported back across the outer membrane and to the periplasmic space via an outer membrane receptor (OMR) through a TonB-dependent mechanism (Figure 1.4).[30,31] A periplasmic binding protein then shuttles the ferric siderophore to an inner membrane ATP-binding cassette (ABC) permease which imports the siderophore to the cytoplasm where it is ultimately reduced by a ferric-siderophore reductase liberating ferrous iron for use by the cell and the apo siderophore is then recycled.[32–36] Interestingly, *E. coli* has evolved the ability to also utilize siderophores from other bacteria, such as ferrichrome from *Aspergillus sp.*, utilizing distinct receptors.[37] In contrast, siderophore-mediated iron uptake systems in Gram-positive bacteria are much less well described, but are known to be simplified due to the need to export and import siderophores across a single membrane. It has been shown that ferric siderophores are recognized by membrane-associated siderophore-binding proteins which facilitate delivery to a permease allowing for import to the cytoplasmic space, but the molecular mechanisms underlying this transport are not well characterized.[38,39]

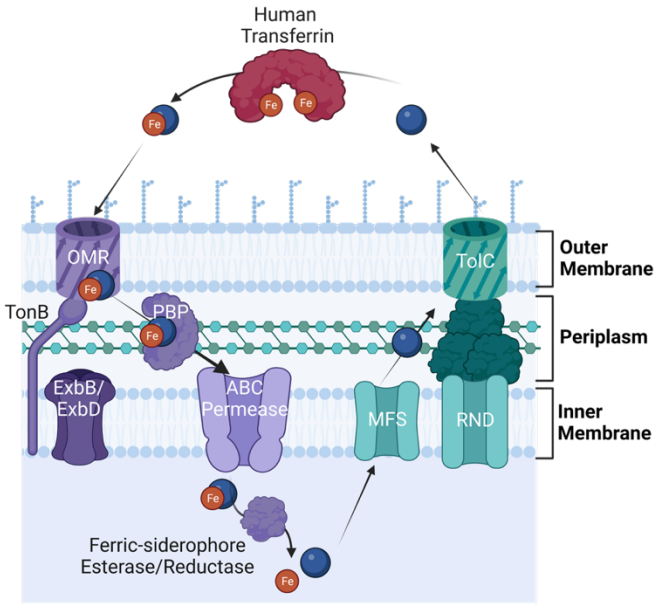


**Figure 1.4**. *E. coli* siderophore export and import mechanisms. The siderophore is the blue sphere, and the orange spheres are iron. Proteins involved in siderophore export are colored in green, while proteins involved in import of ferric-siderophores are colored in purple. In the cytoplasm, the ferric-siderophore esterase induces the release of iron from *E. coli* enterobactin by modification of the siderophore, whereas the ferric-siderophore reductase reduces the iron in non-*E. coli* siderophores to induce its release. In *E. coli*, siderophores are recycled.

## Heme Uptake Pathways in Bacteria

Heme uptake pathways have been discovered in both Gram-negative and Gram-positive bacteria. In Gram-negative bacteria, two main mechanisms of heme uptake have been described: 1) secretion of hemophores which can cleave hemoglobin releasing free heme for uptake by the bacteria (Figure 1.5c)[40–42], or 2) the bacteria produce heme receptors on their outer membranes which directly bind to heme or heme containing proteins such as hemoglobin or hemopexin (Figure 1.5a,b).[43–46] Once this heme has been bound at the outer membrane, it is imported via a TonB-dependent mechanism, transported across the periplasm by a periplasmic binding protein, and then imported across the inner membrane via an ABC permease (Figure 1.5).[44,47]

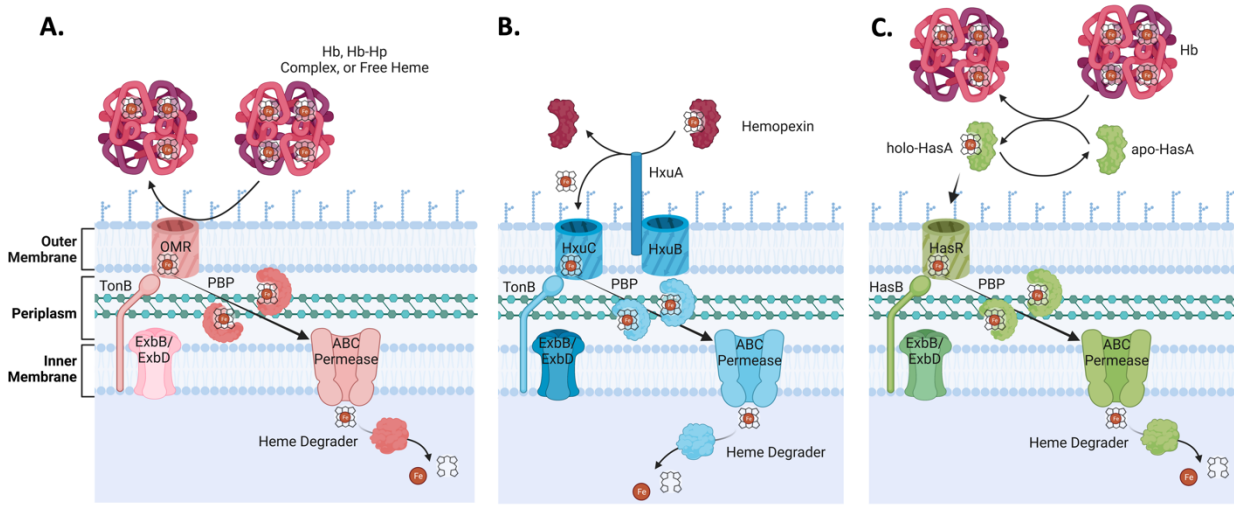


**Figure 1.5.** Heme uptake mechanisms in Gram-negative bacteria. Heme is acquired using an outer membrane receptor specific for either (A) heme-containing proteins such as hemoglobin (HB) or heme, (B) hemopexin, or (C) a secreted hemophore. Heme is transferred across the outer membrane in a TonB-dependent manner, before being shuttled to the inner membrane by a PBP, where an ABC permease translocates heme into the cytoplasm. Heme is then degraded by a cytosolic heme-degrading protein to release iron.

In Gram-positive bacteria, a sophisticated array of heme transport proteins is utilized instead which shuttles the heme across the cell wall environment to the cell membrane ABC transporter (Figure 1.6).[48–51] A feature conserved in Gram-positive heme uptake systems is the utilization of heme-uptake proteins containing a structurally conserved immunoglobulin-like NEAT domain.[52–55] These NEAT domains have been shown to act as cell-surface receptors (as in *S. aureus* IsdB and IsdH)[50,56,57], heme transporters (as in *S. aureus* IsdC and IsdA)[58,59], and have also been shown to function directly as hemophores (as in *B. anthracis* IsdX1).[48,60,61] Once the heme reaches the cytoplasm it is degraded to release iron by a cytosolic heme degrading enzyme (Figure 1.6).[26]

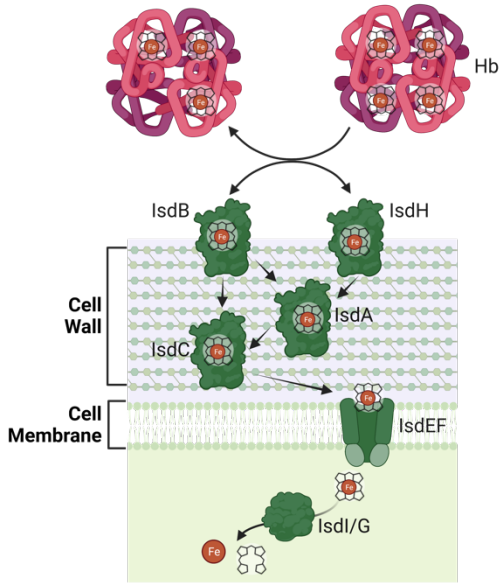


**Figure 1.6.** Heme uptake in Gram-positive *S. aureus*. Heme is acquired using cell-surface receptors that directly interact with and scavenge heme from Hb. Heme is then shuttled across the cell wall through a series of heme transporters via protein–protein interactions. Heme is finally translocated across the membrane using an ABC transporter and degraded via the IsdG-type heme degraders, IsdG and IsdI which are homologous to Mtb MhuD discussed in the next section, as well as Chapter 2.

**Iron Uptake Pathways in Mtb**

To acquire essential host iron, Mtb has both siderophore-mediated and heme-dependent iron uptake pathways (Figure 1.7).[62–67] The Mtb siderophore export (mycobactins) and import (ferric mycobactins) pathways have been quite well-studied; however, there is less known about the heme-uptake pathway as Mtb heme uptake is distinct from other bacteria as there is little to no homology with proteins involved in either Gram-positive or Gram-negative heme uptake systems.[26] For both of these pathways, the proteins involved in transport across the outer membrane, cell wall, and periplasm are poorly understood. Mtb has two predicted periplasmic binding proteins (PBPs), FecB and FecB2, that bear structural homology to known bacterial ferric siderophore and heme PBPs.[26] Previous data suggest that Mtb FecB and FecB2 could be involved in the transport of apo- and ferric-mycobactins or heme across the periplasm by transposon mutagenesis screens (FecB) and knockout studies (FecB2).[68,69]

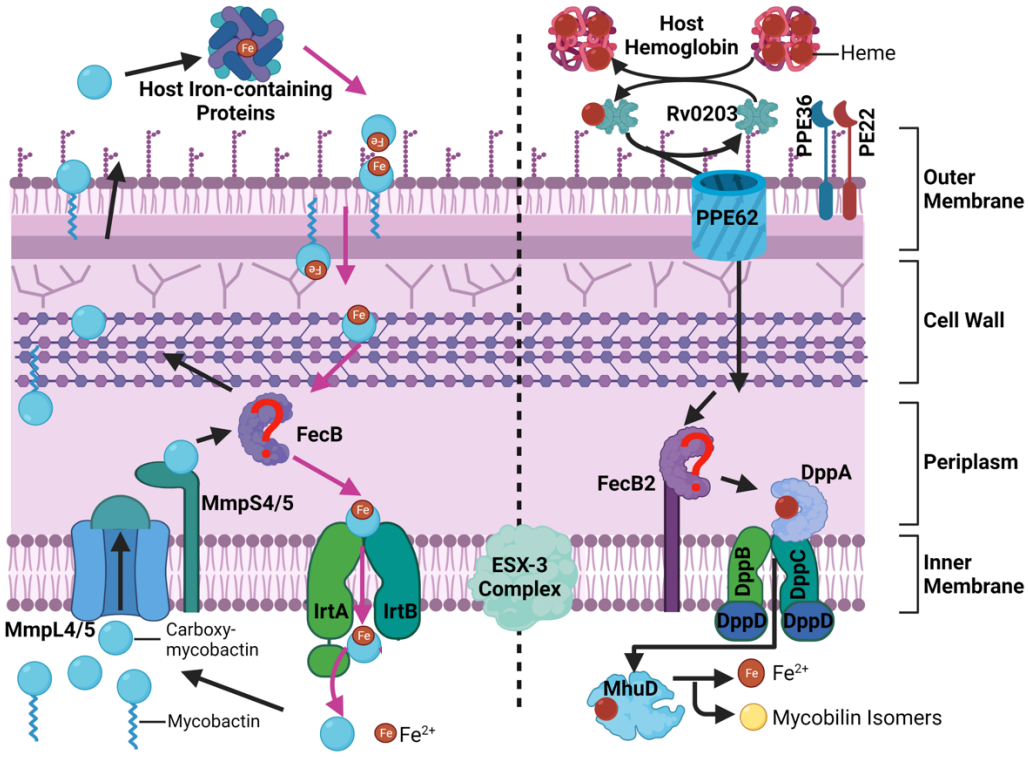


**Figure 1.7.** Proposed iron acquisition pathways in *Mycobacterium tuberculosis.*

As previously stated, Mtb has two mechanisms to acquire iron from its host: a siderophore-mediated pathway, as well as a heme-dependent iron uptake pathway, whereby the latter is the least understood of the two.[62–67] To-date, there is little to no overlap of proteins involved in these two iron acquisition pathways.[69] Notably, ESX-3, is thought to be involved in both iron and heme homeostasis, and perhaps regulation. ESX-3 is one of five Mtb Type VII secretion systems and forms an inner membrane complex, and not only is it involved in iron homeostasis but also the secretion of proteins (Figure 1.7).[70,71]

Mtb synthesizes two different types of siderophores: (1) a smaller hydrophilic siderophore, carboxymycobactin (cMB), which is thought to be exported to scavenge iron from host transferrin, and (2) a larger hydrophobic siderophore, mycobactin (MB), which is thought to anchor in the cell membrane or cell wall and facilitate iron transport from cMB (Figure 1.3b).[26,66] These mycobactins (both MB and cMB) are exported across the inner membrane by MmpL4/5 and their accessory

MmpS4/5 proteins. Once in the periplasmic space both cMB and MB are shuttled to the outer membrane (MB) or secreted into the extracellular space (cMB). It has been proposed that cMB can scavenge iron from the host iron binding proteins such as transferrin (Figure 1.7, Left Panel).[72,73] The ferric-cMB (Fe-cMB) complex is either imported across the outer membrane, or transfers its iron cargo to cell-surface receptors or cell-wall associated MBs for import into the periplasm (Figure 1.7, Left Panel).[67,74] The Fe-mycobactins are then shuttled across the periplasmic space through an unknown mechanism. Then Fe-cMB is imported across the inner membrane by the ABC-transporter complex IrtAB (Figure 1.7, Left Panel).[75] Once in the cytosol, Fe-cMB is reduced by the N-terminal domain of IrtA, which has been shown to be a ferric mycobactin reductase, to release ferrous iron into the cytosol and allowing cMB to be recycled for further rounds of iron uptake (Figure 1.7, Left Panel).[75,76]

Heme import is not well understood. However, cell surface exposed PE and PPE (named for their conservated proline and glutamic acid residues) have been implicated in heme utilization in mycobacteria. PPE36, PE22, and PPE62 are required for hemoglobin and heme utilization as knock-out studies showed either decreased growth (PPE62) or completely abolished growth (PPE36/PE22) when heme or hemoglobin were the sole iron sources.[68] Heme is believed to be sequestered from host hemoglobin and transferred to the surface proteins PPE36/PE22 or PPE62, possibly by the extracellular heme binding protein Rv0203, and then imported into the mycobacterium (Figure 1.7, Right Panel).[64,68,77] Studies suggest that heme is shuttled across the periplasmic space through an unknown mechanism to the inner-membrane tethered periplasmic protein DppA (Figure 1.7, Right Panel).[64] DppA transfers heme to the ABC-transporter DppBCD complex where it is transported into the cytosol and degraded by the cytosolic heme degrading protein MhuD into mycobilin isomers and ferrous iron (Figure 1.7, Right Panel).[64,78]

[798081,828326,84–86]The mechanisms of transport of mycobactins and heme across the periplasmic space are unknown. In other bacteria, there are PBPs that facilitate the transport of ferric-siderophores and heme through the periplasm.[87] In Mtb, there are two predicted ferric-mycobactin and/or heme PBPs, FecB and FecB2 (Rv3044 and Rv0265c, respectively).[87] FecB has been implicated in the mycobactin-mediated iron-uptake pathway as a genome-wide transposon mutagenesis study demonstrated that a *fecB* mutant showed a growth defect when cMB was the sole iron source and is the focus of Chapters 4 and 5.[69] FecB2 has been implicated in the heme uptake pathway as an Mtb *fecB2* deletion strain was shown to be resistant to gallium protoporphyrin IX toxicity, and had a growth defect when heme was the sole iron source.[68] However, notably, the Mtb *fecB2* deletion mutant also had attenuated growth in iron supplemented media indicating it is perhaps also involved in iron uptake.[68]

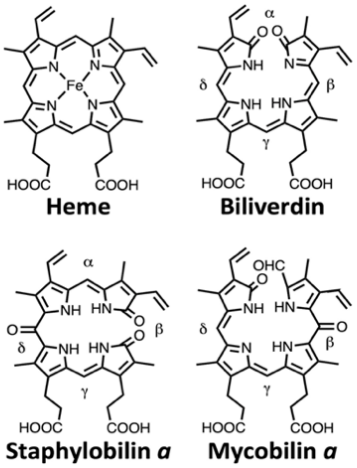


**Figure 1.8.** Structures of heme and heme degradation products. Including products from hHO-1 (BV), *S. aureus* IsdG/IsdI (staphylobilin), and MhuD (mycobilin).

Many pathogens utilize host heme as an iron source, these bacteria express cytosolic heme-degrading proteins to release iron. In Mtb, it has been shown that MhuD is required for normal growth *in vitro* when heme is the sole iron source.[88] In humans, heme degradation is carried out by the canonical human heme oxygenase (hHO-1). hHO-1 catalyzes the oxidative cleavage of heme and releases biliverdin IXα (αBV) (Figure 1.8), ferrous iron, and carbon monoxide.[89–91] HO-produced αBV is acquired and then converted to bilirubin by biliverdin reductase (BVR) in

mammals, and the fate of heme degradation products in bacteria are unknown.[92] Notably, hHO-1 and MhuD are distinct in their primary sequence, tertiary structure, product formation and mechanism of action (Figure 1.9).[93] In Mtb MhuD, like hHO-1, oxidative cleavage of heme occurs at the α-meso carbon, but it also performs an additional oxidation at either the β- or δ-meso carbon and shows no loss of a C1 product, resulting in the formation of two mycobilin isomers (Figure 1.8) and iron.[94,95] The fate of the mycobilin products is unknown, but it has been shown that the mycobilin analogue, αBV, binds with nanomolar affinity to MhuD.[96] Because of this high-affinity interaction, a mycobilin-sequestering protein is likely required for MhuD turnover. We hypothesize that, similar to hHO-1, MhuD product removal is achieved by one of the four Mtb BVR homologs (Rv1155, Rv2074, Rv2991, or Rv3547).[97–99] To date, two of these Mtb BVRs have been tested for αBV reductase activity; Rv2074 was shown to readily reduce αBV while Rv1155 does not, which suggests that Rv1155 may reduce mycobilin.[99] Thus, we investigated if one of the Mtb BVRs is potentially involved in MhuD product removal and processing in Chapter 3.[98,99]

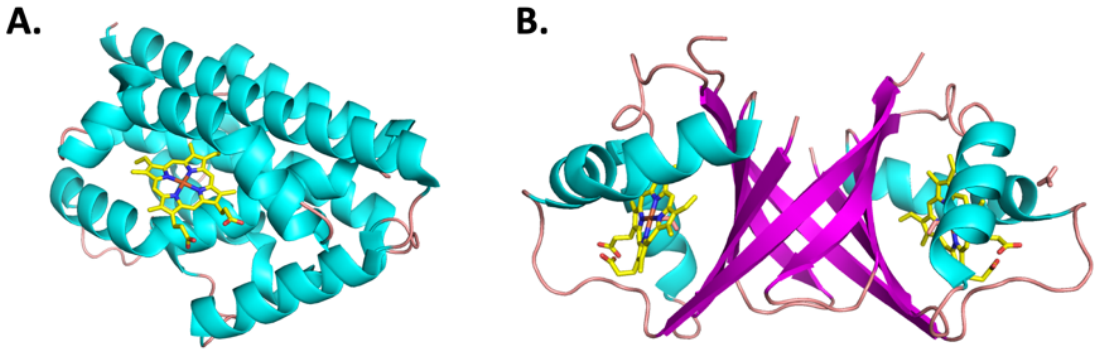


**Figure 1.9.** Comparison of crystal structures of heme degrading enzymes. A) Human heme oxygenase-heme complex (hHO-1, PDB: 1N3U, B), Mtb MhuD-heme-CN complex (PDB: 4NL5, are shown as cartoons with α-helices in cyan, β-sheets in pink, and loop regions in salmon.

## Conclusion

There have been extensive efforts to target iron acquisition pathways as a potential therapeutic strategy to treat Mtb infections. Strategies have utilized the toxic analogues of heme (gallium protoporphyrin IX) and free iron (gallium nitrate)[79], intracellular iron chelators[80], inhibitors of siderophore biosynthesis genes[81,82], and work is being done to design inhibitors of the import of ferric siderophores at the inner membrane adenosine triphosphace (ATP) binding cassette (ABC) permease IrtAB.[83] Due to these factors, new druggable protein targets are necessary for the development of novel anti-TB drugs. One such target is Mtb iron acquisition, as host-acquired iron is essential for its survival.[26,84–86] Further work is needed to fully characterize the heme and siderophore-mediated iron uptake pathways in Mtb so that inhibitors can be designed to target every step of the pathway to find the most efficacious strategy. The work presented herein takes strides towards filling in some these gaps in our knowledge of iron and heme acquisition pathways in Mtb.

As a graduate student, I have had the opportunity to utilize many tools to biochemically characterize proteins in both *in vitro* and *in vivo* contexts. Herein, I begin this dissertation probing the biological relevance of a novel secondary structure seen in the co-crystal complex of a MhuD variant in complex with its product (Chapter 2), then identify the novel Mtb mycobilin reductase activity of Rv2074 (Chapter 3), and finally demonstrate that FecB functions in iron export and potentially import (Chapters 4 and 5). Together, the work presented here has provided insights into how mycobilin is processed after MhuD-mediated heme degradation, and how mycobacterial siderophores are shuttled across the periplasmic space. This work has opened new avenues of research and provided templates for structure-guided inhibitor design to block iron acquisition, and ultimately kill the pathogen.

## References


1. World Health Organization. 2022 Global Tuberculosis Report. https://www.who.int/publications/i/item/9789240061729 (2022).
2. Roberts, L. How COVID is derailing the fight against HIV, TB and malaria. *Nature* **597**, 314 (2021).
3. Harding, E. WHO global progress report on tuberculosis elimination. *Lancet Respiratory Medicine* **8**, 19 (2020).
4. Centers for Disease Control. Treatment for TB disease. https://www.cdc.gov/tb/topic/treatment/tbdisease.htm#Drug-Susceptible (2022).
5. Russel, D. G. TB comes to a sticky beginning. *Nat Med* **7**, 894–895 (2001).
6. Ahmad, F. *et al.* Macrophage: a cell with many faces and functions in tuberculosis. *Front Immunol* **13**, 747799 (2022).
7. Davis, J. M. & Ramakrishnan, L. The role of the granuloma in expansion and dissemination of early tuberculous infection. *Cell* **136**, 37–49 (2009).
8. Humphreys, I. R. *et al.* A role for dendritic cells in the dissemination of mycobacterial infection. *Microbes Infect* **8**, 1339–1346 (2006).
9. Moule, M. G. & Cirillo, J. D. Mycobacterium tuberculosis dissemination plays a critical role in pathogenesis. *Front Cell Infect Microbiol* **10**, 65 (2020).
10. Ernst, J. D. The immunological life cycle of tuberculosis. *Nat Rev Immunol* **12**, 581–591 (2012).
11. Getahun, H., Matteelli, A., Chaisson, R. E. & Raviglione, M. Latent Mycobacterium tuberculosis Infection . *New England Journal of Medicine* **372**, 2127–2135 (2015).

12. Shan Chang, D. P. & Guan, X. L. Metabolic versatility of mycobacterium tuberculosis during infection and dormancy. *Metabolites* **11**, 88 (2021).

13. Nikitushkin, V. *et al.* Shotgun proteomic profiling of dormant, 'nonculturable' Mycobacterium tuberculosis. *PLoS One* **17**, e0269847 (2022).

14. Chandra, P., Grigsby, S. J. & Philips, J. A. Immune evasion and provocation by Mycobacterium tuberculosis. *Nat Rev Microbiol* **20**, 750–766 (2022).

15. Barry, C. E. *et al.* The spectrum of latent tuberculosis: Rethinking the biology and intervention strategies. *Nat Rev Microbiol* **7**, 845–855 (2009).

16. Jarlier, V. & Nikaido, H. Mycobacterial cell wall: Structure and role in natural resistance to antibiotics. *FEMS Microbiology Letters* vol. 123 11–18 Preprint at https://doi.org/10.1111/j.1574-6968.1994.tb07194.x (1994).

17. Ganz, T. & Nemeth, E. Iron homeostasis in host defence and inflammation. *Nat Rev Immunol* **15**, 500–510 (2015).

18. Ratledge, C. Iron, mycobacteria and tuberculosis. *Tuberculosis* **84**, 110–130 (2004).

19. Py, B. & Barras, F. Building Feg-S proteins: Bacterial strategies. *Nat Rev Microbiol* **8**, 436–446 (2010).

20. Ilbert, M. & Bonnefoy, V. Insight into the evolution of the iron oxidation pathways. *Biochim Biophys Acta Bioenerg* **1827**, 161–175 (2013).

21. Muckenthaler, M. U., Rivella, S., Hentze, M. W. & Galy, B. A red carpet for iron metabolism. *Cell* **168**, 344–361 (2017).

22. Piddington, D. L., Kashkouli, A. & Buchmeier, N. A. Growth of Mycobacterium tuberculosis in a defined medium is very restricted by acid pH and Mg 2 levels. *Infect Immun* **68**, 4518–4522 (2000).

23. Wilson, B. R., Bogdan, A. R., Miyazawa, M., Hashimoto, K. & Tsuji, Y. Siderophores in iron metabolism: from mechanism to therapy potential. *Trends Mol Med* **22**, 1077–1090 (2016).

24. Miethke, M. & Marahiel, M. A. Siderophore-based iron acquisition and pathogen control. *Microbiology and Molecular Biology Reviews* **71**, 413–451 (2007).

25. Saha, R., Saha, N., Donofrio, R. S. & Bestervelt, L. L. Microbial siderophores: A mini review. *J Basic Microbiol* **53**, 303–317 (2013).

26. Chao, A., Sieminski, P. J., Owens, C. P. & Goulding, C. W. Iron Acquisition in Mycobacterium tuberculosis. *Chemical Reviews* vol. 119 1193–1220 Preprint at https://doi.org/10.1021/acs.chemrev.8b00285 (2019).

27. Sharman, G. J., Williams, D. H., Ewingt, D. F. & Ratledgej, C. Isolation, purification and structure of exochelin MS, the extracellular siderophore from Mycobacterium smegmatis. *Biochem. J* **305**, 187–196 (1995).

28. Bleuel, C. *et al.* TolC is involved in enterobactin efflux across the outer membrane of Escheriia coli. *J Bacteriol* **187**, 6701–6707 (2005).

29. Horiyama, T. & Nishino, K. AcrB, AcrD, and MdtABC multidrug efflux systems are involved in enterobactin export in escherichia coli. *PLoS One* **9**, e108642 (2014).

30. Hua Zhou, X., van der Helm, D. & Adjimani, J. Purification of outer membrane iron transport receptors from Escherichia coli by fast protein liquid chromatography: FepA and FecA. *BioMetals* **6**, 25–35 (1993).

31. Liu, J., Rutzt, J. M., Feix, J. B. & Klebbatt, P. E. Permeability properties of a large gated channel within the ferric enterobactin receptor, FepA. *Proc. Natl. Acad. Sci. USA* **90**, 10653–10657 (1993).

32. Shea, C. M. & McIntosh, M. A. Nucleotide sequence and genetic organization of the ferric enterobactin transport system: homology to other peripiasmic binding protein-dependent systems in Escherichia coli. *Mol Microbiol* **5**, 1415–1428 (1991).

33. Miethke, M., Hou, J. & Marahiel, M. A. The siderophore-interacting protein YqjH acts as a ferric reductase in different iron assimilation pathways of escherichia coli. *Biochemistry* **50**, 10951–10964 (2011).

34. Piercet, J. R. & Earhart, C. F. Escherichia coli K-12 Envelope Proteins Specifically Required for Ferrienterobactin Uptake. *J Bacteriol* **166**, 930–936 (1986).

35. Stephens, D. L., Choe, M. D. & Earhart, C. F. Escherichia coli periplasmic protein FepB binds ferrienterobact in. *Microbiology (N Y)* **141**, 1647–1654 (1995).

36. Greenwood, K. T. & Luke, R. K. J. Enzymatic hydrolysis of enterochelin and its iron complex in Escherichia coli K-12. *Biochim Biophys Acta* **525**, 209–218 (1978).

37. Moeck, G. S., Coulton, J. W. & Postle, K. Cell envelope signaling in Escherichia coli: ligand binding to the ferricrhome-iron receptor FhuA promotes interaction with the energy-transducing protein TonB. *J Biol Chem* **272**, 28391–28397 (1997).

38. Grigg, J. C., Cooper, J. D., Cheung, J., Heinrichs, D. E. & Murphy, M. E. P. The Staphylococcus aureus siderophore receptor HtsA undergoes localized conformational changes to enclose staphyloferrin a in an arginine-rich binding pocket. *Journal of Biological Chemistry* **285**, 11162–11171 (2010).

39. Dale, S. E., Sebulsky, M. T. & Heinrichs, D. E. Involvement of SirABC in iron-siderophore import in Staphylococcus aureus. *J Bacteriol* **186**, 8356–8362 (2004).

40. Arnoux, P. *et al.* The crystal structure of HasA, a hemophore secreted by Serratia marcescens. *Nat Struct Biol* **6**, 516–520 (1999).

41. Cescau, S. *et al.* Heme acquisition by hemophores. *BioMetals* **20**, 603–613 (2007).

42. Izadi, N. *et al.* Purification and characterization of an extracellular heme-binding protein, HasA, involved in heme iron acquisition. *Biochemistry* **36**, 7050–7057 (1997).

43. Simpson, W., Olczak, T. & Genco, C. A. Characterization and expression of HmuR, a TonB-dependent hemoglobin receptor of Porphyromonas gingivalis. *J Bacteriol* **182**, 5737–5748 (2000).

44. Clarke, T. E., Tari, L. W. & Vogel, H. J. Structural Biology of Bacterial Iron Uptake Systems. *Curr Top Med Chem* **1**, 7–30 (2001).

45. Wong, J. C. Y. *et al.* Affinity, conservation, and surface exposure of hemopexin-binding proteins in Haemophilus influenzae. *Infect Immun* **63**, 2327–2333 (1995).

46. Whitby, P. W., Seale, T. W., VanWagoner, T. M., Morton, D. J. & Stull, T. L. The iron/heme regulated genes of Haemophilus influenzae: Comparative transcriptional profiling as a tool to define the species core modulon. *BMC Genomics* **10**, (2009).

47. Contreras, H., Chim, N., Credali, A. & Goulding, C. W. Heme uptake in bacterial pathogens. *Curr Opin Chem Biol* **19**, 34–41 (2014).

48. Ekworomadu, M. C. T. *et al.* Differential function of lip residues in the mechanism and biology of an anthrax hemophore. *PLoS Pathog* **8**, (2012).

49. Skaar, E. P., Humayun, M., Bae, T., Debord, K. L. & Schneewind, O. Iron-source preference of Staphylococcus aureus infections. *Science (1979)* **305**, 1626–1628 (2004).

50. Grigg, J. C., Vermeiren, C. L., Heinrichs, D. E. & Murphy, M. E. P. Haem recognition by a Staphylococcus aureus NEAT domain. *Mol Microbiol* **63**, 139–149 (2007).

51. Gat, O. *et al.* Characterization of Bacillus anthracis iron-regulated surface determinant (Isd) proteins containing NEAT domains. *Mol Microbiol* **70**, 983–999 (2008).

52. Sheldon, J. R. & Heinrichs, D. E. Recent developments in understanding the iron acquisition strategies of gram positive pathogens. *FEMS Microbiol Rev* **39**, 592–630 (2015).

53. Nobles, C. L. & Maresso, A. W. The theft of host heme by Gram-positive pathogenic bacteria. *Metallomics* **3**, 788–796 (2011).

54. Grigg, J. C., Ukpabi, G., Gaudin, C. F. M. & Murphy, M. E. P. Structural biology of heme binding in the Staphylococcus aureus Isd system. *J Inorg Biochem* **104**, 341–348 (2010).

55. Tong, Y. & Guo, M. Bacterial heme-transport proteins and their heme-coordination modes. *Arch Biochem Biophys* **481**, 1–15 (2009).

56. Kumar, K. K. *et al.* Structural basis for hemoglobin capture by Staphylococcus aureus cell-surface protein, IsdH. *Journal of Biological Chemistry* **286**, 38439–38447 (2011).

57. Torres, V. J., Pishchany, G., Humayun, M., Schneewind, O. & Skaar, E. P. Staphylococcus aureus IsdB is a hemoglobin receptor required for heme iron utilization. *J Bacteriol* **188**, 8421–8429 (2006).

58. Zhu, H. *et al.* Pathway for heme uptake from human methemoglobin by the iron-regulated surface determinants system of Staphylococcus aureus. *Journal of Biological Chemistry* **283**, 18450–18460 (2008).

59. Liu, M. *et al.* Direct hemin transfer from IsdA to IsdC in the iron-regulated surface determinant (Isd) heme acquisition system of Staphylococcus aureus. *Journal of Biological Chemistry* **283**, 6668–6676 (2008).

60. Honsa, E. S., Maresso, A. W. & Highlander, S. K. Molecular and evolutionary analysis of NEAr-Iron Transporter (NEAT) domains. *PLoS One* **9**, e104794 (2014).

61. Honsa, E. S., Fabian, M., Cardenas, A. M., Olson, J. S. & Maresso, A. W. The five near-iron transporter (NEAT) domain anthrax hemophore, IsdX2, scavenges heme from hemoglobin and transfers heme to the surface protein IsdC. *Journal of Biological Chemistry* **286**, 33652–33660 (2011).

62. Jones, C. M. & Niederweis, M. Mycobacterium tuberculosis can utilize heme as an iron source. *J Bacteriol* **193**, 1767–1770 (2011).

63. Tullius, M. V. *et al.* Discovery and characterization of a unique mycobacterial heme acquisition system. *Proc Natl Acad Sci U S A* **108**, 5051–5056 (2011).

64. Mitra, A., Ko, Y. H., Cingolani, G. & Niederweis, M. Heme and hemoglobin utilization by Mycobacterium tuberculosis. *Nat Commun* **10**, (2019).

65. Sritharan, M. Iron homeostasis in Mycobacterium tuberculosis: Mechanistic insights into siderophore-mediated Iron uptake. *Journal of Bacteriology* vol. 198 2399–2409 Preprint at https://doi.org/10.1128/JB.00359-16 (2016).

66. Choudhury, M. *et al.* Iron uptake and transport by the carboxymycobactin-mycobactin siderophore machinery of Mycobacterium tuberculosis is dependent on the iron-regulated protein HupB. *BioMetals* **34**, 511–528 (2021).

67. Ratledge, C. Iron, mycobacteria and tuberculosis. in *Tuberculosis* vol. 84 110–130 (Churchill Livingstone, 2004).

68. Mitra, A., Speer, A., Lin, K., Ehrt, S. & Niederweis, M. PPE surface proteins are required for heme utilization by Mycobacterium tuberculosis. *mBio* **8**, (2017).

69. Zhang, L. *et al.* Comprehensive analysis of iron utilization by Mycobacterium tuberculosis. *PLoS Pathog* **16**, (2020).

70. Tufariello, J. A. M. *et al.* Separable roles for Mycobacterium tuberculosis ESX-3 effectors in iron acquisition and virulence. *Proc Natl Acad Sci U S A* **113**, E348–E357 (2016).

71. Serafini, A., Pisu, D., Palù, G., Rodriguez, G. M. & Manganelli, R. The ESX-3 Secretion System Is Necessary for Iron and Zinc Homeostasis in Mycobacterium tuberculosis. *PLoS One* **8**, (2013).

72. Wells, R. M. *et al.* Discovery of a Siderophore Export System Essential for Virulence of Mycobacterium tuberculosis. *PLoS Pathog* **9**, (2013).

73. Jones, C. M. *et al.* Self-poisoning of Mycobacterium tuberculosis by interrupting siderophore recycling. *Proc Natl Acad Sci U S A* **111**, 1945–1950 (2014).

74. Gobin, J. *et al.* Iron acquisition by Mycobacterium tuberculosis: Isolation and characterization of a family of iron-binding exochelins. *Proceedings of the National Academy of Sciences* **92**, 5189–5193 (1995).

75. Arnold, F. M. *et al.* The ABC exporter IrtAB imports and reduces mycobacterial siderophores. *Nature* **580**, 413–417 (2020).

76. Ryndak, M. B., Wang, S., Smith, I. & Rodriguez, G. M. The Mycobacterium tuberculosis high-affinity iron importer, IrtA, contains an FAD-binding domain. *J Bacteriol* **192**, 861–869 (2010).

77. Owens, C. P., Du, J., Dawson, J. H. & Goulding, C. W. Characterization of heme ligation properties of Rv0203, a secreted heme binding protein involved in mycobacterium tuberculosis heme uptake. *Biochemistry* **51**, 1518–1531 (2012).

78. Chim, N., Iniguez, A., Nguyen, T. Q. & Goulding, C. W. Unusual Diheme Conformation of the Heme-degrading Protein from Mycobacterium tuberculosis. *J Mol Biol* **395**, 595–608 (2010).

79. Choi, S. R., Switzer, B., Britigan, B. E. & Narayanasamy, P. Gallium porphyrin and gallium nitrate synergistically inhibit mycobacterial species by targeting different aspects of iron/heme metabolism. *ACS Infect Dis* **6**, 2582–2591 (2020).

80. Dragset, M. S. *et al.* A novel antimycobacterial compound acts as an intracellular iron chelator. *Antimicrob Agents Chemother* **59**, 2256–2264 (2015).

81. Mori, M. *et al.* Synthesis and assessment of the in vitro and ex vivo activity of salicylate synthase (Mbti) inhibitors as new candidates for the treatment of mycobacterial infections. *Pharmaceuticals* **15**, (2022).

82. Ferguson, L. *et al.* Integrated target-based and phenotypic screening approaches for the identification of anti-tubercular agents that bind to the mycobacterial adenylating enzyme MbtA. *ChemMedChem* **14**, 1735–1741 (2019).

83. Ingale, P., Lad, B., Kabra, R. & Singh, S. Dissecting druggability of ABC transporter proteins in Mycobacterium species through network modeling. *J Biomol Struct Dyn* **40**, 8365–8374 (2022).

84. Pandey, M., Talwar, S., Bose, S. & Pandey, A. K. Iron homeostasis in Mycobacterium tuberculosis is essential for persistence. *Sci Rep* **8**, (2018).

85. Cassat, J. E. & Skaar, E. P. Iron in infection and immunity. *Cell Host and Microbe* vol. 13 509–519 Preprint at https://doi.org/10.1016/j.chom.2013.04.010 (2013).

86. De Voss, J. J., Rutter, K., Schroeder, B. G. & Barry Iii, C. E. *Iron Acquisition and Metabolism by Mycobacteria*. *JOURNAL OF BACTERIOLOGY* vol. 181 (1999).

87. Chu, B. C. H. & Vogel, H. J. A structural and functional analysis of type III periplasmic and substrate binding proteins: Their role in bacterial siderophore and heme transport.

*Biological Chemistry* vol. 392 39–52 Preprint at https://doi.org/10.1515/BC.2011.012 (2011).

88. Contreras, H. *et al.* Characterization of a Mycobacterium tuberculosis nanocompartment and its potential cargo proteins. *Journal of Biological Chemistry* **289**, 18279–18289 (2014).

89. Tenhunen, R., Marver, H. S. & Schmidt, R. Microsomal Heme Oxygenase, Characterization of the Enzyme. *J Biol Chem* **244**, 6388–6394 (1969).

90. Yoshida, T., Noguchi, M. & Kikuchi, G. Oxygenated Form of Heme, Heme Oxygenase Complex and Requirement for Second Electron to Initiate Heme Degradation from the Oxygenated Complex. *J Biol Chem* **255**, 4418–4420 (1980).

91. Matsui, T., Masaki, U. & Masao, I. S. Heme oxygenase reveals Its strategy for catalyzing three successive oxygenation reactions. *Acc Chem Res* **43**, 240–247 (2010).

92. Mantle, T. J. Haem degradation in animals and plants Bilin reduction in plants. *Biochemical Society Trasactions* **30**, 630–633 (2002).

93. Wilks, A. & Ikeda-Saito, M. Heme utilization by pathogenic bacteria: Not all pathways lead to biliverdin. *Acc Chem Res* **47**, 2291–2298 (2014).

94. Nambu, S., Matsui, T., Goulding, C. W., Takahashi, S. & Ikeda-Saito, M. A New Way to Degrade Heme: The Mycobacterium tuberculosis Enzyme MhuD Catalyzes Heme Degradation without Generating CO. *Journal of Biological Chemistry* **288**, 10101–10109 (2013).

95. Thakuri, B. *et al.* The Affinity of MhuD for Heme is Consistent with a Heme Degrading Function in vivo. *Metallomics* **10**, 1560–1563 (2018).

96. Chao, A. *et al.* Structure of a Mycobacterium tuberculosis Heme-Degrading Protein, MhuD, Variant in Complex with Its Product. *Biochemistry* **58**, 4610–4620 (2019).

97. Maines, M. & Trakshel, G. M. Purification and characterization of human biliverdin reductase. *Arch Biochem Biophys* **300**, 320–326 (1993).

98. Ahmed, F. H. *et al.* Sequence-Structure-Function Classification of a Catalytically Diverse Oxidoreductase Superfamily in Mycobacteria. *J Mol Biol* **427**, 3554–3571 (2015).

99. Ahmed, F. H. *et al.* Rv2074 is a Novel F420H2-dependent Biliverdin Reductase in Mycobacterium tuberculosis. *Protein Science* **25**, 1692–1709 (2016).

# CHAPTER 2

# Investigating the Biological Importance of the $^{75}$HisXXXArg$^{79}$ Motif in IsdG-like Heme Degrading Enzymes


## Abstract

Heme degradation to release free iron is one mechanism many pathogenic bacteria utilize to acquire necessary iron from their host. In a recent study from our lab, the first product-bound structure of an IsdG-like heme degrading enzyme revealed a novel secondary structural element, alpha-helix 3(α3), was formed. This α3 helix includes the $^{75}$HisXXXArg$^{79}$ motif. To probe the relevance of this motif, as well as to investigate other active site residues, we investigated changes in heme binding and degradation by the R79S, and T55A variants of MhuD. The $^{75}$HisXXXArg$^{79}$ motif is conserved in IsdI and IsdG, so we generated and investigated the binding affinity of IsdI for α-, β-, and δ-biliverdin to determine a suitable product analogue to be able to probe if the formation of α3 is also conserved in product-bound structures of other IsdG-like enzymes.


## Introduction

Many pathogens utilize host heme as an iron source for various processes such as cell signaling, antioxidant defense, and iron reutilization.[1–3] The most well-studied enzyme which catabolizes heme is the canonical human heme oxygenase (hHO-1), which generates biliverdin IXα (αBV, Figure 2.1a), ferrous iron, and the one-carbon (C1) product carbon monoxide (CO) via the oxidative cleavage of heme.[4–6] Homologs of hHO-1 are also found in some prokaryotes including the pathogens *Corynebacterium diphtheriae*, *Pseudomonas aeruginosa*, and *Neisseria meningitidis* as well as in other eukaryotes.[7–11] HO-produced αBV is acquired and then converted to bilirubin by biliverdin reductase (BVR), which is then conjugated with glucuronic acid and ultimately excreted in eukaryotes.[12,13] Comparatively, we know very little about the fates of HO-

produced biliverdin (BV) isomers in prokaryotes; although, in *P. aeruginosa* it has been shown that the BV isomers produced by HemO, the HO homolog, is excreted without further reduction via an unknown mechanism.[14]

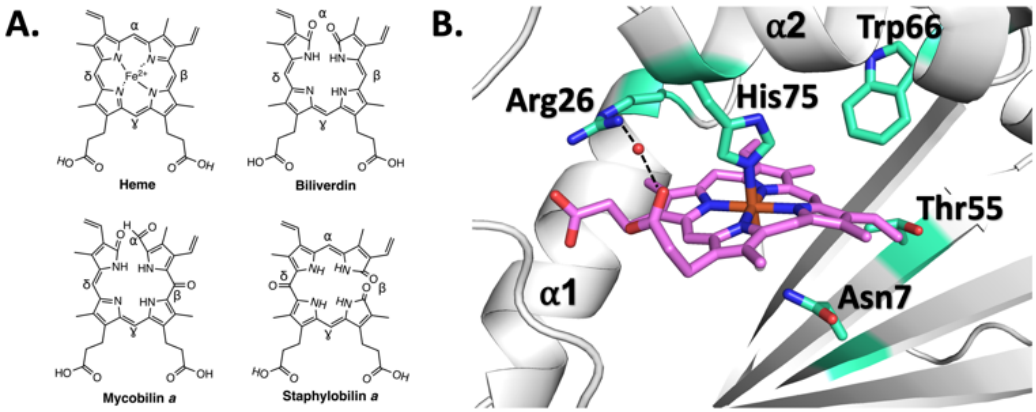


**Figure 2.1.** Structures of heme degradation products and WT-MhuD-monoheme active site. (A) Structure of heme and heme tetrapyrrole degradation products. (B) Structure of the active site of MhuD (cartoon, white), in its cyano-derivatized monoheme form (sticks, pink). Depicted in stick representation (green) are essential Asn7, Trp66, and His75 (which coordinates heme-iron) residues, Arg26 that forms a water-mediated H-bond with one of the heme propionates, and Thr55 which interacts with one of the heme vinyl groups.

There are many families of heme oxygenases, one of which is the iron surface determinant G (IsdG)-type family which is found mainly in Gram-positive bacteria whose members are distinct from canonical HO's in both sequence and structure.[15–17] This family was named for the *Staphylococcus. aureus* heme-degrading enzymes IsdG and IsdI, which were the first members to be characterized.[16,17] These enzymes cleave and oxidize heme at the β- and δ-meso carbon sites to produce staphylobilin isomers (Figure 2.1a), free iron, and formaldehyde rather than degrading heme to BV, iron, and CO as seen in canonical HO's.[18,19] Other IsdG-type enzymes include MhuD from *Mycobacterium tuberculosis* (Mtb) and LFO1 from eukaryotic *Chlamydomonas reinhardtii*, which also degrade heme into unique products.[15,20] While the products of LFO1 heme degradation have yet to be determined,[20] MhuD degrades heme into free iron and mycobilin isomers (Figure 2.1a).[21] Like staphylobilins, the mycobilin isomers are also oxidized at the β- or δ-meso carbons;

however, cleavage occurs at the α-meso carbon with no observed loss of a C1 product.[21] The lack of a C1 product may be of physiological importance, as the CO byproduct of hHO-1 is one of the signals for Mtb to transition from its active to latent state.[21] The fate of the mycobilin products, and those produced by other IsdG-type enzymes, are unknown; however, they may serve in an antioxidant role similar to BV.[22]

The structures of HO and IsdG-type proteins are distinct. HOs are predominately monomeric, comprised of a single α-helical domain (Figure 2.2a),[23] while IsdG-type proteins consist of a homodimeric β-barrel decorated with two α-helices from each subunit (Figure 2.2b,c).[17,24] Unsurprisingly, the two distinct classes of heme-degrading enzymes utilize different mechanisms to degrade heme.[25] Although heme is coordinated by a proximal His residue in both HO and IsdG-type enzymes, the heme molecule in HOs is nearly planar, while the heme is ruffled for IsdG-type proteins.[17,23] Furthermore, HOs have a distal pocket with a network of ordered water molecules, which facilitates the three consecutive monooxygenase steps required for heme degradation.[4] In contrast, the distal heme pocket is quite hydrophobic for IsdG-type proteins, with only one or two ordered waters observed in the proximal pocket.[17,24] In MhuD, it has been proposed that the hydrophobic pocket and the ruffled heme both contribute to the sequential monooxygenase and dioxygenase steps required for MhuD to degrade heme.[25]

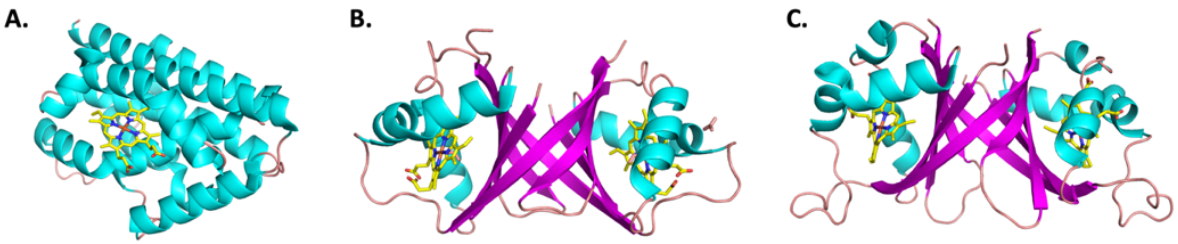


**Figure 2.2.** Comparison of crystal structures of heme degrading enzymes. Human heme oxygenase-heme complex (hHO-1, PDB: 1N3U, A), Mtb MhuD-heme-CN complex (PDB: 4NL5, B), and IsdI-heme complex (PDB: 3LGM, C) are shown as cartoons with α-helices in cyan, β-sheets in pink, and loop regions in salmon.

The structures of both human and *C. diphtheriae* HO complexed with αBV illustrate that the HO heme degradation reaction is coupled with a conformational change from a "closed" to an "open" state.[26,27] In the eukaryotic and prokaryotic HO structures, the open product-bound state results from relaxation of the distal and proximal α-helices, and a rotation of the catalytic His side chain out of the active site pocket, as it is no longer coordinated to heme-iron.[26,27] This structural shift suggests that a degree of protein flexibility is necessary among the HO homologues to facilitate catalysis. Structures of apo and monoheme-bound forms of IsdG-type proteins reveal an analogous conformational change in the catalytic His residue, as it is absent or disordered in the apo structures; however, the ordering of the elongated L2 loop region upon heme binding results in a much more drastic conformational shift compared with those of the canonical HOs (apo-MhuD; PDB code: 5UQ4).[17,24,28] Furthermore, unlike other IsdG-type proteins studied to date, MhuD is exceptionally flexible with its active site, capable of accommodating two molecules of heme, resulting in enzyme inactivation.[15,24] The biological significance of this conformational plasticity and its role in product turnover are not well understood as there is no structure of an IsdG-type enzyme in its product-bound form.

The structure of an IsdG-type protein in complex with its heme degradation product would further our understanding of the mechanism of action of this protein family. Unfortunately, the staphylobilin and mycobilin products of IsdG-type proteins are difficult to purify,[19,21] which has presumably hindered the structural determination of the product-bound form. Recently, we demonstrated that a MhuD variant, MhuD-R26S, upon heme degradation produces αBV, formaldehyde, and iron.[29] In a recent study, we determined the affinity of wild-type (WT) MhuD and the MhuD-R26S variant for both heme and αBV and show they both bind heme and αBV in the nanomolar range.[30] This high affinity for αBV allows the utilization of the MhuD-R26S variant

as a proxy to study IsdG-type proteins in complex with their product, and will be further discussed. Upon determining the crystal structure of the MhuD-R26S−αBV complex, we observed the formation of a novel secondary structural element that has not been seen in previous structures of MhuD bound to the substrate, heme (Figure 2.3), and its implications are the focus of this section.

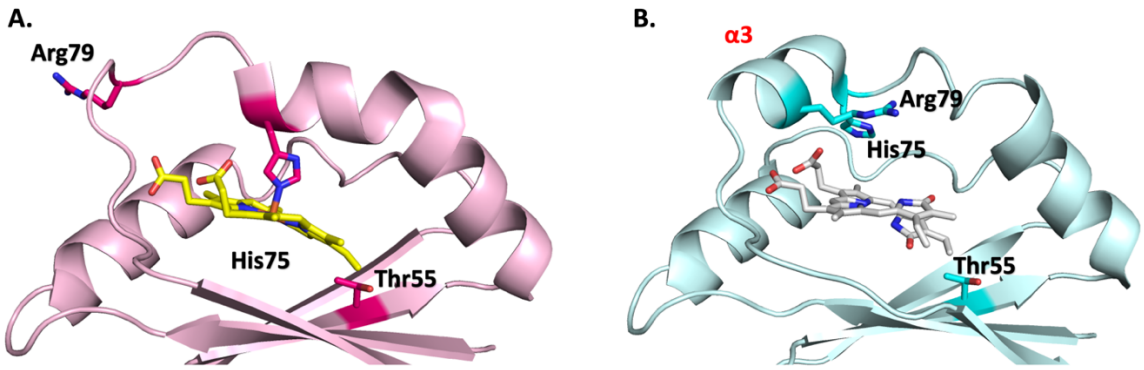


**Figure 2.3.** Comparison of MhuD-monoheme-CN complex (PDB: 4NL5, A) and MhuD-R26S-αBV complex (PDB: 6PLE, B). Residues Arg79 (stabilizes formation of novel α3 helix), His75 (coordinates the iron in the heme bound structure), and Thr55 (is adjacent to the heme vinyl groups) are displayed as sticks.

## Materials and Methods

### *Reagents and Materials*

To avoid contamination of BV isomers during extraction and HPLC separation, only HPLC-grade reagents and solvents were used (Fisher). Similar precautions for the IMS-QToF/MSe validation were taken, and LC-MS grade solvents were used for solubilization and direct injection (Fisher). Specific media, column, and instrument information is listed below where pertinent.

### *Protein Expression and Purification*

Generation of MhuD Variants, Expression and Purification of WT MhuD and Mutants

Site directed mutagenesis using MhuD-T55A-fwd (5’ – CGC TAC TTC GTG GTG GCA CAC TGG GAG TCC GAT - 3’) and MhuD-T55A-rev (5’ – ATC GGA CTC CCA GTG TGC

CAC CAC GAA GTA GCG - 3') primers was used to introduce the T55A mutation. The MhuD R79S construct was produced via site directed mutagenesis using primers MhuD-R79S-fwd (5' – GCC CAT GCC GGA CAC TCA GCC AAC CCC GTG GCG - 3') and MhuD-R79S-rev (5' – CGC CAC GGG GTT GGC TGA GTG TCC GGC ATG GGC- 3'). WT-MhuD, R26S, T55A, and R79S variants were purified as previously reported.[30] Briefly, the expression plasmids were transformed into *E. coli* BL21-Gold(DE3) cells (Agilent, Santa Clara, CA), and were grown in LB media supplemented with 100 μg/mL ampicillin at 37 °C overnight. Growths were then sub-cultured into fresh medium and grown to an $OD_{600}$ of ~0.6 before protein expression was induced by the addition of IPTG (1 mM). Cell growth was continued for 4 h post-induction before the cells were harvested by centrifugation and stored at -80°C. Cells were lysed by sonication on ice in lysis buffer (50 mM Tris-HCl pH 7.4, 350 mM NaCl, 10 mM imidazole) containing 100 μM PMSF and hen egg white lysozyme at 45% amplitude, 15 seconds on 45 seconds off, for 20 cycles. The crude cell lysate was then centrifuged at 14,000 rpm for 1 hour before being filtered with a 0.2 μm filter (Minisart Plus, Sartorius). The clarified lysate was loaded onto a HisTrap FF column (5 mL, GE Healthcare) and washed with lysis buffer. Bound protein was eluted from the column with increasing concentrations of imidazole using an AKTA Start FPLC. Fractions found to contain MhuD by SDS-PAGE analysis (expected MW ~11 kDa) were pooled and dialyzed against 50 mM Tris-HCl pH 7.4, 150 mM NaCl, overnight at 4 °C.

Expression and Purification of IsdI

IsdI was purified as previously reported.[16] Briefly, the expression plasmids were transformed into *E. coli* BL21-Gold(DE3) cells (Agilent, Santa Clara, CA), and were grown in LB media supplemented with 100 μg/mL ampicillin at 37 °C overnight. Growths were then sub-cultured into fresh medium and grown to an $OD_{600}$ of ~0.6 before protein expression was induced

by the addition of IPTG (1 mM). Cell growth was continued for 3 h post-induction before the cells were harvested by centrifugation and stored at -80°C. Cells were lysed by sonication on ice in lysis buffer (50 mM Tris-HCl pH 7.4, 150 mM NaCl, 10 mM imidazole) containing 100 μM PMSF and hen egg white lysozyme at 45% amplitude, 15 seconds on 45 seconds off, for 20 cycles. The crude cell lysate was then centrifuged at 14,000 rpm for 1 hour before being filtered with a 0.2 μm filter (Minisart Plus, Sartorius). The clarified lysate was loaded onto a HisTrap FF column (5 mL, GE Healthcare) and washed with lysis buffer. Bound protein was eluted from the column with increasing concentrations of imidazole using an AKTA Start FPLC. Fractions found to contain IsdI by SDS-PAGE analysis (expected MW ~13 kDa) were pooled and dialyzed against 50 mM Tris-HCl pH 7.4, 150 mM NaCl, overnight at 4 °C.

***Heme Degradation Experiments***

Preparation of MhuD-monoheme

Reconstitution of MhuD-WT and its mutants with heme was achieved as previously described.[29] Briefly, a hemin solution was prepared by dissolving 4-6 mg of heme in 500 μL of 0.1 M NaOH and incubating for 30 minutes. After the addition of 500 μL of 1 M Tris/HCl, pH 7.4, the solution was centrifuged at 15,000 rpm for 15 minutes. The supernatant was then diluted into 15 mL of 50 mM Tris-HCl pH 7.4, 150 mM NaCl and the concentration was determined by UV/Vis ($\varepsilon_{385}$ = 58.44 $mM^{-1}$ $cm^{-1}$ ). Heme was gradually titrated into 100 μM apo-MhuD to a 0.9 heme: 1.0 protein ratio. The samples were incubated overnight at 4°C before being passed through a desalting column to remove unbound heme. Protein concentrations of the eluted samples was determined via UV/Vis ($\varepsilon_{405}$ = 91.5 $mM^{-1}$ $cm^{-1}$ ).

Single turnover heme degradation assays

Single turnover heme degradation assays of 5 or 10 μM MhuD-monoheme were performed in 50 mM Tris-HCl, pH 7.4, 150 mM NaCl as previously described.[29] To eliminate the possibility of non- enzymatic heme degradation, 2.5 μM catalase from *Aspergillus niger* (Sigma-Aldrich) was added to each reaction. The heme degradation reaction was initiated with 10 mM sodium ascorbate and the reaction was monitored spectrophotometrically (DU800, Beckman Coulter) for an hour with scans taken at 5-minute intervals.

***Generation of Biliverdin Isomers***

Chemical cleavage of heme

BV isomers were generated by the ascorbic acid-induced oxidation of heme as described in private communication with the Wilks lab at the University of Maryland, Baltimore. Twenty five mg of heme was dissolved in 100 mL of pyridine before being diluted with water (3:1 water: pyridine). Oxygen was bubbled through the solution with vigorous stirring at 37 °C for 20 minutes. Chemical cleavage was induced by the addition of 4 mM L-ascorbic acid and stirred an additional 3 minutes. The reaction then was removed from heat and acidified by the addition of citric acid to a pH of 4-5. Biliverdin isomers were then extracted into 100 mL of cold chloroform, then washed 5 times with 100 mL 500 mM citric acid, 3 times with water, then residual water was removed with sodium sulfate and the chloroform layer was dried and the crude isomer mixture was stored at -80 °C.

HPLC separation of biliverdin isomers

Dried BV crude mixture aliquots were purified as described in private communication with the Wilks lab at the University of Maryland, Baltimore. Dried aliquots were resuspended in 36% acetonitrile (ACN):0.1% formic acid (FA) and centrifuged at 15,000 rpm for 15 minutes to remove any insoluble particulates. The BV isomers were than separated by HPLC (Beckman Coulter,

System Gold) on a Synergi 4 μm Hydro-RP 80 Å C18 Column (250 × 4.6 mm, Phenomenex) at a flow rate of 3 mL/min. The mobile phase consisted of Solvent A: Water:0.1% FA, and Solvent B: ACN:0.1% FA. A linear gradient was run starting at 36% B and ending at 100% B over 15 minutes. BV isomer retention times were 10.78 minutes, 11.54 minutes, and 12.00 minutes for the α-, δ-, and β-BV isomers, respectively. HPLC fractions were then analyzed by mass spectrometry using direct-injection IMS-QToF/MSe mass spectrometry (Synapt G2, Waters). The injection was performed in 80% $H_2O$, 0.1% FA:20% ACN, and data acquisition was done at high energy with a transfer collision energy ramp from 15-45 V with a mass range of 50-2000 Da acquired in continuum. Separated isomers were then dried, and stored at -80 °C.

***Fluorescence titrations***

Fluorescence quenching titrations of BV isomers were performed as described previously.[30] Stock solutions of IsdI (100 nM), α-biliverdin (αBV, 500 μM), β-biliverdin (βBV, 10 μM) and δ-biliverdin (δBV, 10 μM) were prepared in 50 mM Tris-HCl pH 7.4, 150 mM NaCl. Biliverdin was added in the following titration series: 2 x 1 μL, 4 x 2 μL, 4 x 5 μL, 3 x 10 μL, and 2 x 20 μL injections. In between each titration the solution was incubated for 3 minutes with stirring at 200 rpm at 20 °C before fluorescence spectra were acquired between 300 – 500 nm using a Hitachi F-4500 Fluorescence Spectrophotometer through excitation at 285 nm with the following settings: PMT voltage of 700 V, excitation slit width of 10 nm, emission slit width of 10 nm, and a scan speed of 240 nm/min.

Fluorescence emission spectral analysis

Results from the fluorescence-based assay were fit to Eqn. 1 derived from Conger et al,[31] to determine the equilibrium dissociation-constant ($K_d$) of the biliverdin isomers with IsdI.

*Eqn. 1*:

$$F = \frac{([IsdI] + [ligand] + K_d) - \sqrt{([IsdI] + [ligand] + K_d)^2 - 4[IsdI][ligand]}}{2} \times \left(\frac{F_{min} - F_{max}}{[IsdI]}\right) + F_{max}$$

In Eqn. 1, [IsdI] is the total concentration of IsdI, [ligand] is the total concentration of biliverdin isomer, $F_{max}$ is the emission intensity without ligand, and $F_{min}$ is the emission intensity for fully ligand-bound IsdI. Fitting of the fluorescence emission intensity at 325 nm for $K_d$ determination was performed using GraphPad Prism (Ver 9.3.1).

## Results

### *Investigations into MhuD Oligomeric State in Solution*

When the structure of the MhuD-R26S−αBV complex was determined, the asymmetric unit was found to contain five stacked αBV molecules that link individual subunits from two adjacent, biologically relevant homodimers (2.4a).[30] To determine if the αBV bridge between homodimers is biologically relevant we used size exclusion chromatography to determine the oligomeric state of the MhuD-R26S-αBV complex in solution, which was confirmed to be a dimer (Figure 2.4b).

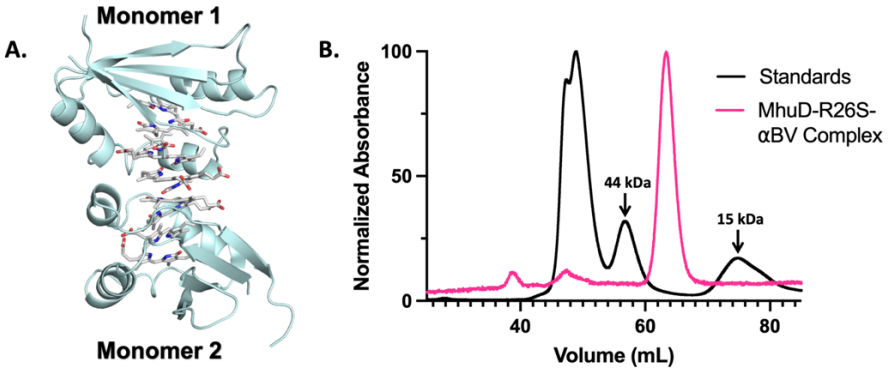


**Figure 2.4.** MhuD R26S-BV is a dimer in solution. A) The crystal structure of MhuD-R26S-αBV complex (PDB: 6PLE) showing two monomers from adjacent homodimers (cartoon, light green) with five stacked αBV molecules (sticks, white). B) Size exclusion chromatography (S75, HiLoad, 16/600) of the MhuD+αBV complex (red trace) and protein standards (black trace, Bio-Rad), which clearly demonstrates that the MhuD-R26S+αBV complex elutes as a dimer (~25 kDa).

***Investigations into Heme Degradation of R79S and T55A MhuD Variants***

From the MhuD-R26S-αBV structure, we see that R79 plays a key role in stabilizing the formation of α-helix 3 by forming hydrogen-bond interactions with backbone atoms (Figure 2.3b).[30] T55 interacts with one of the vinyl groups of the bound heme molecule (Figure 2.3a), and could play a role in ruffling of heme in the active site by repelling the nonpolar vinyl group. To investigate the importance of these residues upon heme binding and degradation, mutants were generated by site-directed mutagenesis. Heme was added at a 0.9:1 ratio of heme: protein before desalting to remove any unbound heme and analyzed by UV/Vis (Figure 2.5a,c solid lines). These spectra indicate that there is a difference in the way the R79S variant coordinates the heme as the Soret peak shifts from ~402 nm in the WT MhuD to ~407 nm in the R79S mutant (Figure 2.5d). Furthermore, the Q-bands at 560 and 608 nm are shifted in the R79S mutant which supports the observation that the heme is coordinated differently (Figure 2.5e). Interestingly, the T55A variant also seems to have a small effect on the way heme is coordinated as compared to WT as the Soret peak shifts by 1 nm and Q-band peaks are less well defined (Figure 2.5b). After initiation of heme degradation the UV/Vis spectra (Figure 2.5d,e dashed lines) show that the R79S mutant lacks the ~560 nm peak seen in WT, and the T55A mutant shows a new peak forming at 647 nm which indicate these variants of MhuD could form different products as seen in the R26S variant (Figure 2.5a,b).[29] When the change in absorbance at the Soret peak of MhuD-heme (~405 nm) is monitored against time, it appears that R79S and T55A degrade heme at a different rate than that of WT; however, as these experiments have only been carried out once, further investigation is required.

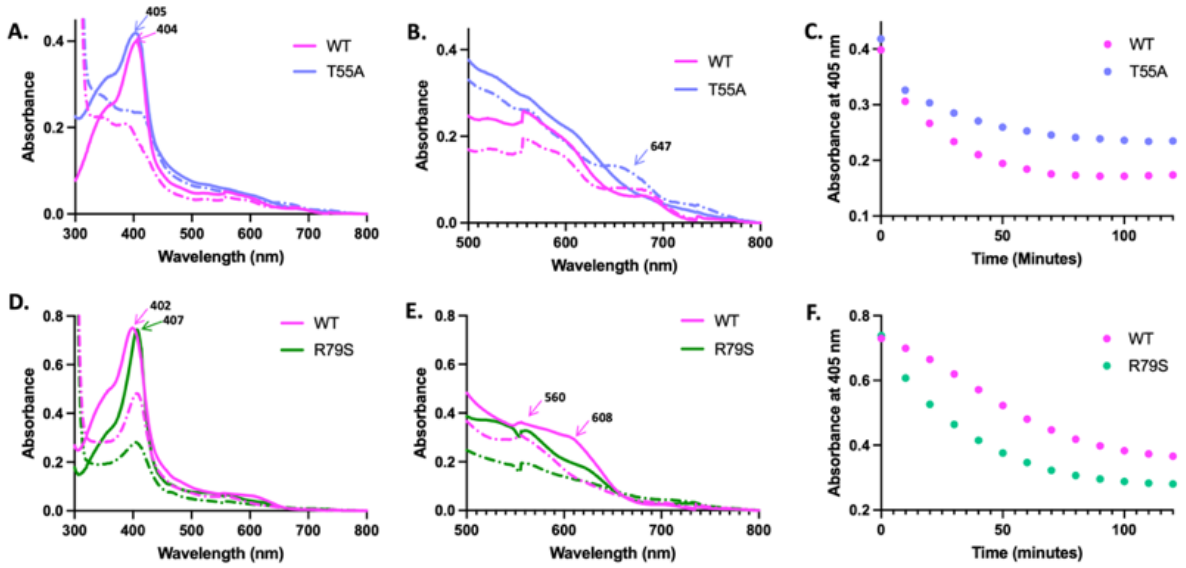


**Figure 2.5.** UV/vis spectroscopy of single turn-over heme degradation of R79S and T55A variants of MhuD. A), and D) show representative spectra before (solid lines) and after (dashed lines) the addition of 10 mM sodium ascorbate to 5 μM T55A and 10 μM R79S MhuD-mediated heme degradation reactions, respectively (with WT at corresponding concentrations for comparison). B) and E) are 5X zoomed in views on the region of 500-800 nm to highlight features in the Q-band regions. C) and F) show the change in absorbance at 405 nm vs. time for T55A and R79S, respectively.

### *Generation and Purification of BV Isomers*

In an effort to determine a suitable product analogue for IsdI, we utilized tryptophan fluorescence quenching assays on α-, β-, and δ-BV isomers which required the generation of BV isomers as only αBV is commercially available. Chemical cleavage of heme using ascorbic acid generates predominantly α-, β-, and δ-BV isomers.[32] Due to this lack of specificity in isomer generation, the isomers then require further purification. All three BV isomers were produced and separated by HPLC (Figure 2.6b), and fractions were analyzed for isomer purity by IMS-QToF/MSe (Fig 2.6c) as the isomers of BV generate distinct fragmentation ions (Figure 2.6a).

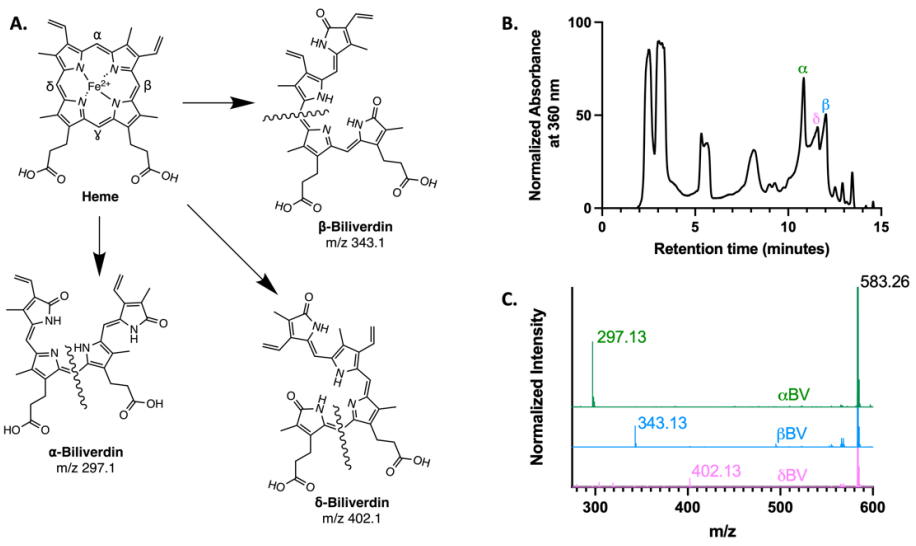


**Figure 2.6.** HPLC purification and mass spectrometry analyses of biliverdin IX isomers. A) Fragmentation patterns of dominant isomers of biliverdin generated by chemical heme cleavage. B) HPLC chromatogram of BV isomers with α-, δ-, and βBV eluting at 10.78 minutes, 11.54 minutes, and 12.00 minutes, respectively. C) IMS-QToF/MSe of purified HPLC fractions.

### *Determining IsdI Specificity for BV Isomers*

Previously, the affinity ($K_d$) of IsdI for heme was measured to be ~13 nM.[33] In MhuD, another IsdG-like heme degrading enzyme, it has been shown that MhuD binds its product analogue (αBV) with high affinity (~30 nM) allowing for a co-crystal structure to be solved.[30] To determine if BV isomers could be used in a similar capacity in IsdI crystallographic experiments, we utilized tryptophan fluorescence quenching assays to determine the affinity of IsdI for α-, β-, and δ-BV. Interestingly, αBV binds to IsdI with the weakest affinity (6.09 ± 0.68 μM, Figure 2.7a) while the β- and δBV isomers bound with ~200-fold tighter affinities of 33.6 ± 5.1 nM (Figure 2.7b) and 30.5 nM (Figure 2.7c), respectively. It is important to note, the affinity for δBV is calculated from a single run as the chemical heme cleavage produced far less of this isomer.

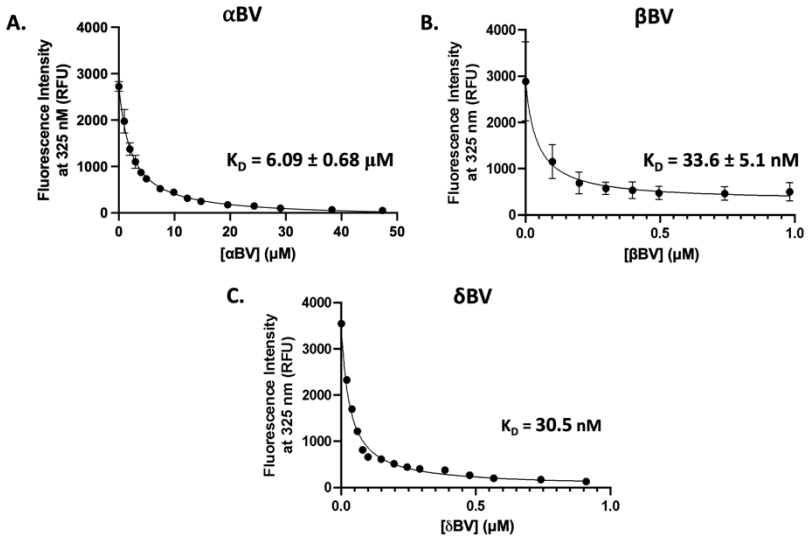


**Figure 2.7.** Affinities of α-, β- and δBV for IsdI. Representative fluorescence emission intensities at 340 nm after excitation at 280 nm of IsdI with increasing concentrations of A) αBV, B) βBV, and C) δBV (Note: data in panel C is from a single run).

## Discussion

Currently the fate of the heme degradation products generated by IsdG-like proteins (MhuD, IsdI, IsdG) are unknown; however, it has been shown that removal of the tetrapyrrole products requires protein denaturation.[19,21] Previous work in the Goulding lab has shown that both the substrate and product analogue of MhuD bind with very high affinities in the low nanomolar range. Therefore, displacement of the product would require high concentrations of substrate which do not typically occur physiologically because free heme is cytotoxic.[31,34] Due to this, we hypothesize that either large conformational changes upon product formation occur, or protein-protein interactions facilitate the removal of these products.

Our lab solved the product-bound co-crystal structure of a variant of MhuD, R26S, which generates αBV as its product.[30] Interestingly, in this structure the asymmetric unit was found to contain five stacked αBV molecules that link individual subunits from two adjacent, biologically relevant homodimers (Figure 2.4a).[30] To determine if this linkage of homodimers is biologically

relevant we used size exclusion chromatography to determine the oligomeric state of the MhuD-R26S-αBV in solution, which was confirmed to be a dimer (Figure 2.4b). This indicates that the stacked biliverdin molecules observed in the structure were a crystallographic artifact and not biologically relevant.

In the structure of the MhuD-R26S-αBV complex, the formation of the novel structural element, α-helix 3 (α3), alters the surface electrostatic potential which could facilitate protein-protein interactions to aid in product removal. Protein–protein interaction-induced product removal is reminiscent of hHO-1 BV removal. Human BVR has been shown to interact with hHO-1, as the rate of product removal from hHO-1 is increased in the presence of BVR and direct binding was observed by fluorescence titration studies.[35] Furthermore, it has been shown that BVR and P450 reductase have competitive binding due to overlapping binding residues on the surface of hHO-1, indicating a potential regulatory mechanism based on the concentrations of these two proteins.[35] This protein-protein interaction between hHO-1 and BVR increases the catalytic rate of hHO-1 by promoting removal of the product BV to further reduce it to bilirubin.[35,36] This novel α-helix in MhuD is formed by the $^{75}$HisXXXArg$^{79}$ motif, which is conserved in the *S. aureus* IsdG-like proteins IsdI and IsdG (Figure 2.8).[30]

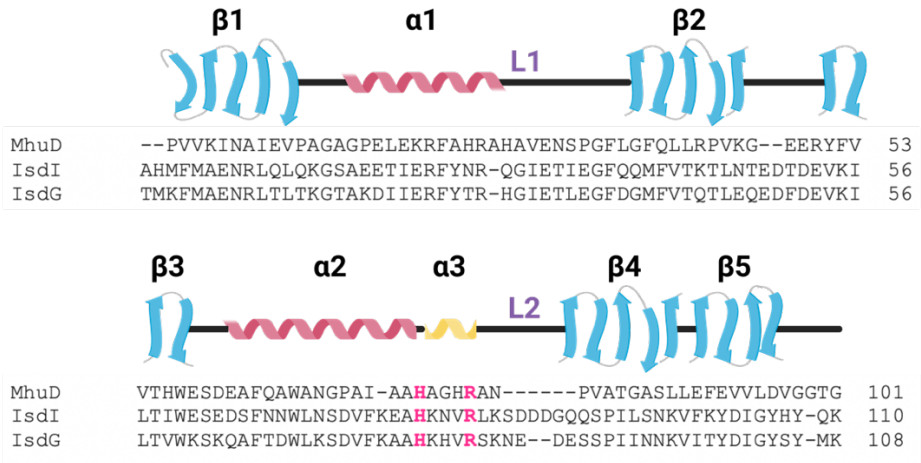


**Figure 2.8.** Structure-based alignment of protein sequences for Mtb MhuD, and *S. aureus* IsdI and IsdG. Secondary structural elements (blue arrows are β-strands, pink helices are α-helices) are based on the WT MhuD-monoheme crystal structure (PDB: 4NL5), apart from the yellow helix which is the novel α-3 helix formed in the MhuD-R26S-αBV structure. The key residues of the $^{75}$HXXXR$^{79}$ motif are labelled in pink.

To further probe the importance of this motif, we generated an R79S variant and examined its ability to bind and turn over heme. R79 was investigated as α-helix 3 is stabilized by R79 moving into the active site vicinity, whereby R79 is a residue previously unresolved in the heme-bound and apo-MhuD structures.[15,24] Interestingly, the Soret peak of MhuD red-shifts 5 nm from 402 to 407 nm in the R79S mutant as compared to wild-type (Figure 2.5d). Furthermore, the Q-band region also red-shifts to slightly higher wavelengths which indicates that the heme is more ruffled in the R79S variant.[37,38] Increases in heme ruffling by more than 1 Å cause a red shift in the Soret and Q-band regions by disrupting **π**-bonding within the porphyrin ring of heme.[37,38] This increase in ruffling is unexpected, as R79 is in a solvent-exposed loop region when heme is bound (Figure 2.3). Disrupting this loop with the R79S mutation could be perturbing the active site leading to the changes in ruffling observed; however, further investigations are required to probe any changes in heme binding caused by this amino acid substitution. Another residue, T55, was similarly investigated by forming a T55A variant. In this variant, there is a slight (1 nm) blue-shift of the Soret peak and the distinct Q-band peaks are lost, indicating a decrease in the heme ruffling

(Figure 2.5a,b).[37,38] This supports our hypothesis that T55 is increasing heme ruffling by repulsive forces on the nearby vinyl group of heme, but further experiments are needed to probe this. Furthermore, T55A degrades heme less completely (Figure 2.5c), and a new peak at 647 nm forms after degradation is complete (Figure 2.5b), which could indicate a non-mycobilin product is being formed.[29,39] In experiments with MhuD and IsdG, previous research has shown that the ruffling of heme is necessary for generation of the mycobilin and staphylobilin products, respectively.[38,39] When mutations cause decreases in ruffling, the major product instead shifts to αBV for these enzymes, and the rate of reaction decreases, and increases in ruffling cause the opposite effect.[38,39] These data suggest that the conserved $^{75}$HisXXXArg$^{79}$ motif is likely physiologically relevant as the loss of R79 causes perturbation of the heme in the active site, and formation of this secondary structural element may also be a conserved mechanism to promote product removal in IsdG-like proteins, therefore we seek to generate a structure of IsdI in complex with a product analogue to validate this hypothesis.

Staphylobilin and mycobilin share similar chemical structures, both of which share an additional oxidation even at the β- or δ-meso-carbon but staphylobilin cleaves at the δ- or β-meso-carbon opposite the oxidation rather than at the α-position as seen in mycobilin (Figure 2.1a). Much like myxobilin, staphylobilin is difficult to produce and purify, we sought instead to identify a suitable BV isomer to utilize as a product analogue. We generated BV isomers using chemical heme cleavage in which chemical oxidation of heme yields predominantly α-, β-, and δBV isomers (Figure 2.6a).[40] These isomers were than separated by HPLC to yield pure β- and δBV isomers as they are not commercially available (Figure 2.6b,c). These isomers were then tested for their affinity to IsdI utilizing tryptophan fluorescence quenching titration assays to determine if any bound with the sub-micromolar affinity amenable to co-crystallography experiments.

Interestingly, αBV was found to have the weakest affinity for IsdI at 6.09 ± 0.68 μM, while both β- and δBV had must tighter binding of 33.6 ± 5.1 nM and 30.5 nM, respectively (Figure 2.7 a-c). This low nanomolar affinity is in the same order of magnitude of the affinity of MhuD for αBV.[30] This higher affinity of β- and δBV is not unexpected, as IsdI cleaves heme at the β- or δ-meso-carbon when generating staphylobilins, therefore these corresponding isomers of BV are close chemical analogues to the natural product of IsdI (Figure 2.1a). The chemical cleavage of heme requires the use of harsh chemicals such as chloroform and pyridine, and generates predominantly αBV, which has hindered efforts to generate sufficient quantities of β- or δBV required for crystallography.[32] New techniques which leverage the *P. aeruginosa* heme degrading enzyme, HemO, which generates only β- and δBV coupled with a specialized *E. coli* system with upregulated heme importers (*E. coli* Nissle T7) have been shown to generate higher yields of β- and δBV which will allow for generation of greater quantities of these isomers to use for crystallographic experiments.[32] Given our results, and the conservation of $^{75}$HisXXXArg$^{79}$ in other IsdG-type proteins, we hypothesize that α-helix 3 formation may be a common structural feature among all product-bound IsdG-type proteins that facilitates protein–protein interactions to promote product egress.

## References


1. Doré, S. *et al.* Bilirubin, Formed by Activation of Heme Oxygenase-2, Protects Neurons Against Oxidative Stress Injury. *Neurobiology* **96**, 2445–2450 (1999).
2. Brouard, S. *et al.* Carbon Monoxide Generated by Heme Oxygenase 1 Suppresses Endothelial Cell Apoptosis. *Journal of Experimental Medicine* **192**, 1015–1026 (2000).
3. Ferris, C. D. *et al.* Haem Oxygenase-1 Prevents Cell Death by Regulating Cellular Iron. *Nat Cell Biol* **1**, 152–157 (1999).
4. Matsui, T., Masaki, U. & Masao, I. S. Heme Oxygenase Reveals Its Strategy for Catalyzing Three Successive Oxygenation Reactions. *Acc Chem Res* **43**, 240–247 (2010).
5. Yoshida, T., Noguchi, M. & Kikuchi, G. Oxygenated Form of Heme, Heme Oxygenase Complex and Requirement for Second Electron to Initiate Heme Degradation from the Oxygenated Complex. *J Biol Chem* **255**, 4418–4420 (1980).
6. Tenhunen, R., Marver, H. S. & Schmidt, R. Microsomal Heme Oxygenase, Characterization of the Enzyme. *J Biol Chem* **244**, 6388–6394 (1969).
7. Schmitt, M. P. Utilization of Host Iron Sources by Corynebacterium diphtheriae: Identification of a Gene Whose Product Is Homologous to Eukaryotic Heme Oxygenases and Is Required for Acquisition of Iron from Heme and Hemoglobin. *J Bacteriol* **179**, 838–845 (1997).
8. Wilks, A. & Schmitt, M. P. Expression and Characterization of a Heme Oxygenase (HmuO) from Corynebacterium diphtheriae. *J Biol Chem* **273**, 837–841 (1998).
9. Zhu, W., Wilks, A. & Stojiljkovic, I. Degradation of Heme in Gram-Negative Bacteria: the Product of the hemO Gene of Neisseriae Is a Heme Oxygenase. *J Bacteriol* **182**, 6783–6790 (2000).

10. Ratliff, M., Zhu, W., Deshmukh, R., Wilks, A. & Stojiljkovic, I. Homologues of Neisserial Heme Oxygenase in Gram-negative bacteria: Degradation of Heme by the Product of the pigA Gene of Pseudomonas aeruginosa. *J Bacteriol* **183**, 6394–6403 (2001).

11. Wilks, A. Heme Oxygenase: Evolution, Structure, and Mechanism. *Antioxid Redox Signal* **4**, 603–614 (2002).

12. Mantle, T. J. Haem Degradation in Animals and Plants, Bilin Reduction in Plants. *Biochem Soc Trans* **30**, 630–633 (2002).

13. Noguchi, M., Yoshida, T. & Kikuchi, G. Specific Requirement of NADPH-cytochrome c Reductase for the Microsomal Heme Oxygenase Reaction Yielding Biliverdin IXα. *FEBS Lett* **98**, 281–284 (1979).

14. Barker, K. D., Barkovits, K. & Wilks, A. Metabolic Flux of Extracellular Heme Uptake in Pseudomonas aeruginosa is Driven by the Iron-regulated Heme Oxygenase (hemO). *Journal of Biological Chemistry* **287**, 18342–18350 (2012).

15. Chim, N., Iniguez, A., Nguyen, T. Q. & Goulding, C. W. Unusual Diheme Conformation of the Heme-degrading Protein from Mycobacterium tuberculosis. *J Mol Biol* **395**, 595–608 (2010).

16. Skaar, E. P., Gaspar, A. H. & Schneewind, O. IsdG and IsdI, Heme-degrading Enzymes in the Cytoplasm of Staphylococcus aureus. *Journal of Biological Chemistry* **279**, 436–443 (2004).

17. Wu, R. *et al.* Staphylococcus aureus IsdG and IsdI, Heme-degrading Enzymes with Structural Similarity to Monooxygenases. *Journal of Biological Chemistry* **280**, 2840–2846 (2005).

18. Matsui, T. *et al.* Heme Degradation by Staphylococcus aureus IsdG and IsdI Liberates Formaldehyde Rather than Carbon Monoxide. *Biochemistry* **52**, 3025–3027 (2013).

19. Reniere, M. L. *et al.* The IsdG-family of Haem Oxygenases Degrades Haem to a Novel Chromophore. *Mol Microbiol* **75**, 1529–1538 (2010).

20. Lojek, L. J. *et al.* Chlamydomonas reinhardtii LFO1 Is an IsdG Family Heme Oxygenase. *mSphere* **2**, e00176-17 (2017).

21. Nambu, S., Matsui, T., Goulding, C. W., Takahashi, S. & Ikeda-Saito, M. A New Way to Degrade Heme: The Mycobacterium tuberculosis Enzyme MhuD Catalyzes Heme Degradation without Generating CO. *Journal of Biological Chemistry* **288**, 10101–10109 (2013).

22. Vanella, L. *et al.* The Non-canonical Functions of the Heme Oxygenases. *Oncotarget* **7**, 69075–69086 (2016).

23. Schuller, D. J., Wilks, A., Ortiz de Montellano, P. R. & Poulos, T. L. Crystal Structure of Human Heme Oxygenase-1. *Nat Struct Biol* **6**, (1999).

24. Graves, A. B. *et al.* Crystallographic and Spectroscopic Insights into Heme Degradation by Mycobacterium tuberculosis MhuD. *Inorg Chem* **53**, 5931–5940 (2014).

25. Matsui, T. *et al.* Unique Coupling of Mono- and Dioxygenase Chemistries in a Single Active Site Promotes Heme Degradation. *Proc Natl Acad Sci U S A* **113**, 3779–3784 (2016).

26. Unno, M., Ardèvol, A., Rovira, C. & Ikeda-Saito, M. Structures of the Substrate-free and Product-bound Forms of HmuO, a Heme oxygenase from Corynebacterium diphtheriae: X-ray Crystallography and Molecular Dynamics Investigation. *Journal of Biological Chemistry* **288**, 34443–34458 (2013).

27. Lad, L. *et al.* Crystal Structure of Human Heme Oxygenase-1 in a Complex with Biliverdin. *Biochemistry* **43**, 3793–3801 (2004).

28. Woo, C. L., Reniere, M. L., Skaar, E. P. & Murphy, M. E. P. Ruffling of Metalloporphyrins Bound to IsdG and IsdI, Two Heme-degrading Enzymes in Staphylococcus aureus. *Journal of Biological Chemistry* **283**, 30957–30963 (2008).

29. Chao, A. & Goulding, C. W. A Single Mutation in the Mycobacterium tuberculosis Heme-Degrading Protein, MhuD, Results in Different Products. *Biochemistry* **58**, 489–492 (2019).

30. Chao, A. *et al.* Structure of a Mycobacterium tuberculosis Heme-Degrading Protein, MhuD, Variant in Complex with Its Product. *Biochemistry* **58**, 4610–4620 (2019).

31. Thakuri, B. *et al.* The Affinity of MhuD for Heme is Consistent with a Heme Degrading Function in vivo. *Metallomics* **10**, 1560–1563 (2018).

32. Robinson, E. A., Frankenberg-Dinkel, N., Xue, F. & Wilks, A. Recombinant Production of Biliverdin IXβ and δ Isomers in the T7 Promoter Compatible Escherichia coli Nissle. *Front Microbiol* **12**, (2021).

33. Conger, M. A., Pokhrel, D. & Liptak, M. D. Tight Binding of Heme to Staphylococcus aureus IsdG and IsdI Precludes Design of a Competitive Inhibitor. *Metallomics* **9**, 556–563 (2017).

34. Larsen, R., Gouveia, Z., Soares, M. P. & Gozzelino, R. Heme Cytotoxicity and the Pathogenesis of Immune-mediated Inflammatory Diseases. *Front Pharmacol* **3**, (2012).

35. Wang, J. & Ortiz de Montellano, P. R. The binding sites on human heme oxygenase-1 for cytochrome P450 reductase and biliverdin reductase. *Journal of Biological Chemistry* **278**, 20069–20076 (2003).

36. Maines, M. D. & Trakshel, G. M. Purification and Characterization of Human Biliverdin Reductase. *Arch Biochem Biophys* **300**, 320–326 (1993).

37. Graves, A. B., Graves, M. T. & Liptak, M. D. Measurement of Heme Ruffling Changes in MhuD Using UV-vis Spectroscopy. *Journal of Physical Chemistry B* **120**, 3844–3853 (2016).

38. Schuelke-Sanchez, A. E., Cornetta, A. R., Kocian, T. A. J., Conger, M. A. & Liptak, M. D. Ruffling is essential for Staphylococcus aureus IsdG-catalyzed degradation of heme to staphylobilin. *J Inorg Biochem* **230**, 111775 (2022).

39. Thakuri, B., O'Rourke, B. D., Graves, A. B. & Liptak, M. D. A Dynamic Substrate is Required for MhuD-Catalyzed Degradation of Heme to Mycobilin. *Biochemistry* **60**, 918–928 (2021).

40. Evans, J. P., Niemevz, F., Buldain, G. & de Montellano, P. O. Isoporphyrin Intermediate in Heme Oxygenase Catalysis: Oxidation of α-Meso-phenylheme. *Journal of Biological Chemistry* **283**, 19530–19539 (2008).

# CHAPTER 3

## Rv2074 is a Novel F420-dependent Mycobilin Reductase


### Abstract

The heme degradation machinery utilized by *Mycobacterium tuberculosis* has been well characterized both structurally and biochemically. The cytosolic protein MhuD generates the tertrapyrrole product mycobilin, whose fate in the cell is unknown. Herein, I present the first evidence that Rv2074 is a mycobilin reductase generating a novel product via a coenzyme F420-dependent mechanism. This product was analyzed by mass spectrometry to determine the putative chemical structure of reduced mycobilin, which has been coined "mycorubin." Finally, we propose the mechanism underlying the Rv2074-mediated reduction of mycobilin.


### Introduction

Mycobilin is a naturally occurring tetrapyrrole produced by *Mycobacterium tuberculosis* (Mtb) when heme is degraded by the cytosolic heme degrading protein MhuD (Figure 3.1).[1] MhuD belongs to the IsdG family of heme degrading enzymes, which differ in sequence, structure, and mechanism from canonical heme oxygenases.[1–3] The ultimate fate of the product produced by MhuD is currently not understood. In humans, heme degradation is carried out by the canonical human heme oxygenase (hHO-1) which catalyzes the oxidative cleavage of heme to produce

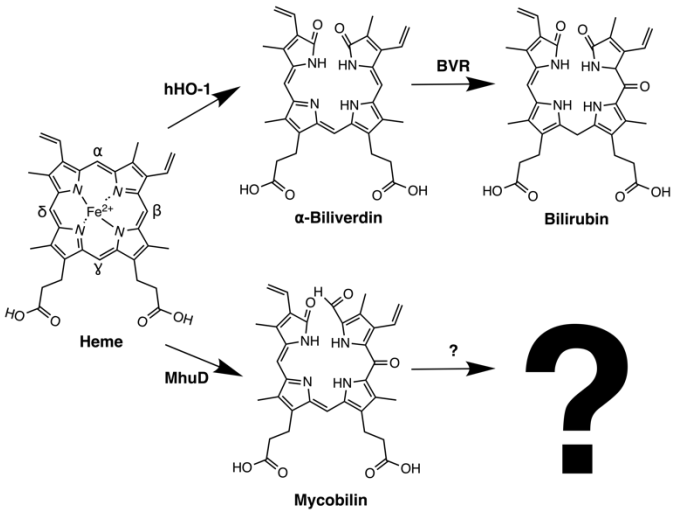


**Figure 3.1.** Scheme of heme degradation with products in humans (top) and *Mycobacterium tuberculosis* (bottom).

biliverdin IXα (αBV, Figure 3.1), ferrous iron, and carbon monoxide.[4–6] After which, αBV is then converted to bilirubin (BR) by biliverdin reductase (BVR, Figure 3.1).[7] BR is then conjugated with glucuronic acid for excretion as high levels of BR are toxic, but low levels act as a strong antioxidant which is capable of neutralizing a 10,000-fold increase in reactive oxygen species levels thereby protecting the cell from oxidative damage.[8–10]

Unfortunately, the products of IsdG-type proteins are difficult to purify,[1,11] which has presumably hindered the structural determination of the product-bound form. Recently, we demonstrated that a MhuD variant, MhuD-R26S, upon heme degradation produces αBV, formaldehyde, and iron.[12] In a recent study, we determined the affinity of wild-type (WT) MhuD and the MhuD-R26S variant for both heme and αBV and show they both bind heme and αBV in the nanomolar range.[3] This high affinity for αBV allowed for the utilization of the MhuD-R26S variant as a proxy to study IsdG-type proteins in complex with their product. Upon determining the crystal structure of the MhuD-R26S−αBV complex, we observed the formation of a novel secondary structural element that has not been seen in the other heme-bound MhuD structures (Figure 3.2).[3] The formation of this novel alpha-helix causes a change in the electrostatic surface potential which could serve to stabilize protein-protein interactions with another protein to facilitate product removal.[3]

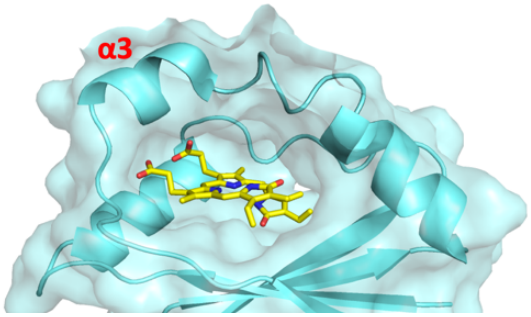


**Figure 3.2.** Structure of MhuD-R26S-αBV complex (PDB: 6PLE) with novel alpha helix 3 labeled.

Protein–protein interaction-induced product removal is reminiscent of hHO-1 αBV removal. Human BVR interacts with hHO-1, albeit via a weak interaction, to remove the product αBV and further reduce it to BR.[13] In contrast, the well-studied bacterial HO from *P. aeruginosa*,

which generates β- and δ-BV isomers, excretes BV without further reduction.[14] We hypothesize that a yet-to-be-identified Mtb protein removes the product from MhuD and potentially aids in its eventual excretion, as observed in the human HO system.

In mycobacteria, there are 22 proposed families of split β-barrel flavin/deazaflavin oxidoreductases (FDORs) identified by sequence-structure-function analyses, and they catalyze a diverse set of redox reactions by facilitating electron transfer between a cofactor binding site and a substrate binding site; however, many of these subfamilies have unknown functions.[15] The cofactors include heme, flavin mononucleotide (FMN), flavin adenine dinucleotide (FAD), and the deazaflavin electron-donating cofactor F420.[15] F420 is typically seen in anaerobic methanogens, however mycobacterial species have evolved to make extensive use of this cofactor in many oxidoreductases.[15,16] Surprisingly, in Mtb two of these FDOR subfamilies contain functional BVRs identified by biochemical and *in silico* docking studies.[15] Notably, Mtb does not have a conventional αBV-producing HO, and these putative BVR homologs share very little sequence identity with human BVR, although a single asparagine residue is conserved (Figure 3.3).[15,17] Two of the FDORs, Mtb Rv2074 and *Mycobacterium smegmatis* MSMEG_3880, have F420-dependent αBV reduction activity.[1515,16]F420 is an obligate two-electron carrying low-potential hydride transfer agent (-360 mV reduction potential),[18] which is similar in reducing potential to the nicotinamide adenine dinucleotide phosphate (NADPH, -400 mV) utilized by human BVR.[19] In contrast, a member of the FDOR B3 family, Rv1155, reduces αBV but at such a low rate the reactivity is thought to not be physiologically relevant.[15] Consequently, it was proposed that one of the αBV inactive Mtb FDORs catabolizes mycobilins. The uncharacterized Rv2991, and the deazaflavin nitroreductase Rv3547 have not been tested for BVR activity and could also act in MhuD product breakdown.[15] Thus, we will investigate if one of these four Mtb

FDORs, Rv1155, Rv2074, Rv2991, or Rv3547, is involved in MhuD product removal and processing.[15,18]

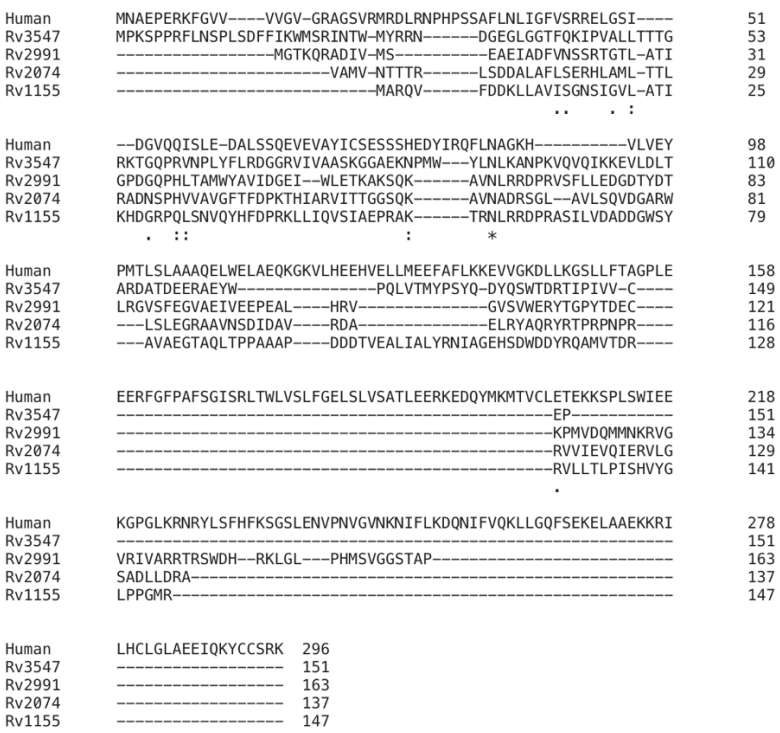


**Figure 3.3.** Clustal Omega alignment of protein sequences for human BVR, and Mtb FDORs with putative BVR activity demonstrates lack of sequence identity.

## Materials and Methods

### *Protein Expression and Purification*

Expression and Purification of Mtb BVR Homologs

Rv1155, Rv2074, Rv2991, and Rv3547 were purified as previously reported with slight modification.[18,19] Briefly, the expression plasmids were transformed into *E. coli* BL21-Gold (DE3) cells (Agilent, Santa Clara, CA), and were grown in LB media supplemented with 100 μg/mL ampicillin at 37 °C overnight. Growths were then sub-cultured into fresh medium and grown to an $OD_{600}$ of ~0.8 before protein expression was induced by the addition of IPTG (1 mM). Cell growth was continued at 18 °C overnight post-induction for all samples except Rv2991, which was grown

for 1.5 h at 37 °C post-induction, before the cells were harvested by centrifugation and stored at -80°C. Cells were lysed by sonication on ice in lysis buffer (50 mM HEPES pH 8, 300 mM NaCl, 10 mM imidazole) containing 100 μM PMSF and hen egg white lysozyme at 45% amplitude, 15 seconds on 45 seconds off, for 20 cycles. The crude cell lysate was then centrifuged at 14,000 rpm for 1 hour before being filtered with a 0.2 μm filter (Minisart Plus, Sartorius). The clarified lysate was loaded onto a HisTrap FF column (5 mL, GE Healthcare) and washed with lysis buffer. Bound protein was eluted from the column with increasing concentrations of imidazole using an AKTA Start FPLC. Fractions found to contain the respective BVR by SDS-PAGE analysis (expected MW: Rv1155 ~18.2 kDa, Rv2074 ~16.9 kDa, Rv2991 ~20.1 kDa, Rv3547 ~17.4 kDa) were pooled and dialyzed against 50 mM HEPES pH 8, 300 mM NaCl, overnight at 4 °C.

*M. smegmatis* Expression and Purification of Mtb FGD

For protein expression, FGD was cloned into the *Mycobacterium smegmatis* expression vector PYUB1049 utilizing site-directed mutagenesis to incorporate the 3' *HindIII* cutsite using the following primers:

Forward 5'-TACGTCGCCTTGGCTAAAAGCTTCTCGAGCACCACCA-3'

Reverse 5'-TGGTGGTGCTCGAGAAGCTTTTAGCCAAGGCGACGTA-3'

The resulting product was then digested using *NcoI* and *HindIII* enzymes, and ligated into PYUB1049 following manufacturer protocols. FGD was expressed and purified as previously reported.[19] Briefly, t[21]he expression plasmid (pYUB1049) was then electroporated into *M. smegmatis* $mc^2$ 4517, and grown in 7H9 media supplemented with 50 μg/mL hygromycin B, 10% ADC, and 0.05 % Tween-80 at 37 °C for 2-3 days. Growths were then sub-cultured into fresh auto-induction medium (ZYP5052/Tween) via a 1:100 dilution and grown for 5 days at 37 °C before the cells were harvested by centrifugation and stored at -80°C. Cells were lysed by sonication on

ice in lysis buffer (50 mM Tris-HCl pH 7.4, 150 mM NaCl, 10 mM imidazole) containing 100 μM PMSF and hen egg white lysozyme at 60% amplitude, 15 seconds on 45 seconds off, for 20 cycles. The crude cell lysate was then centrifuged at 14,000 rpm for 1 hour before being filtered with a 0.2 μm filter (Minisart Plus, Sartorius). The clarified lysate was loaded onto a HisTrap FF column (5 mL, GE Healthcare) and washed with lysis buffer. Bound protein was eluted from the column with increasing concentrations of imidazole using an AKTA Start FPLC. Fractions found to contain FGD by SDS-PAGE analysis (expected MW ~39.4 kDa) were pooled and dialyzed against 50 mM Tris-HCl pH 7.4, 150 mM NaCl, overnight at 4 °C.

***Mycobilin and Coenzyme F420 Production and Purification***

Preparation of Mycobilin Isomers

Reconstitution of MhuD-WT and its mutants with heme was achieved as previously described.[12] Briefly, a hemin solution was prepared by dissolving 4-6 mg of heme in 500 μL of 0.1 M NaOH and incubating for 30 minutes. After the addition of 500 μL of 1 M Tris/HCl, pH 7.4, the solution was centrifuged at 15,000 rpm for 15 minutes. The supernatant was then diluted into 15 mL of 50 mM Tris-HCl pH 7.4, 150 mM NaCl and the concentration was determined by UV/Vis ($\varepsilon_{385}$ = 58.44 $mM^{-1}$ $cm^{-1)}$. Heme was gradually titrated into 500 μM apo-MhuD to a 0.9 heme: 1.0 protein ratio. The samples were incubated overnight at 4 °C before being passed through a desalting column to remove unbound heme. Protein concentrations of the eluted samples was determined via UV/Vis ($\varepsilon_{405}$ = 91.5 $mM^{-1}$ $cm^{-1)}$. Mycobilin was then produced as previously described.[12] Heme degradation was performed in 0.1 M MES, pH 6.0 at 37 °C with 50 μM MhuD-monoheme, 2.5 mM deferoxamine (Sigma-Aldrich), 2.5 μM catalase, and 10 mM sodium ascorbate. Reaction mixtures were incubated at 37 °C for 50 minutes before termination with one half reaction volume of 8 M guanidinium chloride. Samples were incubated at 37 °C for 10 minutes

to ensure full protein denaturation. Mycobilins were then purified via HPLC (Beckman Coulter, System Gold) on a Synergi 4 μm Hydro-RP 80 Å C18 Column (250 × 4.6 mm, Phenomenex) at a flow rate of 3 mL/min. The mobile phase consisted of Solvent A: 0.1 M ammonium acetate, and Solvent B: methanol. A linear gradient was run starting at 50% B and ending at 80% B over 35 minutes. Mycobilin isomers were not resolved and eluted as a single peak with a retention time of 25 minutes; however, UV/Vis analysis indicates the peak was largely mycobilin-a.

Preparation of Coenzyme F420

The production and purification of coenzyme F420 was done as previously described.[20,21] Briefly, the expression plasmid pF420 was transformed into *E. coli* BL21-Gold (DE3) cells (Agilent, Santa Clara, CA), and were grown in LB media supplemented with 25 μg/mL chloramphenicol at 37 °C overnight. Growths were then sub-cultured into LB media and grown to an $OD_{600}$ of ~0.6 before the cells were harvested by centrifugation at 5,000 rpm and transferred into modified M9 media containing 6.78 g/L $Na_2HPO_4$, 1 g/L $NH_4Cl$, 2.5 g/L NaCl, 100X trace elements (1.667 g/L $FeCl_3 \cdot 6\ H_2O$, 0.018 g/L $ZnSO_4 \cdot 7\ H_2O$, 0.012 g/L $CuCl_2 \cdot 2\ H_2O$, 0.012 g/L $MnSO_4 \cdot H_2O$, 0.018 g/L $CoCl_2 \cdot 6\ H_2O$, and 2.225 g/L $Na_2EDTA \cdot 2\ H_2O$), 0.246 g/L $MgSO_4 \cdot 7\ H_2O$, 0.011 g/L $CaCl_2$, and 4.83 g/L fumarate supplemented with 25 μg/mL chloramphenicol at a pH of 7.3. After transfer to M9 media, protein expression was induced by the addition of tetracycline (200 ng/mL) at 28 °C and 200 rpm. Cell growth was continued at 28 °C and 200 rpm overnight post-induction before the cells were harvested by centrifugation and stored at -80°C. To extract F420, cell paste from 1 L of expression was re-suspended in 30 mL of a 75% ethanol solution, and incubated at 90 °C for six minutes before being centrifuged for 15 minutes at 5,000 rpm, and the supernatant was lyophilized. The lyophilized extract was then re-dissolved in 10 mL of $H_2O$, centrifuged at 5,000 rpm for 15 minutes, and filtered with a 0.2 μm filter (Minisart Plus, Sartorius).

The clarified extract was then purified with anion-exchange chromatography using a HiPrep Q XL 16/10 column (GE Healthcare) pre-equilibrated with 25 mM sodium phosphate pH 7.0. A linear salt gradient was then used and fractions containing F420 were determined by absorbance at 420 nm and pooled. These fractions were then desalted using a C18 column (HyperSep C18 cartridge) which was equilibrated with 10 mL 100% MeOH, and 10 mL $H_2O$. F420 was eluted in 2 mL of 20% MeOH which was then lyophilized and stored at -80 °C.

***Fluorescence titrations***

Fluorescence quenching titrations of biliverdin and mycobilin were performed as described previously.[3] Stock solutions of protein (100 nM), α-biliverdin (αBV, 100 μM), and mycobilin (45 μM) were prepared in 50 mM Tris-HCl pH 7.4, 150 mM NaCl for protein and αBV, and 100% MeOH for mycobilin. Small molecules were added in the following titration series: 2 x 1 μL, 4 x 2 μL, 4 x 5 μL, 3 x 10 μL, and 2 x 20 μL injections. In between each titration the solution was incubated for 3 minutes with stirring at 200 rpm at 20 °C before fluorescence spectra were acquired between 300 – 500 nm using a Hitachi F-7100 Fluorescence Spectrophotometer through excitation at 285 nm with the following settings: PMT voltage of 950 V, excitation slit width of 2.5 nm, emission slit width of 5.0 nm, and a scan speed of 240 nm/min.

Fluorescence emission spectral analysis

Results from the fluorescence-based assay were fit to Eqn. 1 derived from Conger et al,[22] to determine the equilibrium dissociation-constant ($K_d$) of the biliverdin isomers with BVRs.

*Eqn. 1*:

$$F = \frac{([BVR] + [ligand] + K_d) - \sqrt{([BVR] + [ligand] + K_d)^2 - 4[BVR][ligand]}}{2} \times \left(\frac{F_{min} - F_{max}}{[BVR]}\right) + F_{max}$$

In Eqn. 1, [BVR] is the total concentration of the biliverdin reductase (BVR) homolog, [ligand] is the total concentration of biliverdin or mycobilin, $F_{max}$ is the emission intensity without ligand,

and $F_{min}$ is the emission intensity for fully ligand-bound BVR. Fitting of the fluorescence emission intensity at 335 nm for $K_d$ determination was performed using GraphPad Prism (Ver 9.3.1).

***Enzymatic assays and product purification***

BVR Activity

Biliverdin reductase activity was investigated as described previously.[18] Biliverdin was prepared by NaOH solubilization and dilution into Tris-HCl as was done for heme in the preparation of mycobilin isomers section above, and concentration was determined by UV/Vis ($\varepsilon_{665}$ = 15.1 $mM^{-1}$ $cm^{-1}$), mycobilin was prepared in 100% MeOH and concentration was estimated using the extinction coefficient for biliverdin ($\varepsilon_{565}$ = 15.1 $mM^{-1}$ $cm^{-1}$). All other stock solutions were prepared in 50 mM Tris pH 7.4 including 10 mM glucose-6-phosphate, 150 μM F420, and 30 μM FGD. Reaction mixtures were prepared consisting of 1 μM FGD, 2.5 mM glucose-6-phosphate, 25 μM biliverdin/mycobilin, 1 μM BVR, and reactions were initiated by the addition of 1 μM F420 and monitored spectrophotometrically (DU800, Beckman Coulter) for half an hour with scans taken at 3-minute intervals. Products were then analyzed by mass spectrometry using LC-MS/MS (ACQUITY UPLC H-class system, Xevo G2-XS QTof, Waters).

The LC method to analyze mycobilin before and after enzymatic reactions was performed by reverse-phase chromatography at 45 °C using a reverse-phase C4 column (Protein BEH C4 Column, 300Å, 1.7 μm, 2.1 mm X 50 mm, Waters) and a 5-minute gradient of Buffer A: 0.1% formic acid in water, Buffer B: acetonitrile (see Table 3.1 for gradient). Data acquisition was begun after a 0.5-minute waste divert (to remove buffer salts). The Xevo Z-spray source was run with a capillary voltage of 300 V, and a cone voltage of 40 V (NaCsI calibration, Leu-enkephalin lock-mass). Nitrogen was used as the desolvation gas at 350 °C and a flow rate of 800 L/hour and data acquisition was done at alternating collision energy with low energy at 0 V and high collision

energy ramp from 15-45 V. Data was acquired in continuum with 0.5 second scans across a mass range of 50-2000 Da.

| Time | Flow (mL/min) | %A | %B | Curve |
|---|---|---|---|---|
| Initial | 0.3 | 97 | 3 | 6 |
| 0.5 | 0.3 | 97 | 3 | 6 |
| 2 | 0.3 | 40 | 60 | 6 |
| 2.5 | 0.3 | 40 | 60 | 6 |
| 3 | 0.3 | 10 | 90 | 6 |
| 3.5 | 0.3 | 10 | 90 | 6 |
| 4 | 0.3 | 97 | 3 | 6 |
| 5 | 0.3 | 97 | 3 | 6 |

**Table 3.1.** Liquid chromatography method used for LC-MS/MS experiments with mycobilins.

## Results

### Expression and Purification of Coenzyme F420 and F420-dependent Glucose-6-Phosphate Dehydrogenase (FGD)

To investigate the activities of the putative BVR homologs, we first needed to generate the coenzyme F420 as well as the F420-dependent glucose-6-phosphate dehydrogenase (FGD) to allow for the reduction of F420 *in vitro* to act as a cofactor for BVR activity (Figure 3.4a). To that end we produced and purified F420 as previously described using Colin Jackson's F420 biosynthesis cassette in *E. coli*.[20,21] Initial FGD expression studies were carried out in *E.* coli, but yielded insoluble protein (data not shown). Efforts to refold the *E. coli*-produced FGD after purifying in denaturing conditions failed to yield active protein, and so *Mycobacterium smegmatis* FGD expression was utilized instead. [20,21]We generated a *Mycobacterium smegmatis* expression construct of FGD in the pYUB1049 vector, electroporated into $mc^2$ 4517 and then the protein was expressed and purified, which yielded soluble FGD enzyme (Figure 3.4b). To ensure the enzyme was active, mixtures containing 5 μM F420, 100 nM FGD, and 10 mM glucose-6 phosphate were mixed in 50 mM Tris-HCl, pH 7.4 at room temperature. The reaction was monitored by UV/Vis

spectroscopy for the loss of the 420 nm peak indicative of the transition from oxidized F420 to reduced $F420H_2$. After 8 minutes, the 420 nm peak was drastically reduced indicating we had purified active FGD (Figure 3.4c).

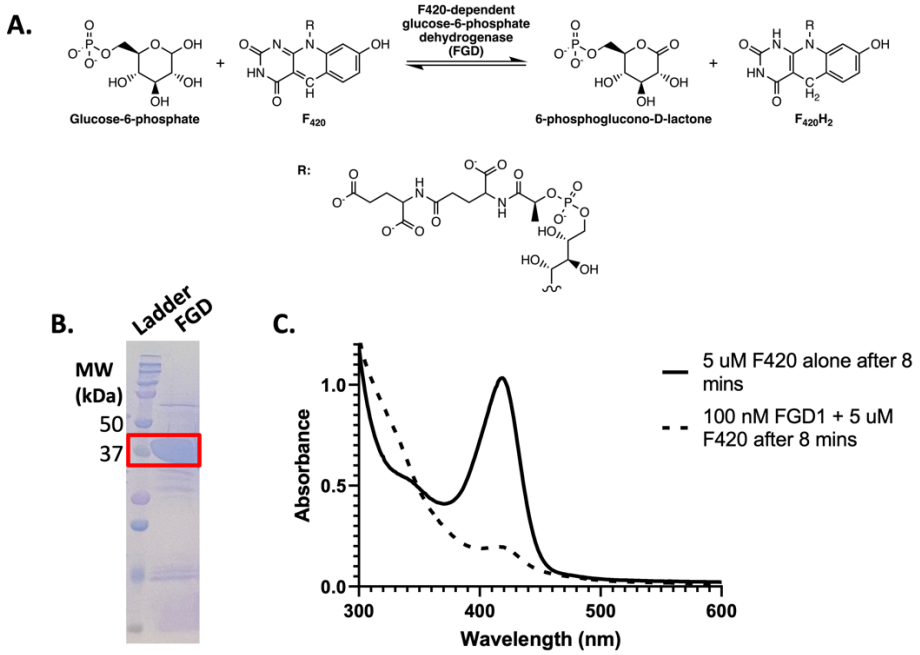


**Figure 3.4.** Purification and validation of *Mycobacterium smegmatis* produced F420-dependent glucose-6-phosphate dehydrogenase (FGD). A) SDS-PAGE analysis of FGD with purified band around 37 kDa highlighted (expected MW: 39.4 kDa). B) UV/Vis analysis of F420 before and after reduction by FGD in the presence of glucose-6-phosphate showing loss of 420 nm peak characteristic of oxidized F420.

**Determining Biliverdin Reductase Homolog Activity Against αBV**

The activities of Rv1155 and Rv2074 against biliverdin had been previously described,[15,18] and therefore served as positive and negative controls for our system. Reaction mixtures were prepared in 50 mM Tris-HCl, pH 7.4, and contained 1 μM FGD, 2.5 mM glucose-6-phosphate, 25 μM αBV, 1 μM BVR, and reactions were initiated by the addition of 1 μM F420, unless otherwise noted, and monitored spectrophotometrically. Mixtures containing F420 alone, and Rv1155 served as negative controls showing no reduction in the peaks at 375 and 665 nm indicative of αBV

(Figure 3.5a, b, c). Rv2074 served as the positive control showing decreases at 375 and 665 nm and an increase at 432 nm as αBV was converted to BR (Figure 3.5a,c). We then investigated the BVR activities of Rv2991 and Rv3547 and found them both to be inactive with αBV as the substrate as there were no shifts in the UV/Vis spectra (Figure 3.5d, e). These data indicate that of the four potential BVR FDORs in the Mtb genome, only Rv2074 is able to reduce αBV.

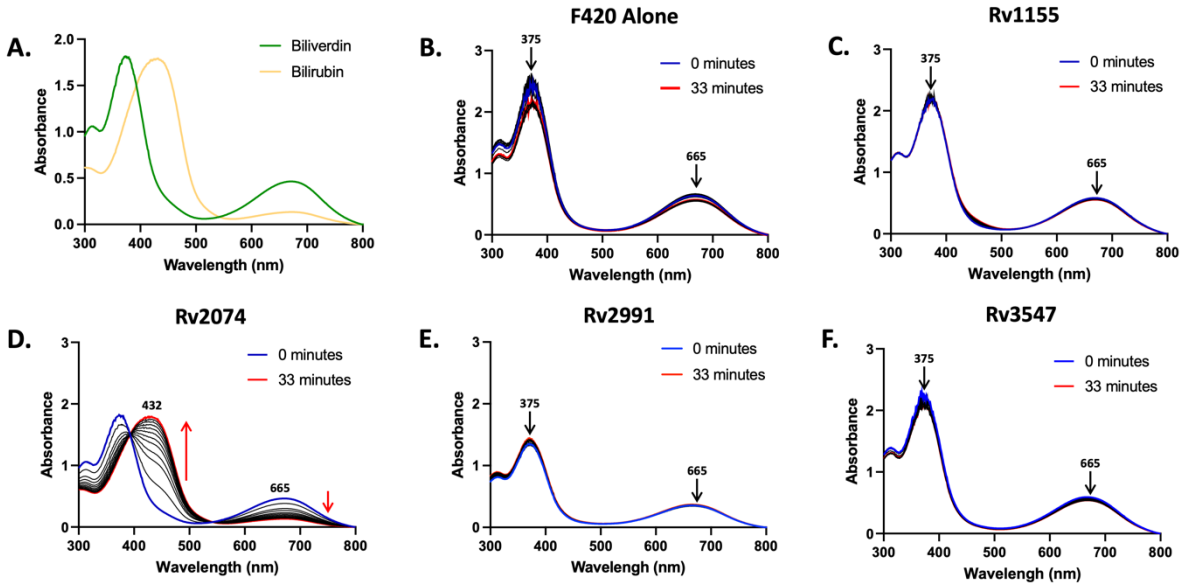


**Figure 3.5.** Activities of putative Mtb biliverdin reductase homologs on α-biliverdin. A) UV/vis spectra of αBV and BR. Reaction mixtures containing: B) 1 µM F420 and 2.5 mM G6P alone, or containing 1 µM FGD, 1 µM F420, 2.5 mM glucose-6-phosphate, 25 µM αBV and 1 µM of: C) Rv1155, D) Rv2074, E) Rv2991, and F) Rv3547 were monitored every 3 minutes for 30 minutes by UV/Vis spectroscopy (Beckman Coulter DU800) for any changes indicating chemical reaction was occurring.

**Investigations into Rv2074 Mycobilin Reductase Activity**

To probe the potential mycobilin reductase activity of the four BVR homologs, we generated and purified mycobilin by single turn-over heme degradation reactions with MhuD (Figure 3.7a).[1,12] This mycobilin was then utilized in identical experiments to those carried out for αBV above, and we found that Rv1155, Rv2991, and Rv3547 had no mycobilin reductase activity (Figure 3.6b,d,e), only Rv2074 showed activity against mycobilin (Figure 3.7c).

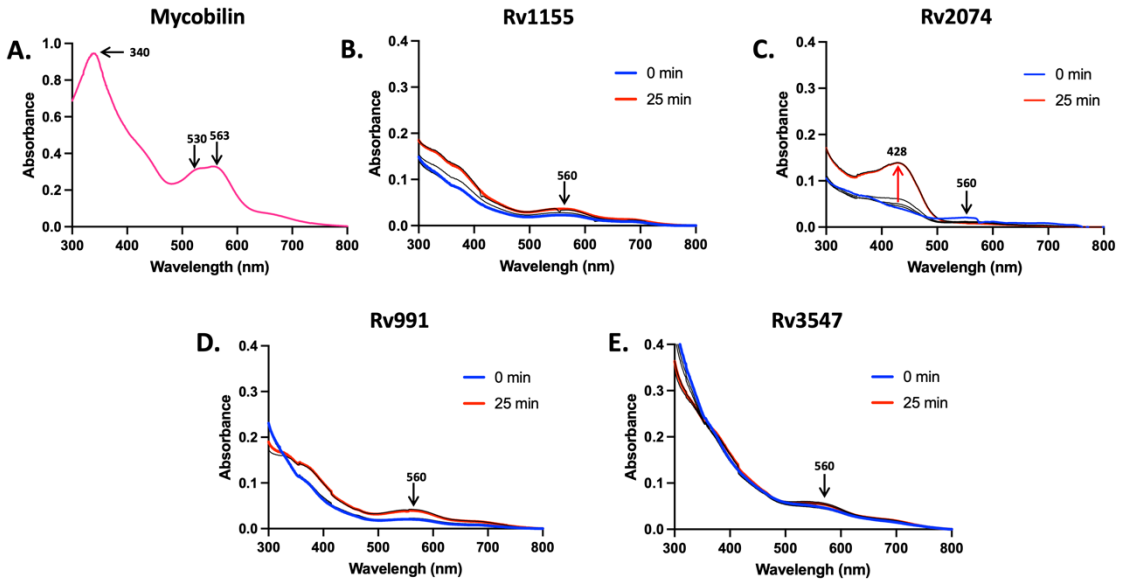


**Figure 3.6.** Activities of putative Mtb biliverdin reductase homologs on mycobilin. A) UV/vis spectra of purified mycobin. Reaction mixtures containing 1 µM FGD, 1 µM F420, 2.5 mM glucose-6-phosphate, 2 µM mycobilin and 1 µM of: B) Rv1155, C) Rv2074, D) Rv2991, and E) Rv3547 were monitored every 3 minutes for 30 minutes by UV/Vis spectroscopy (Beckman Coulter DU800) for any changes indicating chemical reaction was occurring.

When monitoring the scaled up reaction with Rv2074, we saw the loss of the mycobilin peak at 565 nm and the formation of a novel peak at 428 nm as the reaction progressed (Figure 3.7a). When we overlaid the representative spectra of Rv2074-mediated αBV and mycobilin reduction, the reaction mixtures after 30 minutes show distinct spectral differences with the reduced mycobilin product showing one major peak at ~429 nm and bilirubin showing peaks at 432 and 672 nm (Figure 3.7b). These data suggest that Rv2074 is reducing mycobilin to a novel tetrapyrrole product. To further probe the specificity of Rv2074 for mycobilin or αBV we utilized tryptophan fluorescence quenching titrations and found that Rv2074 has an affinity of 0.44 ± 0.02 µM (Figure 3.6d) which is ~4-fold tighter than the affinity observed for αBV (1.64 ± 0.35 µM, Figure 3.7c).

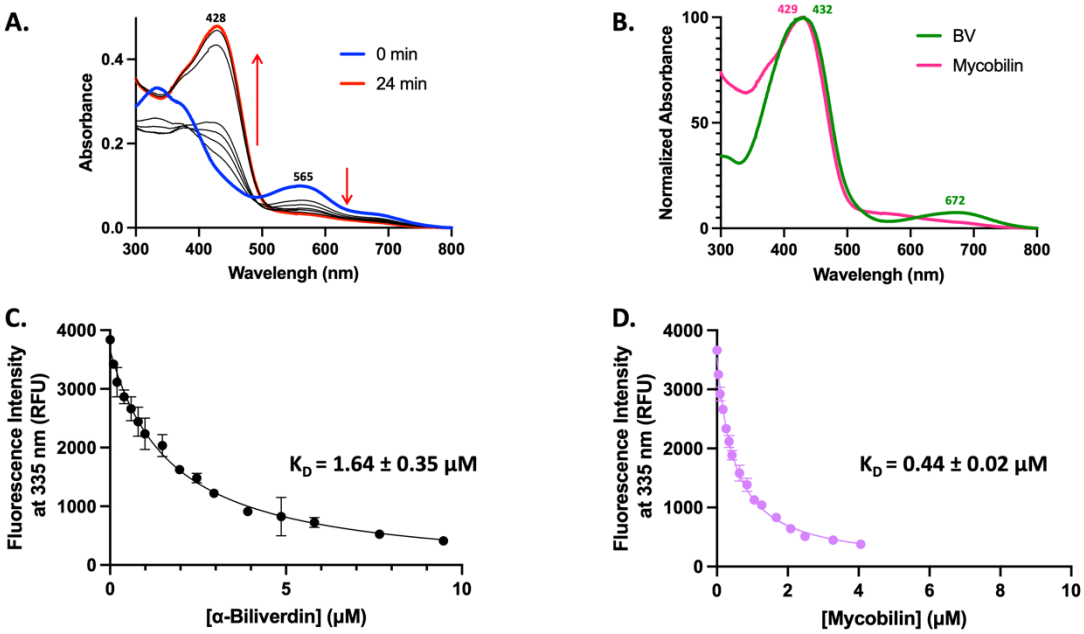


**Figure 3.7.** Examining Rv2074 mycobilin reductase activity. Representative spectra of 5 µM reactions of Rv2074-mediated mycobilin reduction before (blue) and after (red) addition of coenzyme F420 (A) indicate Rv2074 is able to interact with biliverdin. Comparison of representative spectra of reaction mixtures generated by Rv2074 with biliverdin (green) and mycobilin (pink) indicate different products were formed (B). Affinities of αBV and mycobilin for Rv2074. Representative fluorescence emission intensities at 335 nm after excitation at 280 nm of Rv2074 with increasing concentrations of C) αBV, and D) mycobilin.

**Identification of the Product of Rv2074-mediated Mycobilin Reduction**

To determine the chemical structure of the novel product of Rv2074-mediated mycobilin reduction we utilized LC-MS/MS and compared the fragmentation before and after initiating reduction with Rv2074. The mycobilin fragmentation pattern had been previously described, and our data matched that seen previously (Figure 3.7a).[1] The data for the reduced product show the loss of the peak at 297 Da, and the related increase in the peak at 299 Da, as well as the shift of the peak from 325 Da to 327 Da, which together indicate that mycobilin is likely reduced at the ɣ-meso carbon of the tetrapyrrole ring as shown in our putative structure (Figure 3.7b).

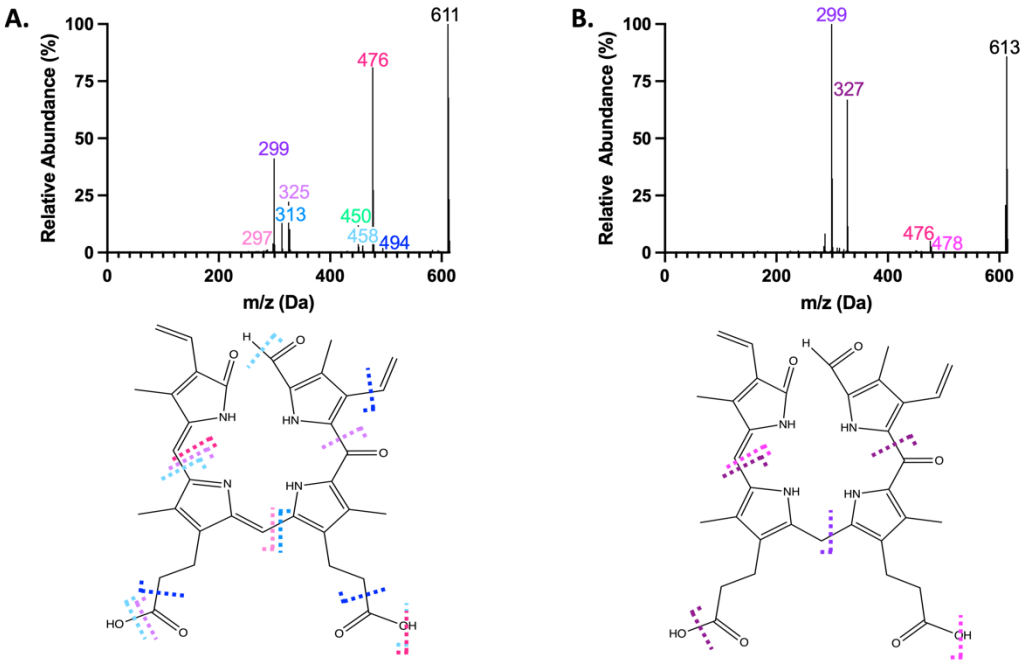


**Figure 3.8.** LC-MS/MS comparison of intact masses (black number) and fragmentation patterns of mycobilin before (A) and after (B) reduction by Rv2074. Proposed fragments are indicated on the structure in corresponding color brackets. Structure of B) is the putative structure of the reduced product of mycobilin.

## Discussion

The mechanism of Mtb heme degradation has been well characterized in which heme is cleaved at the α-mesocarbon generating mycobilin isomers and ferrous iron (Figure 2.1).[1,2,17,22] Although MhuD structural characterization and mechanism of action have been comprehensively studied, the accessory proteins required for MhuD heme degradation as well as the fate of IsdG-like protein products are unknown. It has been shown previously that removal of their tetrapyrrole products requires protein denaturation.[1,11] Indeed, our previous work suggests that both the substrate and the product of MhuD bind in the low nanomolar range, and therefore, the displacement of the product by the substrate would occur only at high heme concentrations *in vivo*.[22] We propose that an accessory protein is required for the removal of the product from the MhuD active site.

The high affinity of MhuD for tetrapyrroles decreases the likelihood that a conformational change alone would promote product release. Because it has been shown that *S. aureus* IsdG is degraded *in vivo* in its apo form yet stabilized in the presence of heme,[23] it seems unlikely that IsdG-type enzymes are also degraded when bound to the product. As the MhuD-R26S−αBV complex structure has a novel structural element and an associated shift in molecular surface electrostatics in comparison to the MhuD–monoheme complex, these conformational changes may promote protein–protein interactions to aid in product removal as discussed in Chapter 2.[3] Our current work served to probe the putative BVR homologs of Mtb to determine if they are in fact able to reduce αBV or mycobilin.

The structures and sequences of the putative Mtb BVRs are highly distinct from human BVR (Figure 3.3, 3.9). Human BVR is a homodimer with each monomer consisting of 296 residues, and consisting of a β-sandwich domain in which an α-helical bundle is sandwiched between two β-sheets (Figure 3.9a). The putative Mtb BVRs are much smaller homodimers (between 137 to 163 residues), and consist of a central β-barrel at the dimer interface decorated with α-helices comprising the active site (Figure 3.9b). It is important to note that Rv3547 was crystalized without 30 N-terminal amino acids in a nonfunctional truncated product that crystallized as a monomer, rather than the dimer traditionally seen for mycobacterial FDORs.[24] The human BVR and bacterial BVR amino acid sequences have no significant similarity when analyzed by BLAST, and a DALI structural homology search does not identify the proteins as structural homologs. This is unsurprising giving the distinct structural features of these proteins discussed above. In an attempt to analyze structural similarities in the four potential mycobilin reductases analyzed in this manuscript, a DALI structural homology search was performed using Rv2074 as the template. Despite having relatively low sequence identities, Rv1155 (Z=14.1, 2.4

Å rmsd, 25% sequence identity) and Rv2991 (Z=14.4, 2.0 Å rmsd, 23% sequence identity) were identified as having high structural homology, while Rv3547 was found to have moderate homology (Z=11.8, 2.4 Å rmsd, 13% sequence identity). This is not surprising as Rv1155, Rv2074, and Rv2991 are from more closely related FDOR subfamilies, while Rv3547 is more distantly related by sequence-structure-function studies and has been shown to have very different activity as a nitroreductase.[15,24] Interestingly, the region which contains the putative catalytic argine (R109 or R112) in Rv2074 are located in a loop region which is an α-helix in the other 3 putative Mtb BVRs (Figure 3.9b). Other proteins with high structural homology include HupZ (Z=14.6, 2.3 Å rmsd, 15% sequence identity), and a predicted F420-binding pyridoxamine 5'-oxidase family protein from *M. smegmatis*, MSMEG_6526 (Z=15.6, 1.8 Å rmsd, 23% sequence identity). HupZ is a heme binding protein from group A *Streptococcus sp*, and as heme and mycobilin are very similar chemical structures with the same tetrapyrrole scaffold (Figure 3.1), it is logical that heme binding proteins would share structural homology to a proteins specific for mycobilin.

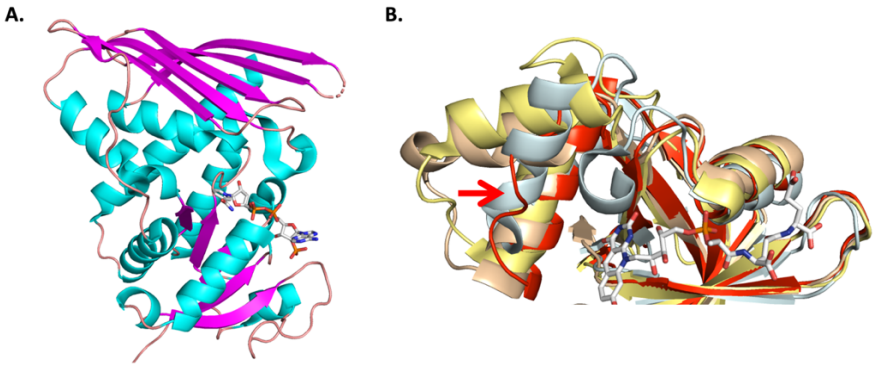


**Figure 3.9.** Comparison of X-ray crystal structures of human BVR and putative bacterial BVRs. A) human biliverdin reductase-NADPH with α-helices are in cyan, β-sheets in pink, and loop regions in salmon (PDB: 2H63), and B) overlay of Rv1155-F420 (yellow, PDB: 4QVB), Rv2074-F420 (red, PDB: 5JAB), Rv2991 (orange, PDB: 1RFE), and Rv3547-F420 (grey, PDB: 3R5R). Red arrow indicates loop region which contains putative catalytic arginines R109 and R112. Cofactors are in white.

To probe the activity of the four putative mycobilin reductases, we utilized enzyme activity assays with reduced coenzyme F420 and the 4 Mtb BVR homologs Rv1155, Rv2074, Rv2991, and Rv3547. Of these enzymes, only Rv2074 showed reductase activity for αBV, as a substrate showing decreases in the peaks associated with αBV at 375 and 665 nm and an increase at 432 nm is indicative of bilirubin formation, confirming previously published results with Rv2074 (Figure 3.5d).[18] Similarly, when probing Rv1155, Rv2991, and Rv3547 for mycobilin reductase activity, all three enzymes showed no effect on mycobilin (Figure 3.6). Interestingly, we were able to demonstrate the novel mycobilin reductase activity of Rv2074 which showed a decrease in the mycobilin peak at 565 nm, and formation of a new peak at 428 nm (Figure 3.7a). When we compare the product peaks generated by Rv2074-mediated reduction of αBV and mycobilin, they have similar peaks at 432 nm and 429 nm respectively (Figure 3.7b). However, the bilirubin produced has a secondary peak at 672 nm which the reduced mycobilin product lacks, indicating that a novel product is being formed upon mycobilin reduction (Figure 3.7b). To determine the chemical structure of this product, we utilized LC-MS/MS before and after Rv2074 reduction. In the intact mycobilin sample we see a parent ion mass of 611 Da, with the fragmentation pattern that has been previously shown for mycobilin (Figure 3.8a).[1] The reduced product, which we have termed mycorubin, shows a shift in the parent ion mass from 611 to 613 Da (Figure 3.8b). This 2 Da shift is the expected mass shift if the mycobilin is reduced in a manner similar to the conversion of αBV to bilirubin, at the ɣ-meso carbon (Figure 3.10).[18] This is supported by the fragmentation data in which we see the loss of the 297 Da peak, and the related increase in the 299 Da peak, as well as the formation of peaks at 327 Da and 478 Da (Figure 3.8b). This indicates that we are likely observing a similar mechanism of action as was proposed for αBV reduction based on the co-crystal structure of Rv2074 with F420 based on the mechanism of BVR in humans.[18,25,26] As

proposed previously for αBV reduction, the initial proton is likely donated by a hydroxonium ion which is formed by R109 or R112, followed by the nucleophilic attack of a hydride from reduced F420 ($F420H_2$) and the resulting reduction of the double bond at the ɣ-meso carbon yielding our mycorubin product (Figure 3.10).[18]

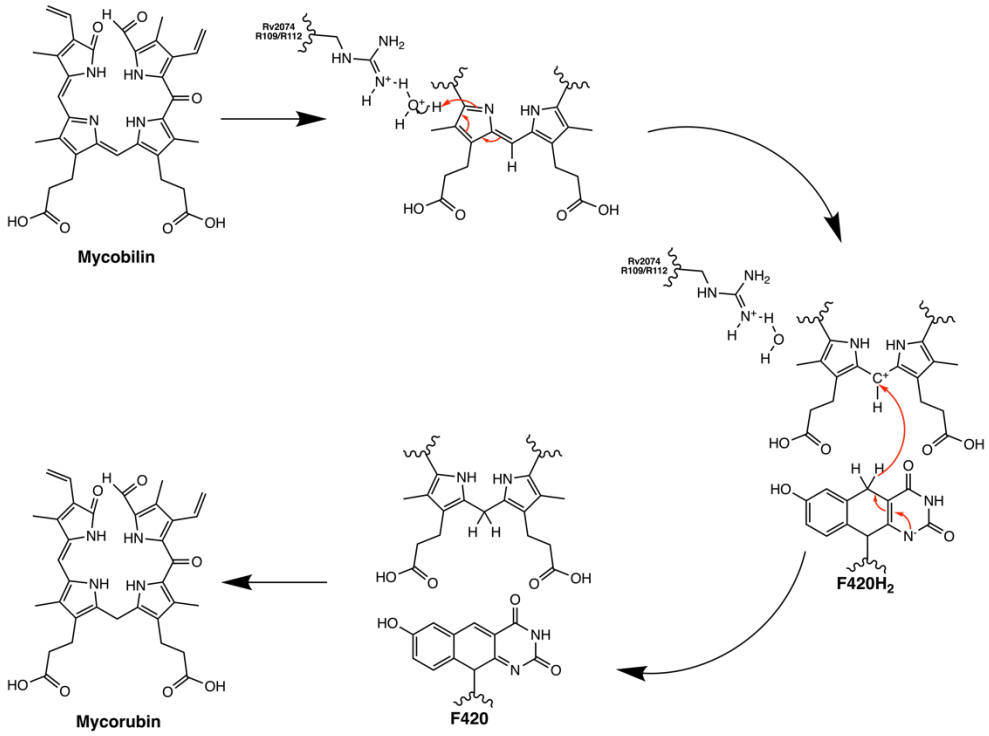


**Figure 3.10.** Proposed mechanism of mycobilin reduction by Rv2074 resulting in the formation of mycorubin. Catalysis is initiated by the formation of a hydroxonium ion via a nearby arginine residue (R109 or R112), followed by hydride transfer from $F420H_2$ to form the final mycorubin product.

To determine if Rv2074 has substrate specificity for mycobilin over αBV we utilized tryptophan fluorescence quenching titrations with both αBV and mycobilin and found that αBV binds with an affinity of 1.64 ± 0.35 μM which is ~4-fold weaker than the affinity for mycobilin of 0.44 ± 0.02 μM (Figure 3.7c, d). Together with the activity and product mass spectrometry data, we have identified Rv2074 as a novel mycobilin reductase in Mtb. Further investigation is required to determine the physiological role of mycorubin, but it potentially acts as an antioxidant similar

to the function of bilirubin in eukaryotes.[8–10] Further work is also required to elucidate the mycobilin reductase kinetics of Rv2074, as well as to determine whether MhuD and Rv2074 directly interact in a manner similar to that seen in human BVR and hHO. The formation of the novel α-helix upon substrate turnover seen in the MhuD-R26S-αBV structure, which was further discussed in Chapter 2, may be a feature that facilitates removal of tetrapyrrole products by stabilizing protein-protein interactions between MhuD and Rv2074, although further work is required to validate this hypothesis.

## References


1. Nambu, S., Matsui, T., Goulding, C. W., Takahashi, S. & Ikeda-Saito, M. A New Way to Degrade Heme: The Mycobacterium tuberculosis Enzyme MhuD Catalyzes Heme Degradation without Generating CO. *Journal of Biological Chemistry* **288**, 10101–10109 (2013).
2. Graves, A. B. *et al.* Crystallographic and Spectroscopic Insights into Heme Degradation by Mycobacterium tuberculosis MhuD. *Inorg Chem* **53**, 5931–5940 (2014).
3. Chao, A. *et al.* Structure of a Mycobacterium tuberculosis Heme-Degrading Protein, MhuD, Variant in Complex with Its Product. *Biochemistry* **58**, 4610–4620 (2019).
4. Tenhunen, R., Marver, H. S. & Schmidt, R. Microsomal Heme Oxygenase, Characterization of the Enzyme. *J Biol Chem* **244**, 6388–6394 (1969).
5. Yoshida, T., Noguchi, M. & Kikuchi, G. Oxygenated Form of Heme, Heme Oxygenase Complex and Requirement for Second Electron to Initiate Heme Degradation from the Oxygenated Complex. *J Biol Chem* **255**, 4418–4420 (1980).
6. Matsui, T., Masaki, U. & Masao, I. S. Heme Oxygenase Reveals Its Strategy for Catalyzing Three Successive Oxygenation Reactions. *Acc Chem Res* **43**, 240–247 (2010).
7. Mantle, T. J. Haem Degradation in Animals and Plants, Bilin Reduction in Plants. *Biochem Soc Trans* **30**, 630–633 (2002).
8. Jansen, T. & Daiber, A. Direct Antioxidant Properties of Bilirubin and Biliverdin. Is there a role for biliverdin reductase? *Front Pharmacol* **3**, (2012).
9. Barañ, D. E., Rao, M., Ferris, C. D. & Snyder, S. H. Biliverdin Reductase: A Major Physiologic Cytoprotectant. *Proceedings of the National Academy of Sciences* **99**, 16093–16098 (2002).

10. Stocker, R., Yamamoto, Y., McDonagh, A., Glazer, A. & Ames, B. Bilirubin is an Antioxidant of Possible Physiological Importance. *Science (1979)* **235**, 1043–1046 (1987).

11. Reniere, M. L. *et al.* The IsdG-family of Haem Oxygenases Degrades Haem to a Novel Chromophore. *Mol Microbiol* **75**, 1529–1538 (2010).

12. Chao, A. & Goulding, C. W. A Single Mutation in the Mycobacterium tuberculosis Heme-Degrading Protein, MhuD, Results in Different Products. *Biochemistry* **58**, 489–492 (2019).

13. Maines, M. D. & Trakshel, G. M. Purification and Characterization of Human Biliverdin Reductase. *Arch Biochem Biophys* **300**, 320–326 (1993).

14. Barker, K. D., Barkovits, K. & Wilks, A. Metabolic Flux of Extracellular Heme Uptake in Pseudomonas aeruginosa is Driven by the Iron-regulated Heme Oxygenase (hemO). *Journal of Biological Chemistry* **287**, 18342–18350 (2012).

15. Ahmed, F. H. *et al.* Sequence-Structure-Function Classification of a Catalytically Diverse Oxidoreductase Superfamily in Mycobacteria. *J Mol Biol* **427**, 3554–3571 (2015).

16. Thauer, R. K., Kaster, A. K., Seedorf, H., Buckel, W. & Hedderich, R. Methanogenic archaea: Ecologically relevant differences in energy conservation. *Nature Reviews Microbiology* vol. 6 579–591 Preprint at https://doi.org/10.1038/nrmicro1931 (2008).

17. Chim, N., Iniguez, A., Nguyen, T. Q. & Goulding, C. W. Unusual Diheme Conformation of the Heme-degrading Protein from Mycobacterium tuberculosis. *J Mol Biol* **395**, 595–608 (2010).

18. Ahmed, F. H. *et al.* Rv2074 is a Novel F420H2-dependent Biliverdin Reductase in Mycobacterium tuberculosis. *Protein Science* **25**, 1692–1709 (2016).

19. Benini, S., Haouz, A., Proux, F., Alzari, P. & Wilson, K. The Crystal Structure of Rv2991 from Mycobacterium tuberculosis: An F420 Binding Protein with Unknown Function. *J Struct Biol* **206**, 216–224 (2019).

20. Shah, M. v. *et al.* Improved Production of the Non-native Cofactor F420 in Escherichia coli. *Sci Rep* **11**, (2021).

21. Bashiri, G. *et al.* A Revised Biosynthetic Pathway for the Cofactor F420 in Prokaryotes. *Nat Commun* **10**, (2019).

22. Thakuri, B. *et al.* The Affinity of MhuD for Heme is Consistent with a Heme Degrading Function in vivo. *Metallomics* **10**, 1560–1563 (2018).

23. Reniere, M. L., Haley, K. P. & Skaar, E. P. The Flexible Loop of Staphylococcus aureus IsdG is Required for its Degradation in the Absence of Heme. *Biochemistry* **50**, 6730–6737 (2011).

24. Cellitti, S. E. *et al.* Structure of Ddn, the deazaflavin-dependent nitroreductase from Mycobacterium tuberculosis involved in bioreductive activation of PA-824. *Structure* **20**, 101–112 (2012).

25. Fu, G., Liu, H. & Doerksen, R. J. Molecular Modeling to Provide Insight into the Substrate Binding and Catalytic Mechanism of Human Biliverdin-IXα Reductase. *Journal of Physical Chemistry B* **116**, 9580–9594 (2012).

26. Smith, L. J., Browne, S., Mulholland, A. J. & Mantle, T. J. Computational and Experimental Studies on the Catalytic Mechanism of Biliverdin-IXβ Reductase. *Biochemical Journal* **411**, 475–484 (2008).

# CHAPTER 4

# *In vitro* Affinities of *Mycobacterium tuberculosis* Periplasmic Binding Proteins, FecB and FecB2, Suggest Roles in Iron/Heme Transport


## Abstract

Many pathogenic bacteria require iron from their human host to survive. To facilitate iron uptake, bacteria have evolved a sophisticated array of proteins to help them uptake, transport and utilize this iron. Mtb has two putative iron or heme periplasmic binding proteins, FecB and FecB2, that have been implicated in these iron acquisition pathways. The crystals structures determined, as well as the *in vitro* affinities of FecB and FecB2, corroborate their roles as putative shuttles of ferric-carboxymycobactin and/or heme across the periplasmic space. The crystal structure of FecB was solved by Alex Chao and Bonnie Cuthbert in the Goulding Lab, and the crystal structure of FecB2 was solved by the Eisenberg lab at UCLA.


## Introduction

Iron is an essential element for all forms of life. It is involved in respiration, electron transfer, energy generation and a variety of biological processes.[1-4] Bacterial pathogens, such as *Mycobacterium tuberculosis* (Mtb), must acquire iron from their host.[5-8] While iron is abundant in nature, free ferric iron ($Fe^{3+}$) is highly insoluble in aerobic environments and can produce toxic free radicals via the Fenton reaction[9]. Due to this, host iron is typically sequestered within iron binding and storage proteins, such as transferrin and ferritin.[10,11] Moreover, a large percentage of the human body's iron is incorporated into heme.[12] Like ferric iron, free heme is relatively insoluble and toxic, and thus is bound to a variety of hemoproteins. As such, most of the host iron and heme reservoirs are protein bound, these proteins pose an additional barrier for bacterial pathogens to overcome in host iron acquisition. Thus, bacteria have developed elaborate iron and heme uptake

systems to acquire iron from their host. Many Gram-negative and Gram-positive bacterial iron uptake systems employ high affinity iron-chelating siderophores. Most bacteria endogenously synthesize one or more structurally unique siderophores, whereby each siderophore requires a distinct biosynthetic pathway and will employ an associated ferric-siderophore uptake system.[13,14] Notably, some microbes have also evolved mechanisms to use siderophores produced by other organisms present within their micro-environment.[15] Likewise, many bacterial pathogens have developed sophisticated heme uptake systems.[16]

In Gram-negative and Gram-positive bacteria, both heme and iron uptake pathways utilize periplasmic binding proteins (PBPs) to shuttle ferric-siderophores (and sometimes apo-siderophores) and heme within the periplasmic or cell-wall environments to the bacterial inner membrane.[13,14,16] In Mtb, evidence suggests that two predicted ferric-citrate binding PBPs, FecB (Rv3044) and FecB2 (Rv0265c), are involved in iron acquisition pathways.[17] FecB is predicted to be part of the IdeR (iron-dependent regulator) regulon, which regulates Mtb iron acquisition [18]. Moreover, a study in *Mycobacterium avium* shows that *fecB* is upregulated under low iron conditions[19], suggesting that Mtb FecB plays a role in iron acquisition. In contrast, a recent study showed that an Mtb∆*fecB* mutant had no significant growth defect when grown in iron-limited conditions, indicating that FecB is not essential for Mtb iron acquisition.[20] Instead, this work suggested that FecB plays a role in maintaining Mtb cell-wall integrity and is involved in the intrinsic resistance of Mtb to multiple antibiotics, including rifampicin, vancomycin and meropenem. FecB2 has also been implicated in iron/heme uptake pathways. In order to identify genes involved in heme uptake, an Mtb transposon library screen was used to identify mutants with greater resistance to the toxic heme analog gallium-protoporphyrin IX (GaPPIX).[21] The interrupted expression of FecB2 resulted in an Mtb variant resistant to GaPPIX toxicity.

Furthermore, the Mtb*ΔfecB2* mutant showed an attenuated growth phenotype when either ferric ammonium citrate or heme were provided as an iron source; however, this growth phenotype was significantly diminished with heme alone, further suggesting that FecB2 could be involved in Mtb heme and alternate iron acquisition mechanisms.[21] Another comprehensive Mtb transposon library study of genes required for growth in the presence of ferric-cMB/MB or heme/hemoglobin as the sole iron sources suggest that *fecB* is required for growth in the presence of Fe-cMB alone[22]; surprisingly this study did not observe that *fecB2* was required for growth in the presence of a specific iron source. Ultimately, these studies suggest that FecB and FecB2 may act as apo- or Fe-cMB or heme periplasmic chaperones.

Herein, we discuss the X-ray crystal structures of both Mtb FecB and FecB2 in their apo-forms. Analysis of the two Mtb PBP structures shows that the ligand-binding pockets have different potential ligand binding residues, shapes, and overall electrostatic surface potential, suggesting they bind different ligands. We carried out binding studies of both FecB and FecB2 with heme and Fe-cMB to determine their preferred ligand. We show that FecB has a higher affinity for heme than FecB2, and interestingly, FecB binds Fe-cMB whereas FecB2 does not. Through mutational analysis, we pinpointed FecB Glu339 as a critical residue for Fe-cMB binding. These results suggest that Mtb FecB2 has a role in the heme uptake pathway, whereas Mtb FecB potentially plays a role in both siderophore-dependent and heme-iron acquisition pathways.

## Materials and Methods

### *Protein Expression and Purification*

Cloning of Rv0265c (FecB2) and Rv3044 (FecB)

For structural studies, the C-terminal portion of *rv0265c* (*fecB2*) was amplified from Mtb H37Rv genomic DNA with primers (Rv0265c-For, and Rv0265c-Rev, Table 4.1) incorporating 5′

*Nco*I and 3′ *Xho*I restriction enzyme sites and cloned into pET28a (Novagen). The resulting construct contains an N-terminal methionine residue followed by the mature FecB2 protein sequence (Ala39-Ala330) and a C-terminal non-cleavable His-tag. As residues 1-38 of FecB encompass the predicted N-terminal signal peptide and lipoprotein attachment site, they were omitted from the expression construct. The sequence of the cloned gene was verified by DNA sequencing (GeneWiz, Piscataway, NJ).

For ligand binding studies, the same gene encoding the mature FecB2 (residues Ala39-Ala330) was subcloned into pET28a to produce a construct with a thrombin-cleavable N-terminal His-tag. The expressed protein after thrombin cleavage includes an additional GSHM sequence at its N-terminus. The primers (Rv0265c-Thrombin-For and Rv0265c-Thrombin-Rev, Table 4.1) incorporate 5′ *Nde*I and 3′ *Hind*III restriction enzyme sites.

For both crystallography and ligand binding studies, the gene (*rv3044*) encoding FecB without the predicted signal peptide (encoding for residues Ala29-Asn359) was cloned into a pET28a vector from Mtb H37Rv genomic DNA to encode for a thrombin-cleavable N-terminal His-tag like the FecB2-construct for ligand binding studies. The primers (Rv3044-For and Rv3044-Rev, Table 4.1**)** incorporate 5′ *Nde*I and 3′ *Hind*III restriction enzyme sites. The resulting mature FecB protein includes Ala29-Asn359 and following thrombin cleavage includes an extra GSHM sequence at the N-terminus.

**Table 4.1.** List of primer sequences used in this study.

| **Oligo Name** | **Sequence (5' to 3')** |
|---|---|
| **Rv0265c-For** | TGCGGACTTTCCATGGCGGCGG TAACTATCAC |
| **Rv0265c-Rev** | GTAGTCACTCGAGTGCGCCCAAGATCTG |
| **Rv0265c-Thrombin-For** | GGGCATATGGCGGCGGTAACTATCACCCACCTGTTCGG |
| **Rv0265c-Thrombin-Rev** | GGGAAGCTTTCATGCGCCCAAGATCTGGC TGATCTGTGGCG |
| **Rv3044-For** | GGCATATGGCGTCACAATCGATGATCACGCCCACCACC C |
| **Rv3044-Rev** | GGAAGCTTCTAGTTGATCGGCGCGTCGACCCAGCG |

| | |
|---|---|
| **R141S-FecB-For** | ATCTGCCCGGTGTCGGTACTTCCAGCGCCCCCGACCT |
| **R141S-FecB-Rev** | AGGTCGGGGGCGCTGGAAGTACCGACACCGGGCAGAT |
| **Q233S-FecB-For** | GTCGATCGTGAGTCTGACCGCCAACACCAT |
| **Q233S-FecB-Rev** | ATGGTGTTGGCGGTCAGACTCACGATCGAC |
| **R240S-FecB-For** | TGACCGCCAACACCATGTCGGTATACGGCGCCAACAAC TT |
| **R240S-FecB-Rev** | AAGTTGTTGGCGCCGTATACCGACATGGTGTTGGCGGT CA |
| **Y242S-FecB-For** | AACACCATGCGGGTATCCGGCGCCAACAACTTCC |
| **Y242S-FecB-Rev** | GGAAGTTGTTGGCGCCGGATACCCGCATGGTGTT |
| **Y270S-FecB-For** | TTCACCGACAAGGCCTCCATCGAGATCGGCACCA |
| **Y270S-FecB-Rev** | TGGTGCCGATCTCGATGGAGGCCTTGTCGGTGAA |
| **E272S-FecB-For** | ACCGACAAGGCCTACATCTCGATCGGCACCA |
| **E272S-FecB-Rev** | TGGTGCCGATCGAGATGTAGGCCTTGTCGGT |
| **D322S-FecB-For** | TCTTCGTCGTCAACAGCCAGGTATGGCAGACCG |
| **D322S-FecB-Rev** | CGGTCTGCCATACCTGGCTGTTGACGACGAAGA |
| **Q336S-FecB-For** | AACGACCAGGTATGGAGTACCGGCGAGGGTATGGT |
| **Q336S-FecB-Rev** | ACCATACCCTCGCCGGTACTCCATACCTGGTCGTT |
| **E339S-FecB-For** | TATGGCAGACCGGCTCAGGTATGGTCGCTG |
| **E339S-FecB-Rev** | CAGCGACCATACCTGAGCCGGTCTGCCATA |

Expression and purification of FecB2 and FecB for crystallization

The FecB2 expression plasmid was transformed into *E. coli* BL21-CodonPlus (DE3)-RIL cells (Agilent, Santa Clara, CA) and cells were grown in LB media supplemented with 50 µg/mL kanamycin to an $OD_{600}$ of 0.6 before protein expression was induced by the addition of 0.5 mM IPTG. Cell growth was continued overnight at 18°C and the cells harvested by centrifugation and stored at -80°C. Cell pellets were resuspended in buffer A (20 mM Tris, pH 8.0, 300 mM NaCl, 10% glycerol) containing a protease inhibitor cocktail (cOmplete, Roche), hen egg white lysozyme and 1mM PMSF, and the cells were lysed by sonication on ice (45% amplitude, 15 seconds on 45 seconds off, for 20 cycles). The lysate was centrifuged for 30 minutes at 30000 x *g* and the clarified supernatant was incubated with Ni-NTA agarose beads at 4°C for 2 hours. The suspension was poured into a gravity column, washed extensively with buffer B (buffer A with 20 mM imidazole), and the bound protein eluted with buffer C (buffer A with 300 mM imidazole). Eluted protein was concentrated and further purified by size exclusion chromatography using a HiLoad Superdex 200

column (GE Healthcare Life Sciences, Piscataway, NJ) equilibrated in buffer A. Protein purity was assessed by SDS-PAGE and fractions containing pure protein were pooled and concentrated to 10 mg/ml for crystallization screening.

A similar protocol was carried out for the expression and purification of FecB. However, the FecB expression plasmid was transformed into *E. coli* BL21-Gold (DE3) cells (Agilent, Santa Clara, CA), and protein expression was induced with 1mM IPTG.

Removal of the N-terminal His-tag for FecB and FecB2

Following Ni-NTA purification, FecB and FecB2 proteins were treated with the thrombin CleanCleave kit (Sigma) following manufacturer protocols to remove His-tags. Briefly, thrombin resin was added to the protein and incubated overnight at 4 °C with stirring. The resin was then removed by centrifugation at 2,500 rpm for 5 minutes and the cleaved protein sample was incubated with Ni-NTA resin (HisPur, Thermo Scientific) for one hour at room temperature. The flow-through was collected and verified to contain cleaved FecB or FecB2 by SDS-PAGE and MALDI-TOF mass spectrometry.

Construction and Purification of FecB variants

The FecB single variants, R141S, Q233S, R240S, Y242S, Y270S, E272S, D322S, Q336S, and E339S, were generated by *in vitro* site-directed mutagenesis using Pfu Ultra Fusion HS DNA polymerase (Agilent) with the primers listed below in Table 4.1, and then confirmed by DNA sequencing (GeneWiz from Azenta Life Sciences).

Each mutant vector was transformed into *E. coli* BL21-Gold (DE3) cells and grown as above. Cells were lysed by sonication on ice in lysis buffer (50 mM Tris-HCl pH 7.4, 350 mM NaCl, 10% glycerol, 10 mM imidazole) containing 10 μM PMSF and hen egg white lysozyme at 45% amplitude, 15 seconds on 45 seconds off, for 20 cycles. The crude cell lysate was then

centrifuged at 14,000 rpm for 1 hour before discarding the supernatant. The pellet was then solubilized in 50 mM Tris-HCl pH 7.4, 350 mM NaCl, 10% glycerol, 6M urea overnight at 4 °C. The resuspended lysate was then centrifuged at 14,000 rpm for 1 hour before being passed through a 1 μm syringe filter to remove insoluble debris. The urea was then sequentially removed by dialysis in buffers of decreasing urea concentration: 4 M urea, 2 M urea, and two rounds of 0 M urea. The re-folded protein was then loaded onto Ni-NTA resin (HisPur Ni-NTA Resin, Thermo Scientific) and eluted with a stepwise elution gradient of imidazole going up to 500 mM imidazole. Fractions found to contain FecB by SDS-PAGE analysis (expected MW ~37 kDa) were pooled and dialyzed against 50 mM Tris-HCl pH 7.4, 350 mM NaCl, 10% glycerol overnight at 4°C. Successful refolding was confirmed by circular dichroism (CD). Far UV CD spectra were collected at 25°C using a Jasco J-810 spectropolarimeter using 0.1 cm cuvettes with FecB variant (5 μM) in 5 mM Tris pH 7.4, 35 mM NaCl, 1% glycerol. The bandwidth and wavelength step were set to 1 nm and the BeStSel tool (https://bestsel.elte.hu/index.php) was used to quantify secondary structural elements.

***Preparation and Purification Carboxymycobactin***

Preparation and purification of Fe-cMB

Carboxymycobactin was purified from *M. smegmatis* growth media as previously described using a Δ*fxbA* variant of *M. smegmatis* $mc^2$ 155 as previously described.[23] Briefly, a culture of a *ΔfxbA* $mc^2$ 155 was streaked on 7H10 agar plates containing 50 μg/mL hygromycin B and grown for 3 days at 37 ℃. A colony was then inoculated into 7H9 media containing 10% ADC supplement and 50 μg/mL hygromycin B and grown for 5 days at 37 ℃. The resulting culture was then inoculated 1:1,000 into minimal media containing 5 g $KH_2PO_4$, 5 g L-asparagine, 60 mL of glycerol, and the pH was adjusted to 7.0 in a final volume of 1 L. After autoclaving, syringe-

filtered (0.2 μm filter, Minisart Plus, Sartorius) $MgSO_4$ (final concentration 1.7 mM), $ZnSO_4$ (6.9 μM) and $MnSO_4$ (1.8 μM) were added with 50 μg/mL hygromycin B and grown for another 5 days at 37 ℃. Finally, the culture was inoculated 1:100 into fresh minimal media as described above with the addition of 0.08 μg/mL $FeSO_4$ and grown for a final 5 days at 37 ℃. To isolate cMB, the bacteria were centrifuged at 5,000 rpm for 30 minutes and the resulting supernatant was filtered with a 0.2 μm filter. The media was then acidified to a pH of 3.5 with HCl before dropwise addition of 10% $FeCl_3$ (w/v) in 100% ethanol until the formation of a reddish-brown precipitate ($FePO_4$) was observed. The solution was then stirred for 1 hour at room temperature before centrifugation at 5,000 rpm for 30 minutes and the resulting supernatant was filtered with a 0.2 μm filter. The Fe-cMB was then extracted into 1 volume of ethyl acetate. The organic later was washed two times with water, dried over anhydrous $MgSO_4$, and filtered using filter paper (Whatman) before being dried by rotary evaporation. The resulting crude Fe-cMB extract was then purified via HPLC (Beckman Coulter, System Gold) on an Ultrasphere ODS 5 μm 80 Å C18 Column (150 × 10 mm, Hichrom) at a flow rate of 2 mL/min. The mobile phase consisted of Solvent A: Water:0.1% FA, and Solvent B: ACN:0.1% FA. A wash was run for 6 minutes at 36% B before a linear gradient was run starting at 36% B and ending at 96% B over 60 minutes, and then holding at this concentration for a further 20 minutes. Carboxymycobactin retention times were 11.5 minutes, 12.7 minutes, 14.0 minutes, 15.8 minutes, 18.5 minutes, and 21.7 minutes for the different chain lengths of carboxymycobactin produced (n=3-8). Carboxymycobactins were pooled based on their characteristic absorbance at 450 nm and lyophilized before being stored at -20 ℃.

Removal of Iron and Isolation of apo-cMB

Fe-cMB was converted to its desiferri form as previously described.[24] Briefly, HPLC-purified Fe-cMB was incubated with 50 mM EDTA, pH 4, for one hour at room temperature. The

resulting desferri-cMB was then separated from EDTA using solid-phase extraction with a Sep-Pak C18 cartridge (Waters) equilibrated with 2 CV each of: acetonitrile (ACN), water, 0.1% trifluoroacetic acid (TFA), and methonal:0.1% TFA (10:90). After sample application the column was washed with 4 CV each of 0.1% TFA, and ACN:0.1% TFA (20:80), and then 2 CV of methanol:0.1% TFA (50:50) and eluted with 1.5 CV of methanol and lyophilized and stored at -20 ℃. The desiferri-cMB was then solubilized in 50 mM Tris-HCl pH 7.4, 150 mM NaCl. To determine concentration, a portion of the solution was ferrated by adding an excess of $FeCl_3$ and then analyzed by UV/vis spectroscopy ($\varepsilon_{450}$ = 3,800.16 $M^{-1}$ $cm^{-1}$).

***Fluorescence Titrations***

Fluorescence quenching titrations of heme, ferric-carboxymycobactin (Fe-cMB), ferric-pyoverdine (Fe-Pyo), and ferric-mycobactin J (Fe-MBJ) were performed as described previously.[25,26] Stock solutions of FecB or FecB2 (100 nM), heme (100 μM), Fe-cMB (80 μM), and Fe-Pyo (1 mM) were prepared in 50 mM Tris-HCl pH 7.4, 150 mM NaCl. Stock solutions of Fe-MBJ (250 μM), and protoporphyrin IX (230μM) were prepared in the same buffer with the addition of 10% DMSO. All small molecules besides Fe-cMB were added in the following titration series: 2 x 1 μL, 4 x 2 μL, 4 x 5 μL, 3 x 10 μL, and 2 x 20 μL injections, while Fe-cMB followed the same titrations without the final three injections. In between each titration the solution was incubated for 3 minutes with stirring at 200 rpm at 20 °C. Fluorescence spectra were acquired between 300 – 500 nm using a Hitachi F-7100 Fluorescence Spectrophotometer through excitation at 285 nm with the following settings: PMT voltage of 950 V, excitation slit width of 2.5 nm, emission slit width of 5.0 nm, and a scan speed of 240 nm/min.

<u>Fluorescence Emission Spectral Analysis</u>

Results from the fluorescence-based assay were fit to Eqn. 1 derived from [26], to determine the equilibrium dissociation-constant ($K_D$) of heme or Fe-cMB with FecB2 or FecB and its mutants.

*Eqn. 1*:

$$F = \frac{([FecB] + [ligand] + K_d) - \sqrt{([FecB] + [ligand] + K_d)^2 - 4[FecB][ligand]}}{2} \times \left(\frac{F_{min} - F_{max}}{[FecB]}\right) + F_{max}$$

In Eqn. 1, [FecB] is the total concentration of FecB or FecB2 or mutants, [ligand] is the total concentration of heme Fe-cMB, Fe-Pyo, or Fe-MBJ, $F_{\max}$ is the emission intensity without ligand, and $F_{\min}$ is the emission intensity for fully ligand-bound FecB(2). Fitting of the fluorescence emission intensity at 335 nm for $K_D$ determination was performed using GraphPad Prism (Ver 9.3.1).

## Results

### *FecB and FecB2 X-ray Crystal Structures*

Mtb FecB and FecB2 are quite different proteins with only 24% sequence identity. FecB2 has a predicted 38-residue signal peptide and potential lipoprotein attachment site (Cys26), while the N-terminus of FecB is predicted to have a 68-residue extension containing both a signal peptide (1-28) and membrane lipid attachment site. As both FecB and FecB2 have a signal peptide, one can predict that they reside in the periplasmic space. The differences in FecB and FecB2 N-termini, however, suggest that FecB and FecB2 may localize to different cellular locations within the Mtb periplasm. Due to the fact that FecB2 localizes to the membrane fraction and is not surface exposed[21], it may be attached to the periplasmic side of the inner membrane or outer membrane.[21] The two Mtb periplasmic binding proteins (PBPs), FecB and FecB2 were cloned in their predicted mature forms without the signal peptide, FecB (without residues 1-28) and FecB2 (without residues 1-38) for *in vitro* biochemical analyses and crystallographic studies. The structure of the mature form of FecB2 (Rv0265c minus the predicted signal peptide residues 1-38) was solved by

molecular replacement using the structure of the *M. smegmatis* homolog (MSMEG_0438; PDB code: 4MDY) as the search model to 2.2 Å resolution. The structure of the mature FecB form was solved by molecular replacement using the structure of Mtb FecB2 (PDB code: 4PM4) as the search model to 2.0 Å.

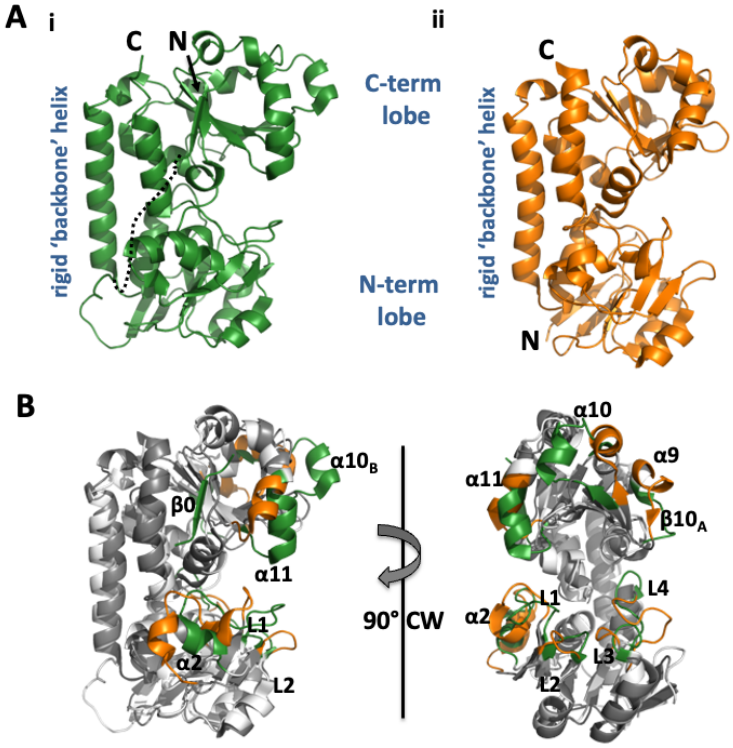


**Figure 4.1.** Overview of Mtb FecB and FecB2 structures. A. FecB (i, green) and FecB2 (ii, orange) structures are shown in cartoon form. Both are multi-domain proteins with an N-terminal lobe and a C-terminal lobe connected by a rigid 'backbone' helix. These features are labelled, as are the N- and C-termini. Notably, FecB has an extra N-terminal sequence that associates with the C-terminal lobe but has an unstructured connection between the N- and C-terminal lobes (dashed black line). B. FecB and FecB2 structures are superimposed to highlight the differences in secondary structure. Secondary structure elements that overlay well are colored in white (FecB) and grey (FecB2), while divergent secondary structure is colored as in (A) and labelled.

Mtb FecB and FecB2 are both members of the type III PBP family.[27] Each protein structure is composed of N- and C-terminal lobes consisting of mixed α/β structures with a central β-sheet surrounded by α-helices, with the two lobes linked by a rigid "backbone" helix (α6) characteristic

of the type III PBP family (Figure 4.1). The two lobes of the protein form a cleft, which is the putative ligand-binding pocket. The substrate binding pocket of FecB is quite different from that of FecB2 in contributing residues, shape, and electrostatic charges (Figure 4.2). The FecB binding pocket has three tyrosine residues (Tyr127, Tyr242, Tyr270), four asparagine residues (Asn119, Asn245, Asn246, Asn331), three glutamine residues (Gln233, Gln333, Gln336), two arginine residues (Arg141, Arg240), a glutamate residue (Glu339) and an aspartate residue (Asp332, Figure 4.3). The resulting FecB pocket is narrower and deeper than the FecB2 ligand-binding pocket, with one side pinched together creating an almost triangular chasm (Figure 4.2). The lip (formed by loop L1) gives the pocket its triangular appearance and the molecular surface is positively charged at the base of the pocket (Figure 4.2b). In contrast, the back of the pocket is negatively charged.

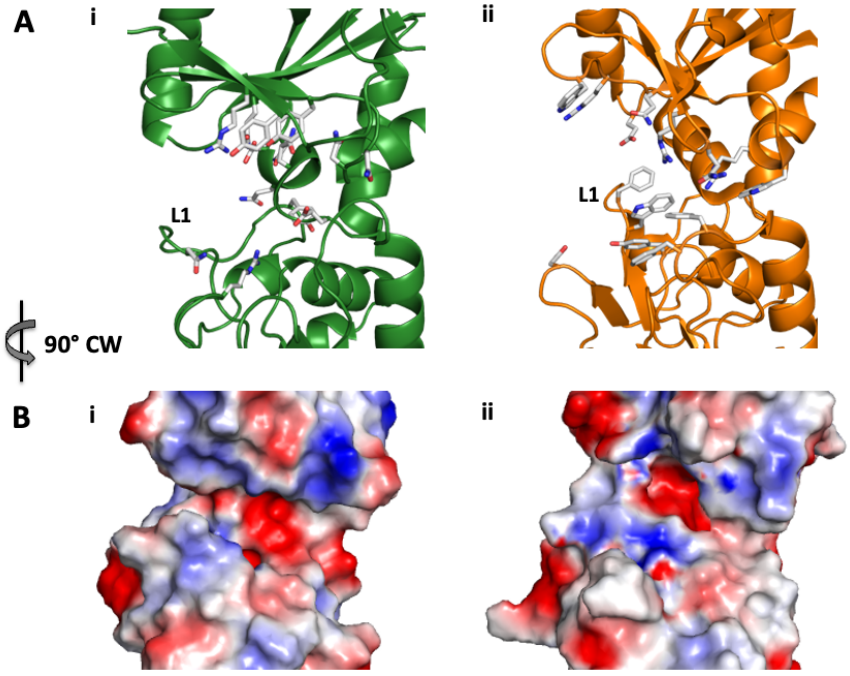


**Figure 4.2.** Comparison of the ligand-binding sites for FecB and FecB2. Putative ligand-binding site of FecB (left panels) and FecB2 (right panels) show that the FecB2 ligand binding pocket is in a more open form compared to that of FecB. A. FecB and FecB2 are represented in cartoon form and colored as in Figure 1A with potential ligand-binding residues shown as white sticks. B. The electrostatic molecular surface for FecB and FecB2 was generated by APBS (Adaptive Poisson-Boltzmann Solver, citation), where white, red and blue represent hydrophobic, negative and positively charged surfaces, respectively.

The substrate binding pocket of FecB2 contains fewer polar or charged residues than that of FecB (Figures 4.2 and 4.3). The binding cleft of FecB2 contains three arginine residues (Arg184, Arg196, Arg221), two glutamine residues (Gln182, Gln220), one glutamate (Glu244), an aspartate (Asp85) and a tyrosine residue (Tyr39) to provide polar contacts with a bound ligand; and several tryptophan residues (Trp58, Trp186, Trp197) and phenylalanine residues (Phe59, Phe131, Phe132), which could further stabilize the substrate backbone (Figure 4.3). The FecB2 binding pocket is wider and shallower than the FecB pocket, and the resulting cleft has a predominately neutral base with a positively charged electrostatic surface surrounding the mouth of the negatively charged tunnel. This positively charged patch at the back of the FecB2 pocket juxtaposes the negatively charged patch in FecB at a similar location (Figure 4.2b).

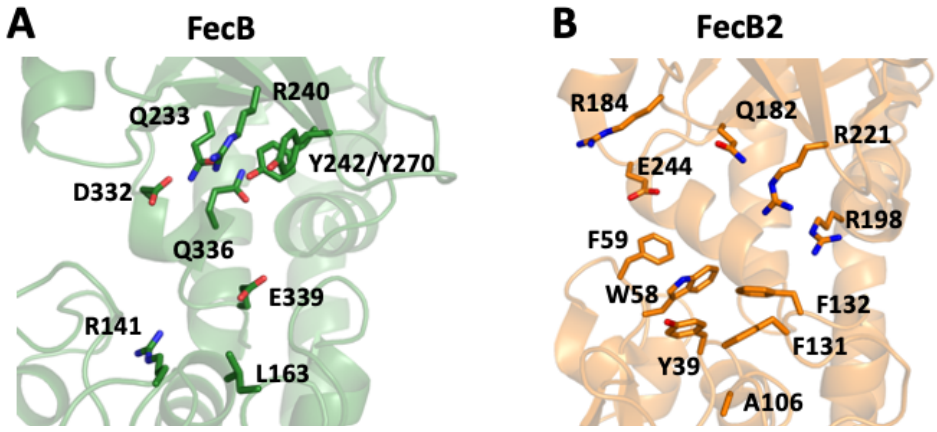


**Figure 4.3.** Structural comparison of Mtb FecB and FecB2. Ligand-binding sites for A. Mtb FecB (green, PDB ID 7UQ0), B. Mtb FecB2 (orange, PDB ID 4PM4), and potential coordinating residues are shown as stick representations.

***Determination of Potential Substrates of FecB and FecB2***

As FecB and FecB2 have multiple tryptophan residues in their substrate binding site pockets, we used a previously described fluorescence-based assay to determine the affinities of heme and Fe-cMB to FecB and FecB2.[25,26] Both FecB and FecB2 constructs with hexa-histidine (His) tags have high nanomolar to micromolar affinities to heme, 1.20 ± 0.10 μM and 0.87 ± 0.02

μM, respectively (Figure 4.4a and e), whereby FecB-His appears to have a reduced affinity to heme compared to FecB2-His. FecB was also tested for its ability to bind to the protoporphyrin IX scaffold to determine if the heme iron was important for binding and found that FecB lost 4-fold affinity as compared to that of heme (4.02 ± 0.04 μM, Figure 4.4d).

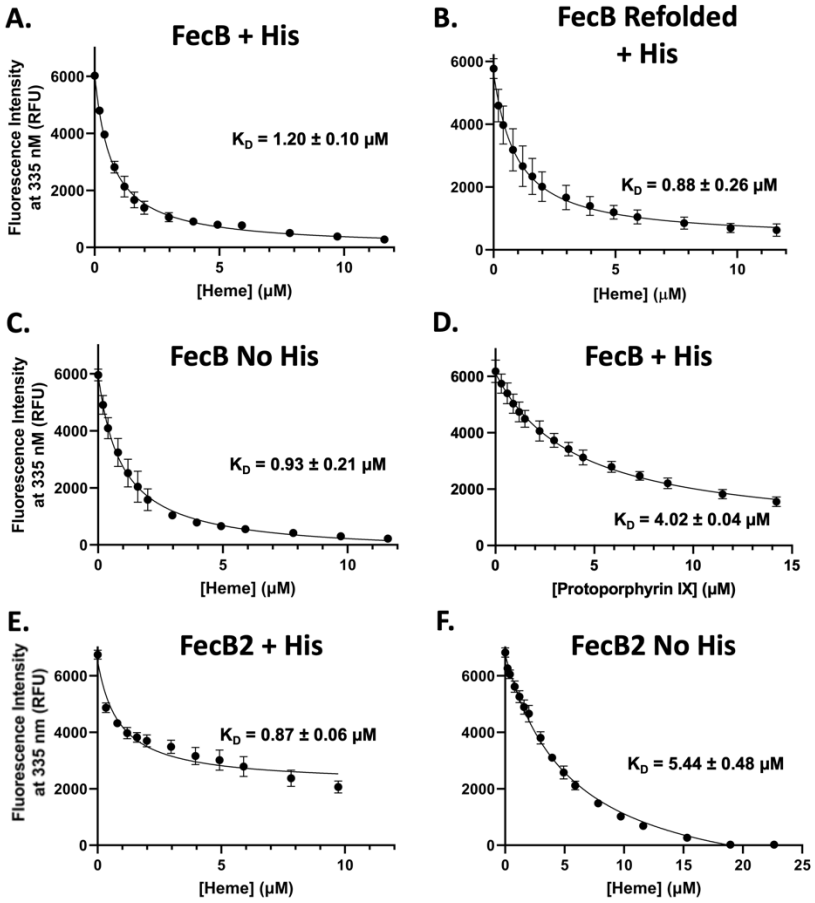


**Figure 4.4.** Affinities of FecB and FecB2 for heme and protoporphyrin IX. Representative fluorescent emission intensities at 335 nm after excitation at 280 nm of 100 nM FecB (A-D) and 100 nM FecB2 (E-F) with increasing concentrations of heme and protoporphyrin IX. Curves were fit using the equation from Conger et al[28] and affinities ($K_D$) are included for each titration.

Previous studies have shown that His tags can interfere with heme binding studies[26,29,30], where the His tag can interact directly with heme.[31] To test that the His tag does not interfere with heme binding, the affinity of heme for FecB and FecB2 without His tags was determined (Figure 4.4c and f). For FecB, its affinity for heme remained similar in the presence or absence of the His tag. However, in the case of FecB2, the affinity for heme was reduced 6-fold in the absence of the His tag (Figure 4.4f). These results suggest that non-tagged FecB (0.93 ± 0.21 μM) preferentially binds heme compared to FecB2 (5.44 ± 0.48 μM). When the affinity of Fe-cMB to FecB-His and

FecB2-His was tested, we observed a dramatic difference in their preference for Fe-cMB. FecB-His has high nanomolar affinity to Fe-cMB (0.68 ± 0.12 μM, Figure 4.5a), whereas the affinity of FecB2-His to Fe-cMB is at least 50-fold weaker, such that it cannot be accurately determined due to the low solubility of Fe-cMB (Figure 4.5e). Interestingly, FecB loses approximately 10-fold affinity for cMB when the iron is removed (Figure 4.5c). Moreover, the affinity of Fe-cMB for FecB was the same in the presence or absence of the His tag, and whether or not the protein was purified in denaturing conditions and refolded (Figure 4.5a and b). These results suggest that while both FecB and FecB2 can bind heme, FecB preferentially binds heme compared to FecB2. In contrast, FecB binds Fe-cMB with high affinity whereas FecB2 does not show measurable binding.

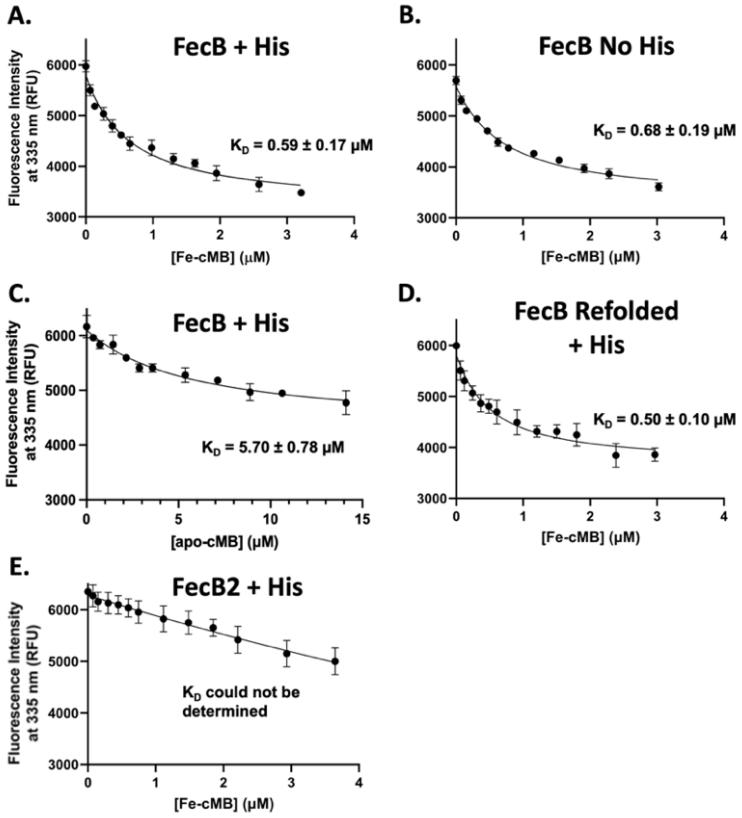


**Figure 4.5.** Affinities of FecB and FecB2 for carboxymycobactin. Representative fluorescent emission intensities at 335 nm after excitation at 280 nm of 100 nM FecB (A-D) and 100 nM FecB2 (E) with increasing concentrations of Fe- (A-B, D-E) or apo-cMB (C). Curves were fit using the equation from Conger et al[28] and affinities ($K_D$) are included for each titration.

Furthermore, some bacteria such as *E. coli* have been shown to be able to utilize siderophores from other bacterial species.[32] As FecB was shown to have an preference for the Mtb siderophore Fe-cMB, we investigated the affinity of FecB for ferric pyoverdine from *Pseudomonas*

*aeruginosa* (Fe-Pyo) and ferric mycobactin J from *Mycobacterium paratuberculosis* (Fe-MBJ). The affinity for Fe-pyo was unable to be determined, as the binding was weak and unable to be determined within the solubility limits of Fe-Pyo (Figure 4.6b). Fe-MBJ did bind to FecB, but with 19-fold weaker affinity than that observed for Fe-cMB (11.34 ± 0.12 µM, Figure 4.6a). Furthermore, a Δ*fecB* mutant had been shown previously to be resistant to the antibiotics rifampin, meropenem, and vancomycin and so we sought to determine if FecB was able to directly bind to these antibiotics.[20] Only rifampin had measurable binding (14.50 ± 0.50 µM, Figure 4.6c-e).

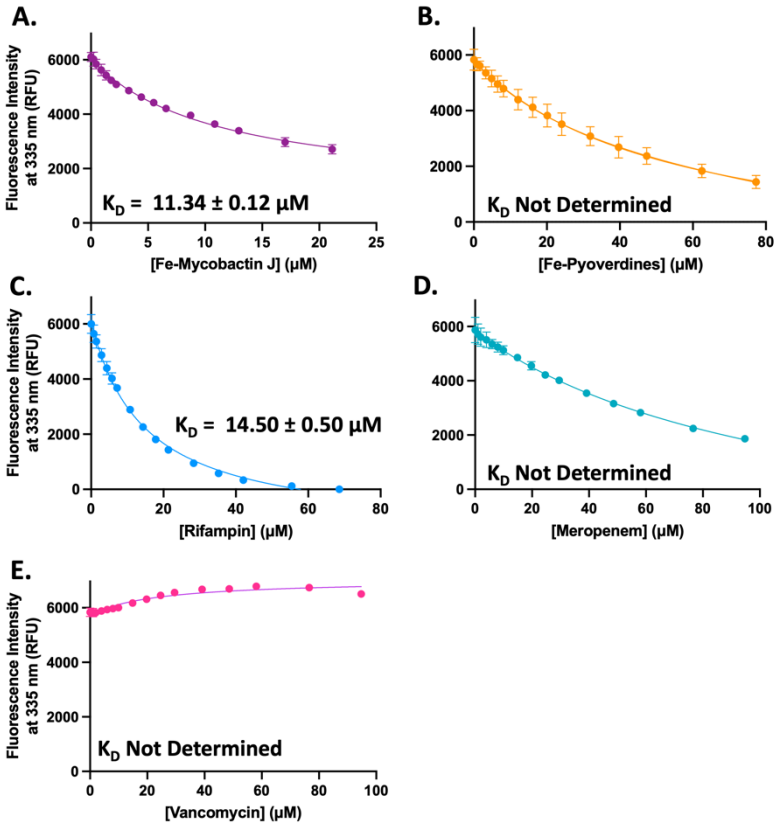


**Figure 4.6.** Affinities of FecB for selected bacterial siderophores and antibiotics. Representative fluorescent emission intensities at 335 nm after excitation at 280 nm of 100 nM FecB with increasing concentrations of Fe-mycobactin J (A), Fe-pyoverdines (B), rifampin (C), meropenem (D), and vancomycin (E). Notably, all experiments were performed with FecB-His. Curves were fit using the equation from Conger et al[28] and affinities ($K_D$) are included for each titration.

***Determination of FecB Residues that Coordinate to Fe-cMB***

As there was a distinct difference in Fe-cMB binding between FecB and FecB2, we interrogated FecB residues that could be involved in Fe-cMB binding. As described above, several potential Fe-cMB-interacting residues were identified in FecB due to conservation with $Fe^{3+}$-siderophore interacting residues from Gram-positive bacterial PBP homologs, or from charged,

polar and aromatic residues located in previously observed PBP binding sites (Figure 4.3). To maintain protein solubility, these surface-exposed potential ligand-coordinating residues (Arg141, Gln233, Arg240, Tyr242, Tyr270, Glu272, Asp322, Gln336, and Glu339) were mutated to serine with one exception: Leu163 was mutated to an arginine as it superimposed onto a conserved arginine residue in the structures of HtsA, SirA and YfiY (Arg126, Arg125 and Arg91, respectively, Figure 4.3). Notably, all resulting FecB variants were insoluble, and were purified under denaturing conditions and refolded. To ensure that the FecB variants were correctly folded, circular dichroism (CD) spectroscopy was utilized. Wild-type (WT) FecB-His and its variants had similar CD traces (Figure 4.7) suggesting that the FecB variants were correctly folded.

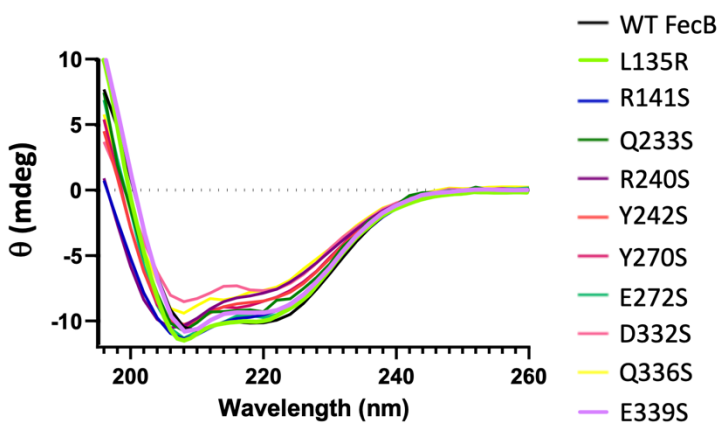


**Figure 4.7**. Circular dichroism (CD) spectra of FecB and its variants. CD was performed to ensure that no major structural changes occurred with the generation of FecB variants compared to wild-type (WT) FecB. Experiments were performed at 25 °C using a Jasco J-810 spectropolarimeter. WT and variant FecB samples (5 μM) were analyzed in 5 mM Tris pH 7.4, 35 mM NaCl, 1% glycerol.

We also tested whether refolded WT FecB had similar affinity for heme and Fe-cMB to that of native WT FecB. We observed that the affinity to Fe-cMB between the refolded and the natively purified FecB proteins were similar (Figure 4.5d). For all nine FecB variants, we determined their affinity to Fe-cMB utilizing fluorescence spectroscopy (Figure 4.8). Out of the nine variants tested (R141S, L163R, Q233S, R240S, Y242S, Y270S, E272S, D322S, Q336S, and E339S), there was only one variant, E339S, (Figure 4.8j) that had a considerably reduced affinity

to Fe-cMB. Ultimately, the affinity of the E339S variant was so diminished that it was unmeasurable due to the solubility limits of Fe-cMB.

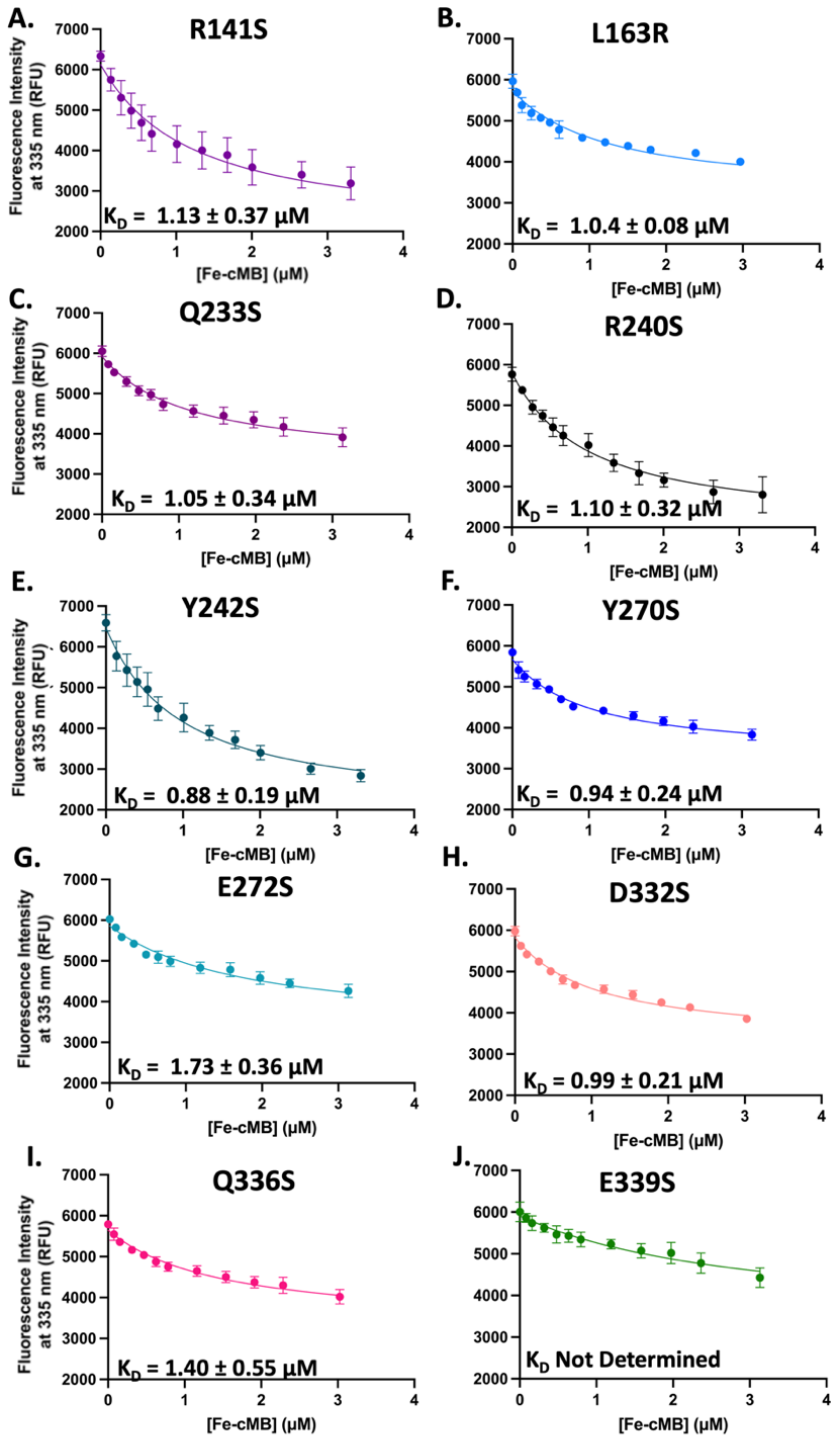


**Figure 4.8.** Affinities of FecB mutants for carboxymycobactin. Representative fluorescent emission intensities at 335 nm after excitation at 280 nm of 100 nM FecB with increasing concentrations of Fe-cMB. Curves were fit using the equation from Conger et al[28] and affinities ($K_D$) are included for each titration.

## Discussion

FecB and FecB2 ligand binding experiments with Fe-cMB and heme indicate that only FecB binds Fe-cMB, but both FecB and FecB2 bind heme. This result places both FecB and FecB2 in the heme iron acquisition pathway but also implicates FecB in cMB iron acquisition. Key differences in the N-terminus of both proteins could suggest different subcellular localizations. The Mtb PBPs enter the periplasm by different routes: FecB is predicted to be secreted by the Sec system which is corroborated by our Msm pull-downs interacting with SecD[33], whereas FecB2 secretion potentially involves the twin-arginine TAT system.[34] Additionally, the different signal peptides and additional sequence at the N-termini of Mtb FecB compared to FecB2 —a predicted 68-residue N-terminal extension containing a signal peptide—and FecB2—a predicted 38-residue signal peptide—could direct the proteins to different cellular locations, such as the cell-wall side or inner-membrane side of the periplasm.

As both FecB and FecB2 bind heme, it is possible that both PBPs are required for the movement of heme through the periplasm to the inner membrane. In *S. aureus*, the iron surface determinant (Isd) heme uptake pathway utilizes a cascade of proteins that contain NEAT domains to capture and shuttle heme across the cell-wall to IsdE, a PBP protein, which transfers its heme cargo to the inner membrane transport complex.[35] In this system, only one PBP, IsdE, is involved in transferring heme from cell-wall proteins to the inner membrane complex, where IsdE utilizes an affinity gradient to ensure unidirectional import of heme from the extracellular space to the periplasmic side of the inner membrane.[36] Notably, in *P. aeruginosa* there are two PBPs, FpvF and FpvC, that work in concert to shuttle its ferric-siderophore through the periplasm to the inner membrane.[37,38] Like in *P. aeruginosa,* Mtb could require a complex of two PBPs, FecB and FecB2, to transport heme or siderophores through the periplasm.

FecB and FecB2 are both Type III PBPs and have high degrees of structural similarity. Nonetheless, there are major differences within the ligand binding pockets as highlighted in the results section (Figure 4.2). There are numerous charged residues observed within the FecB ligand-binding pocket compared to FecB2. PBPs that specifically recognize heme or ferric siderophores coordinate them in different fashions. One major difference is that heme-iron is typically directly coordinated by at least one protein residue such as a histidine or tyrosine[39-41], whereas ferric-siderophores lack iron coordination by a PBP residue and are frequently coordinated solely through hydrogen-bonds with the siderophore scaffold (Figure 4.9).[42-44] As FecB binds Fe-cMB, we sought to not only identify residues that were involved in Fe-cMB binding, but to also determine if perhaps FecB can bind to siderophores from other bacterial species. It has been shown that *E. coli* has evolved the ability to utilize siderophores from other bacteria, such as ferrichrome from *Aspergillus sp.*, utilizing distinct receptors, so perhaps Mtb has evolved a similar mechanism.[32] The two siderophores tested, Fe-Pyo from *P. aeruginosa* and Fe-MBJ from *M. paratuberculosis*, either did not have measurable binding or bound with 19-fold lower affinity than Fe-cMB (Figure 4.6a). This indicates that while FecB can accommodate both heme and Fe-cMB, it is not able to accommodate the larger siderophores tested. This does not preclude FecB's ability to coordinate smaller siderophores such as pyochelin from *P. aeruginosa* or ferrichrome from *Aspergillus sp*, and requires further investigation. Furthermore, a previous study showed that a Δ*fecB* mutant had resistance to many antibiotics including meropenem, rifampin, and vancomycin.[20] To determine if FecB was directly binding and shuttling these antibiotics across the periplasmic space as is proposed for Fe-cMB, we tested the affinity of FecB for these antibiotics (Figure 4.6c-e). Only rifampin showed measurable binding, but that binding was 24-fold weaker than the affinity for Fe-

cMB. This indicates that the effect of FecB on antibiotic resistance is likely not via directly transporting these drugs, but instead an indirect effect via an unknown mechanism.

The direct comparison of the ligand binding pocket of FecB to ferric-siderophore-PBP complex structures allowed for the identification of potential ligand coordinating residues. We tested ten FecB mutants and found that only one mutant, Glu339Ser, significantly attenuated Fe-cMB binding. This acidic residue is situated at the back of the FecB ligand binding pocket (Figure 4.3a). There is one comprehensive, structure-guided study that identified PBP residues that coordinate a ferric-bound siderophore. In this study, only three positively charged residues contributed significantly to the binding of ferric-staphyloferrin A by *S. aureus* HtsA.[45] Therefore, our observation that a single negatively charged glutamate residue had a strong effect on the binding of Fe-cMB by FecB is not surprising.

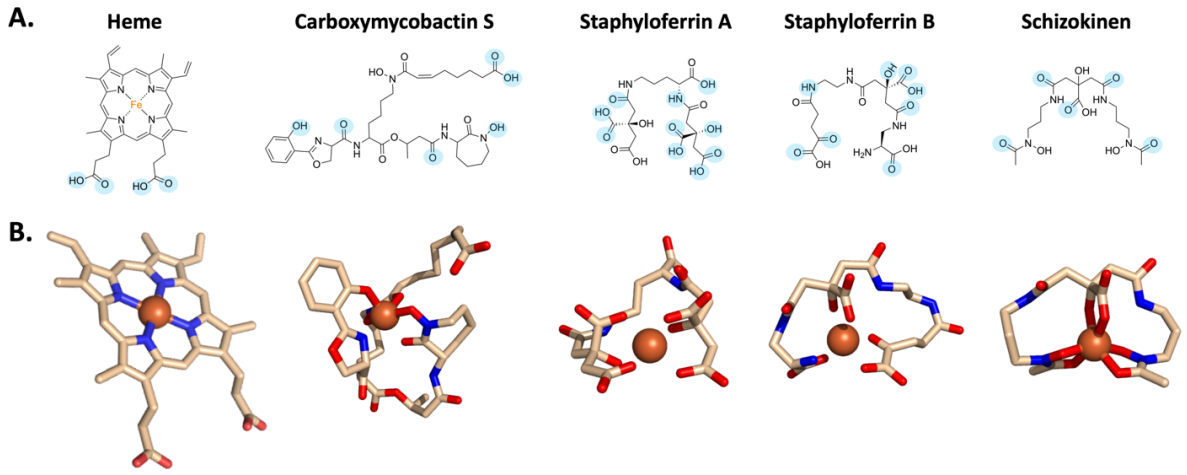


**Figure 4.9.** Structural comparison of a selection of iron-binding molecules and their recognition by periplasmic binding proteins (PBPs). (A) The chemical structures of heme and several apo bacterial siderophores. Highlighted in blue are chemical moieties recognized by protein residues from PDB ID: 2Q8Q, 1X89, 3LI2, 3MWF and 3LI2, respectively. All but ferric carboxymycobactin s were crystallized bound to PBPs, shown here is the only known structure containing ferric carboxymycobactin s, which is bound by siderocalin, a mammalian lipocalin protein. (B) Stick representations from X-ray crystal structures of protein-bound heme and ferric siderophores: heme, ferric carboxymycobactin s, ferric staphyloferrin A and B, and ferric schizokinen.

Additionally, as discussed in the results, the shape and depth of the FecB and FecB2 binding pockets differ significantly. These differences in ligand binding pocket shape could be attributed to differences between open/closed conformations captured in the crystallized apo-structures of FecB and FecB2 or to differences in the ligand the pocket recognizes. It has been observed that Class III PBPs, such as siderophore and heme binding PBPs, usually do not have large conformational changes or motion in the hinge region during ligand binding. Although, as more apo- and holo-siderophore-PBP structures are solved, particularly in Gram-positive bacteria, distinct ligand-binding pocket open and closed conformations have been observed and are usually modulated by the rigid 'backbone' helix and rearrangement in the C-terminal domain.[27] In the apo-FecB structure, this backbone helix is relatively straight which suggests a ligand-binding site that is more closed, whereas in the apo-FecB2 structure, the backbone helix is curved away from the main body of the structure and is more reminiscent of an open conformation (Figure 4.1).[27] Particularly in the case of FecB2, which has a curved backbone helix in its apo form, ligand binding may induce the backbone helix to straighten, causing the N- and C-terminal lobes to clamp down on its cargo. Notably, while the FecB structure appears to be in a more closed conformation than FecB2, the volume of the ligand binding pocket of FecB is substantially larger (526 $Å^3$ vs 156 $Å^3$, as determined by pCast[46]). As FecB binds both heme and cMB, the increased size of its binding pocket could reflect this promiscuity or could explain why FecB is able to bind Fe-cMB—a larger, bulkier ligand than heme (Figure 4.10)—while FecB2 cannot. Obtaining structures of FecB and FecB2 with their native ligands will shed light on the conformational flexibility and ligand-selectivity of FecB and FecB2.

## References


1 Beinert, H., Holm, R. H. & Munck, E. Iron-sulfur clusters: nature's modular, multipurpose structures. *Science* **277**, 653-659 (1997).

2 Gray, H. B. & Winkler, J. R. Electron transfer in proteins. *Annu Rev Biochem* **65**, 537-561 (1996).

3 Perutz, M. F. Mechanisms regulating the reactions of human hemoglobin with oxygen and carbon monoxide. *Annu Rev Physiol* **52**, 1-25 (1990).

4 Poulos, T. L. Heme enzyme structure and function. *Chem Rev* **114**, 3919-3962 (2014).

5 Cairo, G., Bernuzzi, F. & Recalcati, S. A precious metal: Iron, an essential nutrient for all cells. *Genes Nutr* **1**, 25-39 (2006).

6 Doherty, C. P. Host-pathogen interactions: the role of iron. *J Nutr* **137**, 1341-1344 (2007).

7 Ratledge, C. Iron, mycobacteria and tuberculosis. *Tuberculosis (Edinb)* **84**, 110-130 (2004).

8 Skaar, E. P. The battle for iron between bacterial pathogens and their vertebrate hosts. *PLoS Pathog* **6**, e1000949 (2010).

9 Prousek, J. Fenton chemistry in biology and medicine. *Pure and Applied Chemistry* **79**, 2325-2338 (2007).

10 Boradia, V. M. *et al.* Mycobacterium tuberculosis acquires iron by cell-surface sequestration and internalization of human holo-transferrin. *Nat Commun* **5**, 4730 (2014).

11 Malhotra, H. *et al.* Mycobacterium tuberculosis Glyceraldehyde-3-Phosphate Dehydrogenase (GAPDH) Functions as a Receptor for Human Lactoferrin. *Front Cell Infect Microbiol* **7**, 245 (2017).

12 Hooda, J., Shah, A. & Zhang, L. Heme, an essential nutrient from dietary proteins, critically impacts diverse physiological and pathological processes. *Nutrients* **6**, 1080-1102 (2014).

13 Sheldon, J. R. & Heinrichs, D. E. Recent developments in understanding the iron acquisition strategies of gram positive pathogens. *FEMS Microbiol Rev* **39**, 592-630 (2015).

14 Klebba, P. E. *et al.* Iron Acquisition Systems of Gram-negative Bacterial Pathogens Define TonB-Dependent Pathways to Novel Antibiotics. *Chem Rev* **121**, 5193-5239 (2021).

15 Miethke, M. Molecular strategies of microbial iron assimilation: from high-affinity complexes to cofactor assembly systems. *Metallomics* **5**, 15-28 (2013).

16 Donegan, R. K. The role of host heme in bacterial infection. *Biol Chem* **403**, 1017-1029 (2022).

17 Chao, A., Sieminski, P. J., Owens, C. P. & Goulding, C. W. Iron Acquisition in Mycobacterium tuberculosis. *Chem Rev* **119**, 1193-1220 (2019).

18 Prakash, P., Yellaboina, S., Ranjan, A. & Hasnain, S. E. Computational prediction and experimental verification of novel IdeR binding sites in the upstream sequences of Mycobacterium tuberculosis open reading frames. *Bioinformatics* **21**, 2161-2166 (2005).

19 Wagner, D., Sangari, F. J., Parker, A. & Bermudez, L. E. fecB, a gene potentially involved in iron transport in Mycobacterium avium, is not induced within macrophages. *FEMS Microbiol Lett* **247**, 185-191 (2005).

20 Xu, W. *et al.* Chemical Genetic Interaction Profiling Reveals Determinants of Intrinsic Antibiotic Resistance in Mycobacterium tuberculosis. *Antimicrob Agents Chemother* **61** (2017).

21 Mitra, A., Speer, A., Lin, K., Ehrt, S. & Niederweis, M. PPE Surface Proteins Are Required for Heme Utilization by Mycobacterium tuberculosis. *MBio* **8** (2017).

22 Zhang, L. *et al.* Comprehensive analysis of iron utilization by Mycobacterium tuberculosis. *PLoS Pathog* **16**, e1008337 (2020).

23 Paulina Knobloch, H. K.-B., Fabian M. Arnold, Nabil Hanna, Imre Gonda, Sophia Adenau, Nicolas Personnic, Caroline Barisch, Markus A. Seeger, Thierry Soldati, Hubert Hilbi. Mycobacterium marinum produces distinct mycobactin and carboxymycobactin siderophores to promote growth in broth and phagocytes. *Cellular Microbiology* **22**, e13163 (2020).

24 Gobin, J. & Horwitz, M. A. Exochelins of Mycobacterium tuberculosis remove iron from human iron-binding proteins and donate iron to mycobactins in the M. tuberculosis cell wall. *J Exp Med* **183**, 1527-1532 (1996).

25 Chao, A. & Goulding, C. W. A Single Mutation in the Mycobacterium tuberculosis Heme-Degrading Protein, MhuD, Results in Different Products. *Biochemistry* **58**, 489-492 (2019).

26 Thakuri, B. *et al.* The affinity of MhuD for heme is consistent with a heme degrading function in vivo. *Metallomics* **10**, 1560-1563 (2018).

27 Chu, B. C. & Vogel, H. J. A structural and functional analysis of type III periplasmic and substrate binding proteins: their role in bacterial siderophore and heme transport. *Biol Chem* **392**, 39-52 (2011).

28 Conger, M. A., Pokhrel, D. & Liptak, M. D. Tight binding of heme to *Staphylococcus aureus* IsdG and IsdI precludes design of a competitive inhibitor. *Metallomics* **9**, 556-563 (2017).

29 Owens, C. P., Du, J., Dawson, J. H. & Goulding, C. W. Characterization of heme ligation properties of Rv0203, a secreted heme binding protein involved in Mycobacterium tuberculosis heme uptake. *Biochemistry* **51**, 1518-1531 (2012).

30 Snyder, S. N. & Mak, P. J. Structure-function characterization of the mono- and diheme forms of MhuD, a noncanonical heme oxygenase from Mycobacterium tuberculosis. *J Biol Chem* **298**, 101475 (2022).

31 Arnesano, F. *et al.* Solution structure and characterization of the heme chaperone CcmE. *Biochemistry* **41**, 13587-13594 (2002).

32 Moeck, G. S., Coulton, J. W. & Postle, K. Cell envelope signaling in Escherichia coli. Ligand binding to the ferrichrome-iron receptor fhua promotes interaction with the energy-transducing protein TonB. *J Biol Chem* **272**, 28391-28397 (1997).

33 van Winden, V. J. C., Houben, E. N. G. & Braunstein, M. Protein Export into and across the Atypical Diderm Cell Envelope of Mycobacteria. *Microbiol Spectr* **7** (2019).

34 Berks, B. C. The twin-arginine protein translocation pathway. *Annu Rev Biochem* **84**, 843-864 (2015).

35 Mazmanian, S. K. *et al.* Passage of heme-iron across the envelope of Staphylococcus aureus. *Science* **299**, 906-909 (2003).

36 Zhu, H. *et al.* Pathway for Heme Uptake from Human Methemoglobin by the Iron-regulated Surface Determinants System of Staphylococcus aureus. *Journal of Biological Chemistry* **283**, 18450-18460 (2008).

37 Brillet, K. *et al.* An ABC transporter with two periplasmic binding proteins involved in iron acquisition in Pseudomonas aeruginosa. *ACS Chem Biol* **7**, 2036-2045 (2012).

38 Ganne, G. *et al.* Iron Release from the Siderophore Pyoverdine in Pseudomonas aeruginosa Involves Three New Actors: FpvC, FpvG, and FpvH. *ACS Chem Biol* **12**, 1056-1065 (2017).

39 Agarwal, S., Dey, S., Ghosh, B., Biswas, M. & Dasgupta, J. Structure and dynamics of Type III periplasmic proteins VcFhuD and VcHutB reveal molecular basis of their distinctive ligand binding properties. *Sci Rep* **7**, 42812 (2017).

40 Grigg, J. C., Vermeiren, C. L., Heinrichs, D. E. & Murphy, M. E. P. Haem recognition by a Staphylococcus aureus NEAT domain. *Molecular microbiology* **63**, 139-149 (2007).

41 Ho, W. W. *et al.* Holo- and Apo-bound Structures of Bacterial Periplasmic Heme-binding Proteins. *Journal of Biological Chemistry* **282**, 35796-35802 (2007).

42 Clarke, T. E., Ku, S. Y., Dougan, D. R., Vogel, H. J. & Tari, L. W. The structure of the ferric siderophore binding protein FhuD complexed with gallichrome. *Nat Struct Biol* **7**, 287-291 (2000).

43 Grigg, J. C., Cheung, J., Heinrichs, D. E. & Murphy, M. E. Specificity of Staphyloferrin B recognition by the SirA receptor from Staphylococcus aureus. *J Biol Chem* **285**, 34579-34588 (2010).

44 Grigg, J. C., Cooper, J. D., Cheung, J., Heinrichs, D. E. & Murphy, M. E. The Staphylococcus aureus siderophore receptor HtsA undergoes localized conformational changes to enclose staphyloferrin A in an arginine-rich binding pocket. *J Biol Chem* **285**, 11162-11171 (2010).

45 Cooper, J. D., Hannauer, M., Marolda, C. L., Briere, L. A. & Heinrichs, D. E. Identification of a positively charged platform in Staphylococcus aureus HtsA that is essential for ferric staphyloferrin A transport. *Biochemistry* **53**, 5060-5069 (2014).

46 Tian, W., Chen, C., Lei, X., Zhao, J. & Liang, J. CASTp 3.0: computed atlas of surface topography of proteins. *Nucleic Acids Res* **46**, W363-W367 (2018).

# CHAPTER 5

# *In vivo* Protein Partners of FecB Confirm Role in Siderophore-mediated Iron Uptake Pathway in *Mycobacterium tuberculosis*


## Abstract

The mechanisms of transport of iron across the periplasm of *Mycobacterium tuberculosis* (Mtb) are not well understood. Many bacteria utilize periplasmic binding proteins (PBPs) to facilitate the shuttling of iron containing compounds including siderophores and heme across the periplasmic space. In Mtb one of the putative PBPs, FecB, has been implicated in the transport of the Mtb siderophore, carboxymycobactin. Herein, we demonstrate that FecB interacts with known components of the siderophore export and import machinery with co-immunoprecipitation experiments in both *Mycobacterium smegmatis* as well as Mtb, providing the first direct evidence that FecB is involved in the siderophore-mediated iron uptake pathway in Mtb. The *Mycobacterium smegmatis* constructs were generated by Kadamba Papavinasasundaram in the Sassetti lab at UMass Chan Medical School, and the Mtb co-immunoprecipitation experiments were performed by Thaís Klevorn in the Ehrt lab at Weill Cornell Medical College.


## Introduction

Mtb utilizes both iron and heme uptake systems to ensure its survival.[1] Mtb has a relatively well-studied siderophore-dependent iron uptake system, where Mtb siderophores are termed mycobactin (MB) and carboxymycobactin (cMB).[2] MB and cMB are mixed-type siderophores with both phenolate and hydroxamate moieties (Figure 5.1a). While the two siderophores share an identical core [2,3], they differ in hydrophobicity and cellular localization. Owing to its long aliphatic tail, MB is hydrophobic and is thought to be cell-wall and outer membrane associated, though recent studies have observed MB in the culture filtrate as well as the cell-wall/membrane

environment (Figure 5.1a).[4,5] Whereas cMB, which is more hydrophilic than MB due to its shorter tail that terminates with a carboxylate group, is secreted and released from the mycobacterial cell to scavenge for host iron (Figure 5.1a).[6,7] The cytosolic biosynthetic pathways of MB and cMB have been well-characterized.[1,8] Once synthesized, the export of MB and cMB across the inner membrane is facilitated by MmpL4/5 along with their accessory proteins MmpS4/5[5], and a small periplasmic protein Rv0455c, whose precise function is unknown (Figure 5.1b).[9] Iron-loaded- or ferric-cMB (Fe-cMB) is imported across the inner membrane by the heterodimeric IrtA/IrtB (IrtAB) membrane transporter (Figure 5.1b).[10,11] However, the proteins involved in shuttling apo-forms of MB and cMB through the Mtb periplasm and potentially the outer membrane, as well as those that facilitate the transport of iron-loaded MB and cMB from the extracellular space to the inner membrane, are currently unknown. Even less is known about heme uptake in Mtb. Several studies implicate a variety of proteins within the heme uptake pathway by genetic or biochemical methods, which include the secreted protein Rv0203; the cell-surface proteins PPE36, PPE37, PE22, and PE62; a periplasmic binding protein, FecB2; and the DppABC inner-membrane complex dipeptide/heme transporter.[12-15] However, the precise role or mechanism of these proteins in heme acquisition is not fully understood.

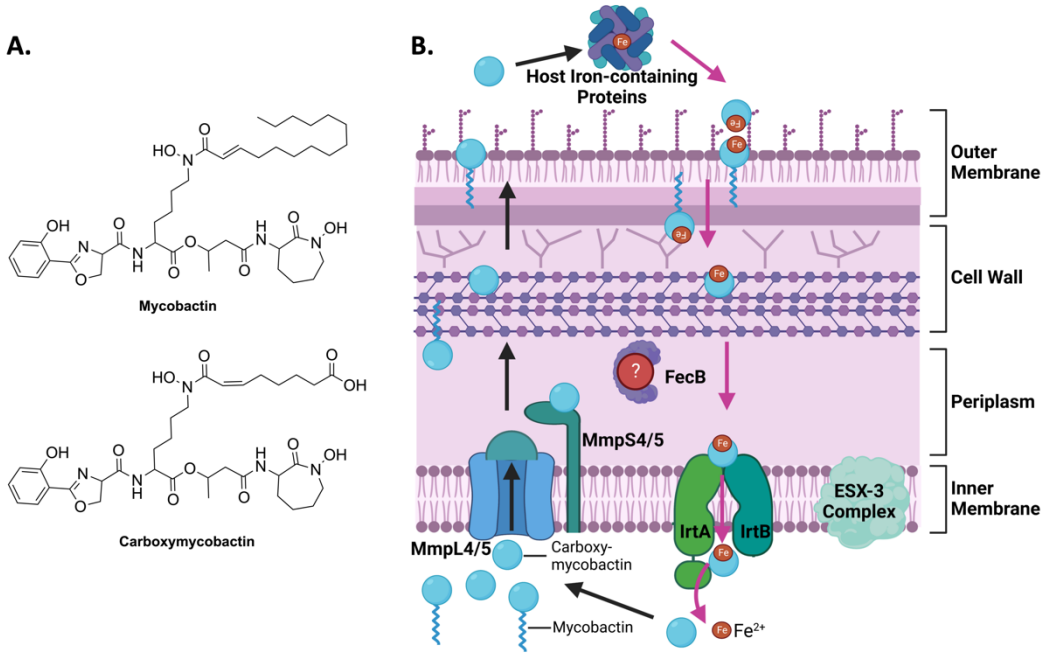


**Figure 5.1.** Chemical structures of Mtb siderophores MB and cMB (A), and representation of the proposed Mtb siderophore-mediated iron uptake pathway (B).

Given that Mtb is the causative agent of the disease tuberculosis (TB), and as iron is essential for the growth and survival of Mtb, targeting its iron/heme uptake pathways is a possible strategy to combat TB. For several decades, there have been on-going efforts to interrupt siderophore-mediated iron acquisition through the inhibition of MB and cMB biosynthesis.[16,17] However, the mechanisms of import and export of iron-scavenging siderophores and import of heme represent an alternate set of anti-TB drug targets. Thus, a more in-depth understanding of these import/export mechanisms at an atomic-level resolution is required.[18-20]

Utilizing both *Mycobacterium smegmatis* (Msm) and Mtb, we identified potential interacting proteins of FecB, placing Mtb FecB in the siderophore-dependent iron acquisition pathway. Finally, the atomic resolution structures of FecB and FecB2 could lead to the development of novel TB treatment strategies. The ligand-binding sites of FecB and FecB2 provide a template for inhibitor design to prevent the transport of iron containing molecules through the Mtb periplasmic space.

## Materials and Methods

### Cloning of M. smegmatis genes - fecB, mmpS4, and mmpS5

*M. smegmatis fecB* (MSMEG_2319), *mmpS4* (MSMEG_0380) and *mmpS5* (MSMEG_0226) coding sequences were amplified from Msm $mc^2155$ genomic DNA using Pfu Ultra Fusion HS DNA polymerase (Agilent) using recommended components and PCR cycle conditions. All these genes were expressed from the constitutive Ptb38 promoter and carried a FLAG epitope coding sequence at the 3' end.

The Msm *fecB* (MSMEG_2319) was cloned into the KanR mycobacterial expression vector pDE43-MEK using the Gateway cloning technology (Invitrogen, and as modified by Blumenthal et al., 2010), and Msm *mmpS4* (MSMEG_0380) and Msm *mmpS5* (MSMEG_0226) genes were assembled into a HygR mycobacterial expression plasmid using the NEBuilder HIFI DNA assembly (New England Biolabs). Appropriate control vectors lacking the coding sequences were prepared by restriction digestion and cloning in a set of annealed oligos. The expression plasmids and the control vectors were electroporated into Msm $mc^2155$ and selected on 7H10 plates supplemented with 25 μg/ml kanamycin or 50 μg/ml hygromycin, as appropriate. The descriptions of plasmids used in this study are listed in Table 5.1.

**Table 5.1.** List of plasmids used in this study (generated by the Sassetii Lab at the UMass Chan Medical School).

| Plasmids | Description | Antibiotic marker | Source |
|---|---|---|---|
| **pDE43-MEK** | Mycobacterial expression vector | $Kan^R$ | [21] |
| **pKP948** | MEK-Ptb38-RBS-fecB1 (MSMEG_2319)-FLAG. Used for the expression of *M. smegmatis* FecB1. | $Kan^R$ | This study |
| **pKP991 (control vector)** | MEK vector lacking the promoter, ORF and the tag. Created by cloning restriction | $Kan^R$ | This study |

| | | | |
|---|---|---|---|
| | sites between PacI and NdeI sites in pDE43-MEK. | | |
| **pDE43-MEH** | Mycobacterial expression vector | $Hyg^R$ | [21] |
| **pKP1230** | MEH-Ptb38-RBS-MmpS5 (MSMEG_0226)_TEV_FLAG. Used for the expression of *M. smegmatis* MmpS5. | $Hyg^R$ | This study |
| pKP1231 | MEH-Ptb38-RBS-MmpS4 (MSMEG_0380)_TEV_FLAG. Used for the expression of *M. smegmatis* MmpS4. | $Hyg^R$ | This study |
| pKP1234 (control vector) | MEH-Ptb38-MCS_TEV_FLAG. MEK control vector lacking the ORF but carrying the constitutive promoter, multiple cloning sites and the TEV-FLAG tag. | $Hyg^R$ | This study |
| pGMEK-$P_{hsp60}$-*fecB*-FLAG | Mycobacterial expression vector for FecB-FLAG | $Kan^R$ | This study |
| pGMCS-$P_{750}$-*mmpS5*-HA | Mycobacterial expression vector for MmpS5-HA | $Strep^R$ | This study |

**Co-immunoprecipitation of FLAG-tagged M. smegmatis constructs**

*M. smegmatis* variants were streaked on Middlebrook 7H10 agar plates supplemented with 10% albumin/dextrose/catalase (ADC), 0.05% Tween-80, and 50 μg/mL kanamycin and grown for 3 days at 37 °C. A single colony was then used to inoculate growth cultures in Middlebrook 7H9 media supplemented with 10% ADC, 0.05% Tween-80, and 50 μg/mL kanamycin and grown for 2 days at 37 °C before the cells were harvested by centrifugation at 5,000 rpm for 20 mins, and then washed twice with TBS (Tris-Buffered Saline, 50 mM Tris-HCl pH 7.4 + 150 mM NaCl). The cells were then resuspended in iron-free 7H9 media supplemented with 10% ADC, 0.05% Tween-80, and 50 μg/mL kanamycin and grown for an additional 2 days at 37 °C to deplete intracellular iron levels. The media was then supplemented with 20 μM ferric ammonium citrate and grown for a final 2 days at 37 °C before harvesting the cells by centrifugation at 5,000 rpm for

25 minutes. The cells were then resuspended and lysed in buffer (1 mL per 25 mg cell mass, 50 mM Tris-HCl pH 7.4, 350 mM NaCl, 10% glycerol) by sonication (60% amplitude, 15 seconds on, 45 seconds off, 10 cycles). N-dodecyl-β-D-maltoside, a mild detergent used for membrane protein research, was then added to a concentration of 1% w/v and incubated for 2 hours at 4 °C. To remove cellular debris the lysate was centrifuged at 14,000 rpm for 30 minutes and syringe filtered with a 0.1 μm filter. FLAG-tagged FecB and potential interacting partners were then precipitated using ANTI-FLAG M2 affinity gel slurry (Sigma) following manufacturer protocols. Briefly, 40 μL of resin slurry and lysate were incubated overnight at 4 °C before centrifuging for one minute at 2,500 rpm and washed 2x with 500 μL of TBS. The proteins were then eluted from the slurry by treating with 100 μL of 1% formic acid and heating at 95 °C for 10 minutes. The supernatant was then neutralized by adding 400 μL of 50 mM ammonium bicarbonate. The proteins were then treated with 0.5 mg/mL dithiothreitol for 30 minutes at 80 °C, followed by treatment with 0.5 mg/mL iodoacetamide for one hour in the dark. The proteins were then digested using 1.5 ng/μL of trypsin and incubated overnight at 37 °C. The peptides were then de-salted using Sep-Pak C18 cartridges (Waters) following manufacturer protocols to prepare them for mass spec analysis.

**Mass spectrometry data acquisition**

Proteomics data were acquired via liquid chromatography (LC)-MS/MS using an UltiMate 3000 UHPLC (Thermo Fisher Scientific) coupled in-line with an Orbitrap Fusion Lumos mass spectrometer (Thermo Fisher Scientific) using a Nanospray Flex ion source. Mobile phase A is comprised of 0.1% FA in water, while mobile phase B is 0.1% FA in ACN. The total flow rate was 300 nL $min^{-1}$, and the C18-cleaned peptides were separated over a 57 min gradient from 4% to 25% buffer B (total run time is 90 min) on an Acclaim PepMap RSLC column (50 cm x 75 μm).

Survey (MS1) scans were acquired in Orbitrap (FT) with automated gain control (AGC) target 1E6, maximum injection time 50 ms, and dynamic exclusion of 60 s after 2 selections across the scan range of 375-1800 m/z. MS/MS spectra were acquired in data-dependent acquisition mode at top speed for 3 s per cycle. The AGC target was set to 1E4 with maximum injection time of 35 ms. Ions were subjected to stepped-energy higher-energy collision dissociation (seHCD) fragmentation at a normalized collision energy (NCE) of 20±5%.

**MaxQuant Protein Identification**

The raw LC-MS/MS data files were analyzed using MaxQuant (version 1.5.2.8), with the spectra searched against the Uniprot *M. smegmatis* database (updated June 2018). For identification of the peptides, the mass tolerances were 20 ppm for initial precursor ions and 0.5 Da for fragment ions. Two missed cleavages in tryptic digests were allowed. Cysteine residues were set as static modification. Oxidation of methionine was set as the variable modification. Filtering for the peptide identification was set at a 1% false discovery rate (FDR).

**Co-immunoprecipitation of FLAG- or HA-tagged Mtb proteins**

For co-immunoprecipitation of *M. tuberculosis* proteins, *fecB* (*rv3044*) was synthesized with a C-terminal FLAG-tag (GenScript) and cloned via Gateway cloning technology (Invitrogen) under control of the hsp60 promoter on an episomal plasmid. *MmpS5* (*rv0677c*) was synthesized with a C-terminal HA-tag and expressed under control of a synthetic promoter (P750) on a plasmid that integrates into the attL5 site of the Mtb genome.

150 mL of Mtb$\Delta$*fecB*[22] culture transformed with pGMEK-$P_{hsp60}$-*fecB*-FLAG and pGMCS-$P_{750}$-*mmpS5*-HA was grown in roller incubator until the culture reached $OD_{580}$=1. The bacteria were collected by centrifugation at 4000 rpm, 8 min, 4°C, followed by resuspension in 20 mL PBS 0.05% Tween 80. After a second centrifugation step (4000 rpm, 8 min, 4°C), the pellet was

resuspended in 1.2 mL of lysis buffer (50 mM Tris-HCl pH7.4, 50 mM NaCl) with protease inhibitor (Roche cOmplete, Mini, EDTA-free protease inhibitor cocktail, Cat. # 11836170001). 600 mL of suspension was bead-beaten with ~"300 mL" of zirconia beads 4 times for 30 seconds each, with chilling on cold rack between each round. Lysates were centrifuged at 11,000 x g, 5 min, 4°C to remove unbroken cells and insoluble material. An aliquot of the lysate fraction was saved for Western-blot and the rest was added either to 50 mL slurry of "FLAG" magnetic agarose (Thermo Scientific Pierce™ Anti-DYKDDDDK Magnetic Agarose, Cat. # A36798) that had been pre-washed in lysis buffer according to the manufacturer's protocol, or to 25 mL of HA magnetic beads (Thermo Scientific Pierce™ Anti-HA Magnetic Beads, Cat. # 88836) that had been pre-washed in 0.05% TBS-T (Tris-Buffered Saline, 50 mM Tris-HCl pH 7.4 + 150 mM NaCl, with 0.05% of Tween 20) according to the manufacturer's protocol. Lysates were incubated with magnetic agarose/beads for 1 hr at room temperature on a rotating platform. After incubation, the flow-through fraction was collected using a magnetic stand and subsequent washing steps were performed according to the magnetic agarose/bead manufacturer's protocol. The elution of immunoprecipitated proteins was performed first with addition of (i) 1.5 mg/mL Pierce 3x DYKDDDDK Peptide (in PBS) to "FLAG" magnetic agarose, or (ii) 2 mg/mL Pierce HA Peptide (in TBS) to HA magnetic beads, which were incubated for 10 min at room temperature on a rotating platform. Further recovery of immunoprecipitated proteins was obtained by resuspending magnetic agarose/beads in PBS with 4x Laemmli sample buffer (Bio-Rad Cat. # 1610747) containing 2-mercaptoethanol and boiling for 10 min at 95°C. 1:4 dilution of 4x Laemmli sample buffer containing 2-mercaptoethanol was also added to all other fractions (lysate, flow-through and eluate) which were also boiled for 10 min at 95°C. Samples were stored at -80°C prior to running the western-blots to detect the proteins of interest.

**Western-Blot to detect FLAG and HA tagged proteins**

Samples were thawed and boiled at 95°C for 10min prior to loading on a 4-20% precast polyacrylamide gel (Bio-Rad Mini-PROTEAN® TGX™ Precast Protein Gels, Cat. # 4561094). After running at 100 V for 60 min, proteins were transferred to a nitrocellulose membrane (Invitrogen iBlot™ 2 Transfer Stacks, Cat. # IB23001) in an iBlot2 dry blotting system (Invitrogen, Cat. # IB21001). Membranes were blocked with Intercept (TBS) Blocking Buffers (Li-Cor Cat. # 927-40000) for 1 hr at room temperature, followed by incubation with primary antibodies anti-FLAG (monoclonal anti-FLAG M2, Sigma Cat. # F3165-5MG, at 1:800) or anti-HA (HA Tag Monoclonal Antibody 2-2.2.14, Invitrogen Cat. # 26183, at 1:10,000) or polyclonal anti-FecB antiserum (at 1:5000 dilution; produced by Thermofisher) in dilution buffer (1:1 PBS:Intercept buffer plus 0.1% Tween 20) on a rocking platform, at 4°C, overnight. After washing the primary antibody with PBS 0.1% Tween 20 three times, membranes were incubated with a fluorescent secondary antibody (Goat anti-Mouse IgG (H+L) Cross-Adsorbed Secondary Antibody DyLight800, Thermo Fisher Cat. # SA5-10176, or IRDye 680LT Donkey anti-rabbit, Thermo Fisher Cat # SA5-10042 at 1:10,000 in dilution buffer) for 1h at room temperature on a rocking platform. After three washes with PBS 0.1% Tween 20, the membranes were visualized using the Azure 600 Imaging System.

## Results

***Investigation into the Protein Interaction Partners of FecB***

As shown in Chapter 4, FecB appears to bind both Fe-cMB and heme; however, FecB binds Fe-cMB with a higher affinity than heme. To better understand the role that FecB plays in mycobacterium iron acquisition, we sought to identify FecB interacting protein partners *in vivo*. To achieve this, we utilized co-immunoprecipitation (co-IP) followed by protein identification

using tandem mass spectrometry (MS/MS) in the non-pathogenic Mtb model organism, *Mycobacterium smegmatis* $mc^2155$ (Msm). The closest Msm homolog to Mtb FecB, Msmeg_2319 (63% sequence identity) was cloned to encode a C-terminal FLAG tag.[23] With the intention of upregulating the iron acquisition machinery, Msm cultures were first grown under iron deplete condition before supplementing with low iron (20 μM ferric ammonium citrate), and a control consisting of Msm bearing a FLAG expressing vector was run in tandem. As FecB is a periplasmic protein, we limited our search to predicted periplasmic proteins, and membrane proteins and complexes. The resulting co-IP of Msm-FecB-FLAG lysate with anti-FLAG beads, followed by MS/MS revealed potential Msm-FecB-FLAG interacting protein partners that were not observed in the control co-IP.

Several identified interacting partners of FecB suggest that it is involved in siderophore-dependent iron acquisition (Table 5.2). One of the interacting proteins of FecB is IrtB, which together with IrtA forms the heterodimeric inner membrane complex (IrtAB) that imports Fe-cMB into the mycobacterial cytosol.[10,11] Another interactor is MmpL5, where MmpL5 is an inner membrane protein involved in the export of Mtb siderophores.[5] We also observed MmpS5 and MmpS4 as FecB interacting candidates, which are known accessory proteins of MmpL5 and its family member MmpL4, respectively.[5] Finally, we identified one of the subunits involved in the ESX-3 complex, EccE3, where ESX-3 is a Type VII secretion system known to be involved in iron and heme homeostasis.[4,24,25] Several interacting partners are involved in the upregulation of iron sequestration machinery, indicating that FecB is involved in Mtb apo-siderophore export, ferric-siderophore import, or both.

**Table 5.2.** Top periplasmic and membrane protein hits from Msm co-IPs with FecB-FLAG

| Protein | Msm # | Mtb # | Coverage | Spectral Counts |
|---|---|---|---|---|
| **FecB** | **MSMEG_1039/2319** | **Rv3044** | **87.1%** | **953** |
| MmpS5 | MSMEG_0226 | Rv0677c | 26% | 4 |
| IrtB | MSMEG_6553 | Rv1349 | 6.9% | 4 |
| MmpS4 | MSMEG_0380 | Rv0451c | 41% | 11 |
| MmpL5 | MSMEG_0225 | Rv0676c | 2.7% | 2 |
| EccE3 | MSMEG_0626 | Rv0292 | 8.7% | 5 |

To corroborate our co-IP results, we performed reverse co-IPs with the small periplasmic proteins, MmpS4 and MmpS5. As Msm has several homologs of Mtb MmpS4 and MmpS5, we used the closest Msm homolog to Mtb MmpS4 and MmpS5 as the bait proteins: MSMEG_0380 (Msm-MmpS4, 60% sequence identity) and MSMEG_0226 (Msm-MmpS5, 57% sequence similarity), respectively. As with Msm-FecB, both Msm-MmpS4 and Msm-MmpS5 were engineered to encode C-terminal FLAG tags. Msm cells containing the Msm-MmpS4-FLAG or Msm-MmpS5-FLAG vectors were grown under similar conditions to the Msm-FecB-FLAG experiment, followed by co-IPs and protein identification by MS/MS. For both Msm-MmpS4-FLAG and Msm-MmpS5-FLAG lysates, the reverse co-IP results indicated that Msm-FecB is an interacting protein partner (Table 5.3a,b). These results corroborate that FecB does indeed interact with MmpS4 and MmpS5 in Msm *in vivo* and lends credence to the original co-IP interacting partners described above.

**Table 5.3.** Top periplasmic and membrane protein hits from Msm co-IPs with (A) MmpS4-FLAG, and (B) MmpS5-FLAG.

**A.**

| Protein | Msm # | Mtb # | Coverage | Spectral Counts |
|---|---|---|---|---|
| **MmpS4** | **MSMEG_0380** | **Rv0451c** | **97.1%** | **294** |
| FecB | MSMEG_1039/2319 | Rv3044 | 15.4% | 5 |

**B.**

| Protein | Msm # | Mtb # | Coverage | Spectral Counts |
|---|---|---|---|---|
| **MmpS5** | **MSMEG_0226** | **Rv0676c** | **80.3%** | **54** |
| FecB | MSMEG_1039/2319 | Rv3044 | 25.2% | 12 |

***FecB Interacts with MmpS5 in Mtb***

To determine if FecB interacts with MmpS5 in a pathogenic mycobacterium, the Ehrt lab tested this protein-protein interaction in Mtb utilizing co-IP experiments followed by western blot. Using the Mtb$\Delta$*fecB* variant[22], we introduced two vectors: the first encoded a C-terminal FLAG tagged FecB and the second encoded a C-terminal hemagglutinin (HA) tagged MmpS5. We used WT Mtb with vectors only expressing the tags alone as the control. Cells were grown in regular 7H9 media and co-IPs were performed from cell lysates with anti-FLAG beads and anti-HA beads. Western blots were carried out and were blotted with either anti-FLAG or anti-HA primary antibodies, or anti-FecB antiserum (data not shown). The western blot of the co-IP using FecB-FLAG as the bait protein and analyzed with anti-HA primary antibody showed a band corresponding to MmpS5 from the eluted anti-FLAG beads (Figure 5.2a), indicating FecB pulled down MmpS5. The reverse experiment, in which MmpS5-HA was used as the bait protein, and probed with anti-FLAG primary antibody, showed an eluted band corresponding to FecB (Figure 5.2b), indicating MmpS5 pulled down FecB. Finally, when the Western blot of the eluted anti-HA beads that pulled down MmpS5-HA (data not shown) was probed with anti-FecB antiserum, a

clear band corresponding to FecB was observed (Figure 5.2c), reinforcing the results that MmpS5 binds to FecB. These results confirmed the above observation in the Msm FecB co-IP experiments, and suggest that Mtb FecB interacts with Mtb MmpS5 *in vivo*.

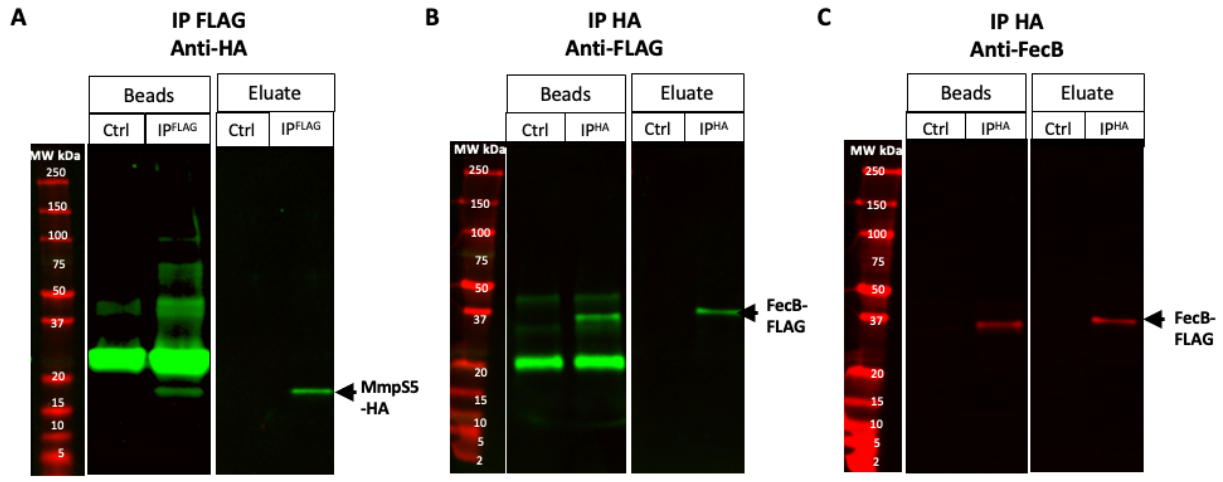


**Figure 5.2.** Western Blot analysis of Mtb co-IPs suggest that FecB interacts with MmpS5. Western Blot analysis of protein co-IPs with Mtb∆*fecB* with vectors expressing FecB-FLAG and MmpS5-HA, and the negative control whereby Mtb contains vectors that express the tags alone. Western Blot analysis of both the boiled beads and eluate of the (A) co-IP using the anti-FLAG beads to pull down FecB-FLAG, probed with an anti-HA antibody that recognizes MmpS5-HA, (B) co-IP using the anti-HA beads to pull down MmpS5-HA, probed with an anti-FLAG antibody that recognizes FecB-FLAG, and (C) co-IP using the anti-HA beads to pull down MmpS5-HA, probed with an anti-FecB antiserum that recognizes FecB.

## Discussion

The role FecB plays in the Mtb periplasm has been a source of controversy in the field, therefore we set out to determine the protein-interaction partners of FecB in the cell utilizing co-IP experiments in Msm and Mtb. The FecB protein-protein interaction experiments described herein place FecB in the cMB-mediated iron acquisition pathway. Further, as FecB binds Fe-cMB *in vitro*, there is strong evidence for the involvement of FecB in Fe-cMB import. It should be noted that previously under iron-limiting and iron-replete conditions the Mtb∆*fecB* mutant did not display major growth defects relative to the wild-type Mtb, suggesting that it is not essential for iron acquisition.[22] This indicates that there may be functional redundancy in the Mtb proteome

whereby another protein can also play a similar role as FecB in iron acquisition. Interestingly, *E. coli* FecB is part of the larger Fec system that sequesters ferric citrate from the host and shuttles it to the cytosol.[26] The Fec system consists of a TonB-dependent outer membrane receptor (FecA) and an inner membrane ABC transporter FecCDE complex, which interacts with periplasmic FecB. In contrast, Mtb, apart from FecB and FecB2, does not encode any homologs of other Fec system proteins. Instead, in the Msm FecB co-IP experiment, we observe that IrtB is an interaction partner of FecB. IrtA and IrtB form the heterodimeric inner membrane ATP-dependent transporter that imports Fe-cMB into the mycobacterial cytosol (Table 5.2).[10,11] We propose that Fe-cMB loaded FecB docks to the periplasmic side of IrtAB and induces a conformational change in IrtAB to facilitate ATP-dependent import of Fe-cMB to the cytosol.

FecB is not only implicated in Fe-cMB import; this study also supports the involvement of FecB in cMB export. In both the Msm and Mtb FecB co-IP experiments, we observe MmpS5 as a FecB interacting partner, and MmpS4 was observed in Msm co-IP experiments (Table 5.2). The inverse co-IPs with MmpS4 or MmpS5 confirm that they interact directly or indirectly with FecB (Table 5.2). MmpS4 and MmpS5 are essential periplasmic accessory proteins of the inner membrane cMB/MB exporters MmpL4 and MmpL5[5], suggesting that FecB may also play a role in cMB efflux. In mycobacteria, MmpL proteins are important inner membrane exporters of essential cell-wall polysaccharide and lipid components along with MB and cMB.[27,28] However, once MmpL proteins transport these small molecules into the periplasm, little is known about the final translocation or incorporation of these molecules into the cell-wall and outer membrane architectures. While some Gram-negative bacteria couple inner membrane efflux pumps with TolC channels that span the outer membrane to secrete siderophores into the extracellular environment[29,30], Mtb does not possess a TolC homolog so this avenue is not available. Two

components have been implicated in the extracellular export or cell-wall incorporation of these small molecules. First, a small helical periplasmic protein, Rv0455c, was recently shown to be important in the secretion of Mtb siderophores into the extracellular space.[9] Second, some lipoproteins are thought to be involved in the efflux of small molecules via unknown mechanisms.[28] For example, the lipoprotein LpqN is a putative periplasmic transporter of trehalose monomycolate, an important inner and outer membrane lipid.[31] We propose, as FecB directly or indirectly interacts with MmpS4/5, that FecB could chaperone Mtb apo-siderophores across the periplasm.

As discussed above, our results indicate that FecB could be involved in both the export of cMB and the import of Fe-cMB. Although most PBPs are thought to bind only ferric-siderophores, several PBPs appear to bind both their iron-loaded and iron-free siderophores.[32,33] Furthermore, recognition of apo- and iron-bound siderophores appears to be a common feature of *P. aeruginosa* and *E. coli* outer membrane β-barrel siderophore transporters.[34,35] Notably, *P. aeruginosa* utilizes a complex of two PBPs, FpvF and FpvC, that forms when bound to the *Pseudomonas* ferric-siderophore, $Fe^{3+}$-pyoverdine, and shuttles it through the periplasm to the inner membrane, where ferric iron is reduced to ferrous iron and imported into the cytosol. FpvF also shuttles the apo-siderophore to the siderophore export system.[33,36] *E. coli* FecB (25% sequence identity to Mtb FecB) binds both ferric-citrate and citrate, although ferric-citrate is bound with higher affinity than citrate alone.[32] While FecB appears to be involved in both apo-cMB export and iron-bound cMB import, and we have shown that FecB binds Fe-cMB *in vitro* (See Chapter 4), it remains to be seen if FecB can bind both forms of cMB *in vitro* or *in vivo*. Because Mtb relies on host-acquired iron for survival and growth, iron acquisition pathways are attractive drug targets. A comprehensive transposon mutagenesis study undertaken by the Niederweis group[37] showed that a *fecB*

transposon mutant had a growth defect when grown with Fe-cMB as the sole iron source, indicating that FecB may play a role in utilizing Fe-cMB. The data presented herein have shown that FecB intereacts with known components of the siderophore import and export machinery, demonstrating direct evidence for the first time that FecB is involved in Fe-cMB utilization in Mtb.

## References


1 Chao, A., Sieminski, P. J., Owens, C. P. & Goulding, C. W. Iron Acquisition in Mycobacterium tuberculosis. *Chem Rev* **119**, 1193-1220 (2019).

2 Ratledge, C. Iron, mycobacteria and tuberculosis. *Tuberculosis (Edinb)* **84**, 110-130 (2004).

3 De Voss, J. J., Rutter, K., Schroeder, B. G. & Barry, C. E., 3rd. Iron acquisition and metabolism by mycobacteria. *J Bacteriol* **181**, 4443-4451 (1999).

4 Tufariello, J. M. *et al.* Separable roles for Mycobacterium tuberculosis ESX-3 effectors in iron acquisition and virulence. *Proc Natl Acad Sci U S A* **113**, E348-357 (2016).

5 Wells, R. M. *et al.* Discovery of a siderophore export system essential for virulence of Mycobacterium tuberculosis. *PLoS Pathog* **9**, e1003120 (2013).

6 Gobin, J. *et al.* Iron acquisition by Mycobacterium tuberculosis: isolation and characterization of a family of iron-binding exochelins. *Proc Natl Acad Sci U S A* **92**, 5189-5193 (1995).

7 Wong, D. K., Gobin, J., Horwitz, M. A. & Gibson, B. W. Characterization of exochelins of Mycobacterium avium: evidence for saturated and unsaturated and for acid and ester forms. *J Bacteriol* **178**, 6394-6398 (1996).

8 Madigan, C. A. *et al.* Lipidomic discovery of deoxysiderophores reveals a revised mycobactin biosynthesis pathway in Mycobacterium tuberculosis. *Proc Natl Acad Sci U S A* **109**, 1257-1262 (2012).

9 Zhang, L. *et al.* A periplasmic cinched protein is required for siderophore secretion and virulence of Mycobacterium tuberculosis. *Nat Commun* **13**, 2255 (2022).

10 Arnold, F. M. *et al.* The ABC exporter IrtAB imports and reduces mycobacterial siderophores. *Nature* **580**, 413-417 (2020).

11 Rodriguez, G. M. & Smith, I. Identification of an ABC transporter required for iron acquisition and virulence in Mycobacterium tuberculosis. *J Bacteriol* **188**, 424-430 (2006).

12 Mitra, A., Ko, Y. H., Cingolani, G. & Niederweis, M. Heme and hemoglobin utilization by Mycobacterium tuberculosis. *Nat Commun* **10**, 4260 (2019).

13 Mitra, A., Speer, A., Lin, K., Ehrt, S. & Niederweis, M. PPE Surface Proteins Are Required for Heme Utilization by Mycobacterium tuberculosis. *MBio* **8** (2017).

14 Tullius, M. V. *et al.* Discovery and characterization of a unique mycobacterial heme acquisition system. *Proc Natl Acad Sci U S A* **108**, 5051-5056 (2011).

15 Tullius, M. V., Nava, S. & Horwitz, M. A. PPE37 Is Essential for Mycobacterium tuberculosis Heme-Iron Acquisition (HIA), and a Defective PPE37 in Mycobacterium bovis BCG Prevents HIA. *Infect Immun* **87** (2019).

16 Shyam, M., Shilkar, D., Rakshit, G. & Jayaprakash, V. Approaches for targeting the mycobactin biosynthesis pathway for novel anti-tubercular drug discovery: where we stand. *Expert Opin Drug Discov*, 1-17 (2022).

17 Shyam, M. *et al.* The Mycobactin Biosynthesis Pathway: A Prospective Therapeutic Target in the Battle against Tuberculosis. *J Med Chem* **64**, 71-100 (2021).

18 Mislin, G. L. & Schalk, I. J. Siderophore-dependent iron uptake systems as gates for antibiotic Trojan horse strategies against Pseudomonas aeruginosa. *Metallomics* **6**, 408-420 (2014).

19 Owens, C. P., Chim, N. & Goulding, C. W. Insights on how the Mycobacterium tuberculosis heme uptake pathway can be used as a drug target. *Future medicinal chemistry* **5**, 1391-1403 (2013).

20 Wilson, B. R., Bogdan, A. R., Miyazawa, M., Hashimoto, K. & Tsuji, Y. Siderophores in Iron Metabolism: From Mechanism to Therapy Potential. *Trends Mol Med* **22**, 1077-1090 (2016).

21 Blumenthal, A., Trujillo, C., Ehrt, S. & Schnappinger, D. Simultaneous analysis of multiple Mycobacterium tuberculosis knockdown mutants in vitro and in vivo. *PLoS One* **5**, e15667 (2010).

22 Xu, W. *et al.* Chemical Genetic Interaction Profiling Reveals Determinants of Intrinsic Antibiotic Resistance in Mycobacterium tuberculosis. *Antimicrob Agents Chemother* **61** (2017).

23 Ehrt, S. *et al.* Controlling gene expression in mycobacteria with anhydrotetracycline and Tet repressor. *Nucleic Acids Res* **33**, e21 (2005).

24 Serafini, A., Pisu, D., Palu, G., Rodriguez, G. M. & Manganelli, R. The ESX-3 secretion system is necessary for iron and zinc homeostasis in Mycobacterium tuberculosis. *PLoS One* **8**, e78351 (2013).

25 Siegrist, M. S. *et al.* Mycobacterial Esx-3 is required for mycobactin-mediated iron acquisition. *Proc Natl Acad Sci U S A* **106**, 18792-18797 (2009).

26 Braun, V. & Mahren, S. Transmembrane transcriptional control (surface signalling) of the Escherichia coli Fec type. *FEMS Microbiol Rev* **29**, 673-684 (2005).

27 Domenech, P., Reed, M. B. & Barry, C. E., 3rd. Contribution of the Mycobacterium tuberculosis MmpL protein family to virulence and drug resistance. *Infect Immun* **73**, 3492-3501 (2005).

28 Jackson, M., Stevens, C. M., Zhang, L., Zgurskaya, H. I. & Niederweis, M. Transporters Involved in the Biogenesis and Functionalization of the Mycobacterial Cell Envelope. *Chem Rev* **121**, 5124-5157 (2021).

29 Bleuel, C. *et al.* TolC is involved in enterobactin efflux across the outer membrane of Escherichia coli. *J Bacteriol* **187**, 6701-6707 (2005).

30 Furrer, J. L., Sanders, D. N., Hook-Barnard, I. G. & McIntosh, M. A. Export of the siderophore enterobactin in Escherichia coli: involvement of a 43 kDa membrane exporter. *Mol Microbiol* **44**, 1225-1234 (2002).

# CHAPTER 6

## Summary and Future Directions: Furthering our Understanding of Heme and Iron Acquisition Pathways in *Mycobacterium tuberculosis*

Iron acquisition systems in *Mycobacterium tuberculosis* have been of interest for their potential use as therapeutic targets as iron is known to be essential for the growth and persistence of Mtb infection.[1,2] To acquire this iron, Mtb utilizes two main iron acquisition pathways: 1) a siderophore-mediated pathway in which Mtb secretes small molecules that scavenge host iron, and 2) a heme uptake pathway in which Mtb directly imports heme and degrades it in the cytosol to release free iron.[2] Many stages of both pathways remain unknown, such as how heme and iron-bound siderophores are transported across the cell wall and periplasmic environments to the inner membrane, as well as the ultimate fate of the product of cytosolic heme degradation. Herein, I take steps towards filling in these knowledge gaps.

In Chapter 2, I describe the potential importance of a novel motif seen in the co-crystal complex of a MhuD mutant, R26S, in complex with its product α-biliverdin (αBV).[3] My co-authors on the manuscript solved the MhuD-R26S-αBV X-ray crystal structure and noted that the conserved $^{75}$HisXXXArg$^{79}$ motif amongst IsdG-like heme degrading proteins, may stabilize the formation of a novel α-helical element, α3, and used molecular dynamics simulations to probe its biological relevance.[3] In the MhuD-R26S-αBV structure five stacked molecules of αBV link to adjacent monomers of MhuD.[3] To probe if this was biologically relevant I utilized size-exclusion chromatography on MhuD-R26S-BV and found that in solution this protein complex exists solely in its dimeric form, demonstrating that this linkage by stacked αBV was a crystallographic artifact. To further investigate the importance of the $^{75}$HisXXXArg$^{79}$ motif I generated a R79S variant and tested its ability bind and degrade heme. Interestingly, the R79S mutant seems to cause increased

heme ruffling as evidenced by the red-shift of the Soret and Q-band regions as compared to wild-type MhuD.[4,5] To test if the formation of the new secondary structure element, α3 after turnover of IsdG-like heme degrading enzymes is a conserved, we sought to determine a product analogue amenable to co-crystallography with *Staphylococcus aureus* IsdI. To that end, I generated β- and δBV isomers and compared their affinity to IsdI to that of αBV. Both isomers bound >150-fold tighter than αBV in the 30 nM range, indicating they are excellent candidates for co-crystallographic trials; however, crystallography requires mg quantities of small molecules, and the ascorbic-acid mediated chemical cleavage of heme was only generating μg amounts. There is a novel way of generating β- and δBV that leverages the heme oxygenase (HemO) from *Pseudomonas aeruginosa* in a specialized strain of *E. coli* with upregulated heme importers (T7 Nissle) which secretes these isomers to the media pioneered by the Wilks lab.[6] Utilizing this methodology, future work will focus on generating sufficient quantities of β- or δBV isomers to carryout co-crystallization trials with IsdI, with the hope that structure determination of the IsdI-β/δBV complex will provide evidence of the a new α3 compared to the structure of IsdI/heme complex, and will be the first steps towards examining the biological relevance of this secondary structural element.

In Chapter 3, I shift towards identifying the fate of the tetrapyrrole product generated in MhuD-mediated heme degradation, mycobilin. Previous studies had identified four putative biliverdin reductases (BVRs) in Mtb, Rv1155, Rv2074, Rv2991, and Rv3547.[7,8] I tested each of them for BVR activity, and only Rv2074 was able to readily reduce αBV to bilirubin (BR). Both Rv1155 and Rv2074 had been investigated for BVR activity previously, and these results agreed with those previously published.[7,8] These putative Mtb BVRs were then tested for mycobilin reductase activity, and again it was found that only Rv2074 showed activity. I then further analyzed

the product formed to determine its chemical structure by mass spectrometry and found that, similar to BV reduction to BR, mycobilin is reduced at the ɣ-meso-carbon of the porphyrin ring forming a novel product which has been coined "mycorubin."[7]

Together, Chapters 2 and 3 suggest that upon turnover of MhuD, the formation of α3 could stabilize protein-protein interactions to facilitate MhuD product removal followed by the reduction of mycobilin to 'mycorubin' in a manner similar to that observed with human heme oxygenase and BVR.[9] To test this, protein-protein interaction studies with mycobilin-bound MhuD and Rv2074 need to be undertaken to see if Rv2074 is able to remove mycobilin bound to MhuD, this will be monitored with UV/vis spectroscopy. To determine if MhuD R79, whereby R79 has been proposed to stabilize the new α3 via a hydrogen-bonding network, is necessary for this transfer to occur the experiment could be performed both with WT MhuD and the R79S variant – discussed in Chapter 2. This, combined with crystallographic studies would provide deeper insight into the mechanism of product removal and turnover in IsdG-like heme degrading enzymes. Further work is also required to determine the physiological role of mycorubin, which could serve as a potent antioxidant in much the same manner as bilirubin protects the cell from reactive oxygen species.[10–12]

Mtb periplasmic binding proteins FecB and FecB2 have been implicated in host iron acquisition; however, their precise roles are not well understood.[2] In Chapters 4 and 5 we sought to differentiate the roles FecB and FecB2 play in Mtb iron acquisition. In Chapter 4, the crystallographic structures of Mtb FecB and FecB2 were determined were determined by my coauthors to 2.0 Å and 2.2 Å resolution, respectively, and show distinct ligand binding pockets. *In vitro* ligand binding experiments for FecB and FecB2 were performed with heme and ferric-carboxymycobactin (Fe-cMB), revealing that both FecB and FecB2 bind heme, while only FecB

binds Fe-cMB. Subsequent structure-guided mutagenesis of the FecB ligand binding site identified a single glutamate residue—Glu339—that significantly contributes to Fe-cMB binding. Furthermore, FecB was investigated for its ability to bind to other bacterial siderophores as well as several antibiotics, and showed little to no binding of all compounds tested. These antibiotics were investigated as it had been previously shown that a Mtb∆*fecB* variant had increased resistance to meropenem, vancomycin, and rifampin; however, the binding studies showed little to no direct binding of these compounds, which indicates that this resistance mechanism in the Mtb∆*fecB* variant is not due to loss of periplasmic transport by FecB and is instead more indirect.[13] Further work is needed to determine how FecB coordinates to Fe-cMB. To that end, crystallographic studies of FecB in complex with Fe-cMB would increase our understanding of FecB-mediated Fe-cMB transport.

In Chapter 5. *in vivo* interaction experiments performed with FecB in *Mycobacterium smegmatis* showed interactions with known members of the mycobacterial siderophore export and import machinery, placing FecB in the Mtb siderophore-mediated iron acquisition pathway. Finally, the FecB interacting partner MmpS5, part of the apo-siderophore export complex, was corroborated in Mtb by co-immunoprecipitation by my coauthors. Ultimately, due to ligand preference and protein partners, our data suggest that Mtb FecB plays a role in siderophore-dependent iron acquisition pathways; whereas Mtb FecB2 is likely to be involved in the heme uptake pathway. MmpS4 and MmpS5 are the only *in vivo* interacting partners of FecB that have been verified by reciprocal immunoprecipitation. Further work is needed to verify interactions with the Fe-cMB iron import machinery, IrtAB, which could include generating soluble periplasmic domain constructs of this complex to examine for interactions with FecB using biolayer interferometry or isothermal titration calorimetry. Furthermore, now that MmpS5 has

been confirmed to interact with FecB in both *M. smegmatis* and Mtb, the protein-protein interaction strength, and interface need to be determined particularly in the presence and absence of cMB to determine if the protein-protein interaction requires the presence of cMB.

Together in Chapters 4 and 5, we have greatly expanded the knowledge on Mtb FecB. We have solved the structure of FecB and determined its ligand specificity. Furthermore, we have also solved the structure of FecB2 and confirmed that it preferentially binds heme over Fe-cMB. Using this structural information, one could utilize FecB and FecB2 to overcome the difficulty of cellular entry for many Mtb drugs. For example, Mtb could be therapeutically targeted with a drug that is specifically recognized by FecB, and shuttled across the periplasm to the Fe-cMB import machinery as has been done in *P. aeruginosa*.[14] We have also shown that FecB interacts with known components of the siderophore-mediated iron acquisition pathway, and that it potentially plays a dual role in both siderophore export and import. With this information, other avenues for therapeutic development include preventing interactions between FecB and other components of the Mtb iron acquisition machinery to limit iron availability.[15] These strategies could weaken or kill Mtb or act synergistically with other TB treatments allowing for more efficacious combinatorial therapies to help combat the rising infection and death counts of TB.

## References


1. Ratledge, C. Iron, mycobacteria and tuberculosis. *Tuberculosis (Edinb)* **84**, 110–130 (2004).
2. Chao, A., Sieminski, P. J., Owens, C. P. & Goulding, C. W. Iron Acquisition in Mycobacterium tuberculosis. *Chem Rev* **119**, 1193–1220 (2019).
3. Chao, A. *et al.* Structure of a Mycobacterium tuberculosis Heme-Degrading Protein, MhuD, Variant in Complex with Its Product. *Biochemistry* **58**, 4610–4620 (2019).
4. Graves, A. B., Graves, M. T. & Liptak, M. D. Measurement of Heme Ruffling Changes in MhuD Using UV-vis Spectroscopy. *J Phys Chem B* **120**, 3844–3853 (2016).
5. Schuelke-Sanchez, A. E., Cornetta, A. R., Kocian, T. A. J., Conger, M. A. & Liptak, M. D. Ruffling is essential for Staphylococcus aureus IsdG-catalyzed degradation of heme to staphylobilin. *J Inorg Biochem* **230**, 111775 (2022).
6. Robinson, E. A., Frankenberg-Dinkel, N., Xue, F. & Wilks, A. Recombinant Production of Biliverdin IXβ and δ Isomers in the T7 Promoter Compatible Escherichia coli Nissle. *Front Microbiol* **12**, (2021).
7. Ahmed, F. H. *et al.* Rv2074 is a Novel F420H2-dependent Biliverdin Reductase in Mycobacterium tuberculosis. *Protein Science* **25**, 1692–1709 (2016).
8. Ahmed, F. H. *et al.* Sequence-Structure-Function Classification of a Catalytically Diverse Oxidoreductase Superfamily in Mycobacteria. *J Mol Biol* **427**, 3554–3571 (2015).
9. Wang, J. & Ortiz de Montellano, P. R. The binding sites on human heme oxygenase-1 for cytochrome P450 reductase and biliverdin reductase. *Journal of Biological Chemistry* **278**, 20069–20076 (2003).

10. Jansen, T. & Daiber, A. Direct Antioxidant Properties of Bilirubin and Biliverdin. Is there a role for biliverdin reductase? *Front Pharmacol* **3**, (2012).

11. Barañ, D. E., Rao, M., Ferris, C. D. & Snyder, S. H. Biliverdin Reductase: A Major Physiologic Cytoprotectant. *Proceedings of the National Academy of Sciences* **99**, 16093–16098 (2002).

12. Stocker, R., Yamamoto, Y., McDonagh, A., Glazer, A. & Ames, B. Bilirubin is an Antioxidant of Possible Physiological Importance. *Science (1979)* **235**, 1043–1046 (1987).

13. Xu, W. *et al.* Chemical Genetic Interaction Profiling Reveals Determinants of Intrinsic Antibiotic Resistance in Mycobacterium tuberculosis. *Antimicrob Agents Chemother* **61**, (2017).

14. Ji, C., Juárez-Hernández, R. E. & Miller, M. J. Exploiting bacterial iron acquisition: Siderophore conjugates. *Future Med Chem* **4**, 297–313 (2012).

15. Shin, M. *et al.* Characterization of an antibacterial agent targeting ferrous iron transport protein FeoB against Staphylococcus aureus and Gram-positive bacteria. *ACS Chem Biol* **16**, 136–149 (2021).